

Renormalised Mean-Field Analysis of the 2D Hubbard Model

Von der Fakultät Mathematik und Physik der Universität Stuttgart
zur Erlangung der Würde eines Doktors der Naturwissenschaften
(Dr. rer. nat.) genehmigte Abhandlung

vorgelegt von

Julius Reiß
aus Heidelberg

Hauptberichter: Prof. Dr. W. Metzner

Mitberichter: Prof. Dr. A. Muramatsu

Tag der mündlichen Prüfung: 19. Dezember 2006

Max-Planck-Institut für Festkörperforschung

Stuttgart 2006

Meinen braven Eltern

Die Zeit ist ein Flugzeug, es fliegt durch den Raum
Wir sitzen im Cockpit, es ist wie im Traum
Wir sitzen ganz vorn, das ist eigentlich verboten
Doch wir sind die Kinder vom Autopiloten

(Funny van Dannen)

Contents

Abbreviations	iii
1 Introduction	1
1.1 Outline of the Work	5
2 Renormalisation Group Equations	9
2.1 Derivation of the RG Equations	12
2.2 Discussion of the RG Equations	17
2.3 Integrating the RG Equation & Introducing MF	18
3 The Mean-Field Approximation	21
3.1 Symmetry Breaking	21
3.2 Derivation of Gap Equations	25
3.2.1 Operator Formalism	25
3.2.2 Functional Integral Formalism	28
3.3 The Gap Equations	31
4 AF Mean-Field Solutions	35
4.1 The Right Hand Side	35
4.1.1 Zero Next-Nearest Neighbour Hopping	37
4.1.2 Finite next-nearest Neighbour Hopping	39
4.1.3 Electron-doped side	43
4.2 Solutions of the Gap Equation & Free Energies	47
4.3 RG and AF-Mean-Field Theory	50
4.3.1 Flow without Gap	52
4.3.2 Flow with Gap	53
4.3.3 Numerical Results	53
5 SC, Pi-Pair and Coexistence	59
5.1 Only Pi Gap	59
5.2 Only SC Gap	60
5.3 Coexistence	61
5.3.1 SC and AF	61
5.3.2 Interplay with the Pi-pair	63

6	Numerical Results	67
6.1	Attractive Hubbard model	68
6.2	Repulsive Hubbard Model	70
6.2.1	Only Superconducting Gap	70
6.2.2	Only Antiferromagnetic Gap	72
6.2.3	Interplay of both Gaps	75
6.2.4	The Pi-pairing	85
6.2.5	Electron-doped Side	86
7	Conclusions and Outlook	89
A	Analogy of the RG in ODE Theory	93
A.1	Stating the Problem	93
A.2	Deriving the RG equations	95
B	Gap Equations in Operator Formalism	99
B.1	Antiferromagnetism	99
B.2	Superconductivity and the π -Pairing	101
B.3	The Pomeranchuk and Magnetic Gap	102
B.4	The Mean-Field Hamiltonian	102
B.5	Gap Equations	104
B.6	Grand Canonical Potential for $T = 0$	109
C	Gap Equations in Path Integral Formalism	111
C.1	Effective Action	111
C.2	Bosonic Action	118
C.3	Saddle-Point Approximation	119
D	Mathematical Details	127
D.1	Determinants and Minors	127
D.2	Matrices with Big Values	129
D.3	Simplification of the Gap Equations	130
D.4	Performing the Matsubara Sum	131
E	Technical details	135
F	Deutsche Zusammenfassung	137
F.1	Übersicht der Arbeit	138

Abbreviations

AF AntiFerromagnet(ic), often also the combined spin/charge density wave

BZ Brillouin-Zone

$\delta_{vH} = \mu - 4t'$, shifted chemical potential; distance to the van Hove points

EV EigenValues; often a synonym for the mean-field dispersions

HM two-dimensional Hubbard Model

HS Hubbard-Stratonovich (transformation)

MF Mean-Field

$\mu_{vH} = 4t'$, chemical potential for which the bare Fermi surface includes the van Hove points $(0, \pm\pi), (\pm\pi, 0)$

$\mu_{1/2} = 2t'$, chemical potential for which a system with a finite self-consistent AF-gap is half-filled, see figure (4.6) and section (4.2)

pp particle-particle

ph particle-hole

RG Renormalisation Group

RHS Right-Hand Side of the gap equations or sometimes of the flow equations

RPA Random Phase Approximation

SC SuperConductor/SuperConducting

t Nearest neighbour hopping, used also as energy scale for all energies

t' Next nearest neighbour hopping, $t' \leq 0$ in this work

The prime (\sum_k') marks summation over the magnetic BZ.

Chapter 1

Introduction

Systems with strong correlations and competing instabilities have attracted much attention over the last years. Strong stimulation to this field came by the ground-breaking finding of Bednorz and Müller [Bednorz and Müller 1986], who in 1986 discovered an unexpected high superconducting transition temperature of 30K in Ba-La-Cu-O. Not only was its transition temperature higher than that of any other known superconductor, but the probe also belonged to a material class where superconductivity was believed to be a rare feature. Especially the proximity to magnetism and the poor conductivity in the normal state, obtained by doping the antiferromagnetic parent-compound, was untypical for superconductors. Further investigation revealed other strange, and largely still not understood features, such as the deviation from Fermi liquid behaviour in the normal state, seen for example in the linear (instead of quadratic) temperature dependence of the resistivity and the onset of a pseudo-gap, i.e., a suppression of the density of states near the Fermi surface. The nature of the ground state for certain doping regions is still under debate.

Other features are widely, but not generally, agreed on. The superconductivity is due to pairing of two electrons, like in (classical) BCS superconductors [Bardeen et al. 1957], as is seen from analysing the a.c. Josephson effect [Esteve et al. 1987] and from flux quantisation [Gammel et al. 1987]. These electrons pair with antiparallel spin, forming a singlet, which is concluded from Knight-shift measurements of the spin susceptibility [Barrett et al. 1990], [Takigawa et al. 1989]. The symmetry of the pair-function, which first was controversial, is *d*-wave in contrast to the conventional *s*-wave symmetry, as seen in ARPES data [Shen et al. 1993] and in the famous tri-crystal experiments [Tsuei et al. 1994].

The electron motion seems to be mainly restricted to the Cu-O planes, leading to a strong anisotropy of the conductivity within and perpendicular to these planes. The coupling to the third dimension might therefore be of less importance.

Since the first works this new, unconventional superconductivity has been observed in lots of similar materials. The unusual electronic properties, the closeness to antiferromagnet ordering and the layered structure of the lattice are common to most of these materials.

These new, spectacular experimental discoveries unleashed a tremendous amount of theoretical work trying to explain the different features, but until today the key issue, the pairing mechanism, is strongly controversial. Among others phonon mechanisms resonating valence bond (RVB) theories [Anderson et al. 1987; Anderson 1987], high symmetries like SO(5) [Zhang 1997], Schrieffer's spin bag [Schrieffer et al. 1988] and spin-fluctuation mechanisms [Scalapino 1995] have been suggested.

The d -wave symmetry seems to favour an electronic mechanism over a phonon mechanism, which usually yields s -wave superconductivity [Scalapino 1995]. Also the lack of an isotope effect at optimal doping¹ is interpreted as evidence against a phonon mechanism. An electronic mechanism for superconductivity has already been suggested in the famous paper of [Kohn and Luttinger 1965]. Although the transition temperatures estimated there are extremely low, they already suggest that a suitable dispersions might increase this transition temperature considerably.

Numerical and analytical calculations for the Hubbard model, one model suggested as a model for cuprates, yielded evidence for d -wave pairing on the basis of an electronic mechanism ([Scalapino 1995], and references therein).

The two dimensional (2D) Hubbard model is given by

$$\mathcal{H} = - \sum_{i,j} t_{ij} a_{i\sigma}^\dagger a_{j\sigma} + U \sum_i n_{i\uparrow} n_{i\downarrow}. \quad (1.1)$$

Even though it was originally proposed as a model describing ferromagnetism of narrow-band electrons it was found to exhibit also antiferromagnetism and superconductivity close to half filling. The model contains only electronic degrees of freedom and does not include effects due to lattice distortion, i.e., it neglects phonons.

The two dimensional structure is identified with the two dimensional Cu-O planes, widely believed to be the crucial part of the high- T_c materials, responsible for the superconducting features. Although a three-band model seems appropriate on first sight [Hybertsen et al. 1992], it was found that this can be mapped on an effective one-band model [Zhang and Rice 1988]. The coupling to the third dimension is assumed to be much smaller than the coupling within the planes. It might however be important to stabilise certain order parameters which are known to be suppressed by thermal fluctuations in two dimensions² [Mermin and Wagner 1966].

This seemingly simple model has proven a tremendous task in two dimensions. It is agreed on that the ground state for half-filled systems with large interactions is antiferromagnetically (AF) ordered. For special choices of the hopping amplitudes it may favour ferromagnetism [Honerkamp and Salmhofer 2001; Katanin and Kampf 2005]. Superconductivity (SC) with a d -wave form factor was found by numerous calculations for small doping.

¹ Although an isotope effect is seen in some experiments away from optimal doping.

² To avoid these problems in the present work $T = 0$ is always assumed.

The Fourier transformation of (1.1) leads to

$$\mathcal{H} = \sum_{k,\sigma} \varepsilon_k a_{k\sigma}^\dagger a_{k\sigma} + \sum \frac{1}{4} U (\delta_{\sigma_1\sigma'_1} \delta_{\sigma_2\sigma'_2} - \delta_{\sigma_1\sigma'_2} \delta_{\sigma_2\sigma'_1}) a_{k_1\sigma_1}^\dagger a_{k_2\sigma_2}^\dagger a_{k'_2\sigma'_2} a_{k'_1\sigma'_1}.$$

The tight-binding dispersion is $\varepsilon_k = \varepsilon_k^t + \varepsilon_k^{t'}$ with

$$\begin{aligned} \varepsilon_k^t &= -2t(\cos k_x + \cos k_y), \\ \varepsilon_k^{t'} &= -4t' \cos k_x \cos k_y. \end{aligned}$$

While ε_k^t is antisymmetric under translation by $Q = (\pi, \pi)$, $\varepsilon_k^{t'}$ is symmetric under this translation. The t' contribution is often neglected; however, in this work it is found to be of great importance for the possibility of doping a system with finite AF and the coexistence of the AF and SC order parameter.

The renormalisation group (RG) has been one tool to study the Hubbard model. Although developed first in the high-energy context to remove divergencies in field theories and in the context of critical phenomena, where it paved the way to calculate critical exponents, it also became important in solid state physics, most prominently for Kondo physics [Wilson 1975].

Early works for the high- T_c problems include [Schulz 1987; Dzyaloshinskii 1987; Lederer et al. 1987] where the coupling function was parametrised by a few couplings. Due to the line of divergencies on the Fermi surface no RG with a finite number of renormalised couplings seems to be sufficient, so that the functional RG seems more appropriate. At least the momentum dependence of the coupling function parallel to the Fermi surface (FS) has to be taken into account, see e.g. [Shankar 1994].

This functional RG follows the spirit of the momentum-shell RG of Wilson³, which provides a mapping of the original Hamiltonian on a series of effective Hamiltonians. Since by this procedure terms of all orders of the original interaction are summed up, studying this mapping can reveal physics which is not caught by naïve perturbation theory (PT). Even though other formulations of the RG were found more practical for calculations [Amit 1978], later [Polchinski 1984] used the concept of Wilson to prove renormalisability of the φ^4 -theory, without relying on combinatorics to show that indeed all divergencies can be absorbed into renormalised couplings (see ref. (3-5) of [Polchinski 1984]). Renormalisability in this context means that all divergencies in any order of PT can be absorbed by redefining a finite number of couplings.

The functional RG in the Polchinski scheme was used by [Zanchi and Schulz 1998, 2000] to treat the relevant dependences of the coupling function parallel to the FS; to allow a numerical treatment the momentum dependence parallel to the FS was discretised.

Other formulations of the functional RG were developed. The one-particle irreducible scheme [Wetterich 1993; Morris 1994; Salmhofer and Honerkamp 2001] allowed an easy inclusion of the self-energies and naturally produced a local one-loop equation for the interactions. In the Wick-ordered scheme introduced by [Salmhofer 1998], the flow of the vertices is given by (a sum over)

³ Early, but still worth reading is [Wilson and Kogut 1974].

bilinear terms; the one-loop equation follows naturally from it. All propagators have an upper bound given by the cut-off, which allows in certain cases rigorous statements for the validity of common approximations. This scheme was used by [Halboth and Metzner 2000; Halboth 1999], [Rohe and Metzner 2005] for a numerical treatment of the Hubbard model.

While the cut-off is usually a sharp momentum cut-off function also other procedures were used, for example the temperature flow [Honerkamp and Salmhofer 2001], [Katanin and Kampf 2003; Kampf and Katanin 2003] and the interaction flow [Honerkamp et al. 2004].

The works cited above were done in the symmetric phase. The symmetry-broken state was not allowed for so that tendencies to a symmetry broken-ground state had to be deduced from strongly enhanced couplings or susceptibilities. To gain insight into the symmetry-broken ground state with the RG [Berges et al. 2002; Wetterich 2002] used (partial) bosonisation. To keep the computational effort manageable the vertices were phenomenologically parametrised.

In the fermionic RG a symmetry-breaking field can be introduced yielding anomalous propagators and vertices; after reorganising the flow equations of the one-particle irreducible scheme [Katanin 2004] the correct contribution to the anomalous self energy was accounted for. This allowed to reproduce the Eliashberg equations [Honerkamp and Salmhofer 2005] and to recover the exact solutions of MF-models [Salmhofer et al. 2004; Gersch et al. 2005]. In combination with the interaction flow and a counter term, also first-order phase transition and metastable phases can be treated [Gersch et al. 2006]. Within these schemes the flow equations can be (numerically) integrated. Since introducing a symmetry-breaking term leads to a considerably larger complexity only mean-field models have been treated so far.

In this work a different route will be followed. The fermionic RG in the symmetric phase is combined with a mean-field calculation allowing symmetry breaking. The RG scheme employed here is the Wick-ordered scheme in one-loop approximation. The numerical implementation of [Rohe 2005; Rohe and Metzner 2005] is used to solve the flow equations. The energy dependence as well as the radial momentum dependence of the effective interaction are neglected, see section 2.3. Since divergent couplings hinder the complete integration of the flow equations ($\Lambda \rightarrow 0$), only the high-energy modes $|\varepsilon_k - \mu| > \Lambda_{\text{MF}}$ can be treated within the RG; the low-energy modes $|\varepsilon_k - \mu| < \Lambda_{\text{MF}}$ are treated within a mean-field ansatz. The one-loop approximation is expected to be controlled for moderate initial interaction⁴ [Salmhofer 1998; Salmhofer and Honerkamp 2001]. For the low-energy model the cut-off Λ_{MF} provides a small parameter [Feldman et al. 1993].

⁴The estimates work only for Fermi surfaces *without* van Hove points. However here the scheme will also be used close to the van Hove points.

1.1 Outline of the Work

In chapter 2 the renormalisation scheme will be motivated and derived. As an intermediate step the Polchinski scheme will be obtained from which the Wick-ordered scheme immediately follows. The Wick-ordered scheme is especially useful for our purposes, since the scale-dependent interactions can unambiguously be interpreted as an effective low-energy model. To gain some insight into the one-loop approximation used here, the interaction resulting from the integration of the flow equation will be interpreted graphically as the so called parquet diagram approximation. Finally the flow to large couplings, invalidating the one loop approximation, will be explained, and as a way to circumvent this problem the obtained interactions together with the low-energy cut-off will be understood as an effective low-energy model, which then is treated in a different manner, namely within a mean-field approximation. From the RG treatment the couplings of the effective model have a non-trivial momentum dependence and become attractive in various channels. This allows to obtain non-trivial results within a mean-field approximation which would not have been obtained in a mean-field theory for the bare model.

In chapter 3 the mean-field (MF) equations are presented. After a short introduction to symmetry breaking and mean-field theory, understood as a self-consistent perturbation theory, the MF equations are derived. The equations are coupled MF equations for several order parameters; a superconducting pair with zero momentum and a spin/charge-density wave with $Q = (\pi, \pi)$ modulation, since these instabilities are found to be important in both experimental and theoretical works. A pair with momentum Q , called π -pair, is found to be a natural combination with the former two order parameters. A Fermi surface distortion in the spin/charge-channel can be introduced into the scheme without complicating the gap equations.

The gap equations are derived in two manners. On the one hand, within the Grassmann path integral formalism, using a Hubbard-Stratonovich transformation, and performing a saddle-point approximation for the obtained action. On the other hand, they are derived within the operator formalism using a mean-field decoupling. While the first scheme is more general, and annexed naturally to the RG scheme, and could for example easily be modified for different cut-off procedures, the latter is shorter and less technical. Both derivations make only little use of specific properties of the gaps or the model and are therefore easy to generalise to more or other order parameters, or to other models.

In chapter 4 the mean-field theory for only the spin-density wave having non-zero amplitude is discussed in detail. Frustration due to the chemical potential μ and due to next-nearest-neighbour hopping t' lead to a richer and more complex behaviour compared with an antiferromagnet in the perfect nesting case or the BCS theory. Meta-stability and antiferromagnetic systems with and without Fermi surfaces are found. Despite this complexity, a rather transparent picture emerges.

For $t' = 0$ homogeneous systems with a finite gap are always half-filled.

Doping leads to a complete breakdown of the gap⁵. A finite⁶ chemical potential μ within the band gap changes the free energy of the gapped solution and leads for a finite μ to metastable gapless solutions. For an even larger μ the gapless solution becomes the thermodynamically stable solution.

A finite t' can allow for doped antiferromagnetic solutions. Therefore, finite gap solutions with an effective Fermi surface are possible. The behaviour of the solution as a function of μ and the interaction is to a wide extent determined by these effective Fermi surfaces. Metastable phases are mainly restricted to occur only below $\mu_{vH} = 4t'$.

In the final section of chapter 4 the interplay of the RG and the AF mean-field calculation is discussed. It is shown that due to the possibility of first order transitions the usual RG scheme does not always create adequate low energy models, nor does a non-divergent flow exclude a symmetry-broken state. Further it is shown that even in cases where no metastable solutions exist inadequate low-energy models can be created by the RG. All these effects can be attributed to the strong change of the Fermi surface structure with the antiferromagnetic gap. It becomes clear for which scales the low-energy models are still valid.

Understanding the mean-field theory of the antiferromagnet proved essential for interpreting the calculations for full RG+MF combinations.

In chapter 5 the mean-field theory for only the π -pair having non-zero amplitude is discussed in brevity. Since this order parameter is, in agreement with the expectations, found to be unimportant, the discussion is restricted to the main facts. Already in bare mean-field theory it is apparent that this order parameter plays only a minor rôle. The coexistence of the AF and SC gap creates a π -pair, as stated by [Kyung 2000]. The relevant facts for the numerical calculation are discussed.

The interplay of the superconducting and antiferromagnetic gap in the coupled mean-field theory is discussed. It is found that in contrast to the general belief a finite AF gap can increase the SC gap under suitable circumstances. This increase is due to the enlargement of the effective Fermi surfaces with a small AF gap for systems with a bare FS below the van Hove points, discussed in chapter 4.

Since the gap equations are obtained as derivatives of the grand canonical potential, the changes of the SC gap equation due to an AF gap can be connected with the change of the AF gap equation with the SC gap. This proves helpful in understanding certain features of the AF gap equation, especially the possibility of changing a first- to a second-order transition.

In chapter 6 the results of the numerical calculations of the combined renormalisation group and mean-field method are presented. First the case of an attractive Hubbard model is examined. This allows qualitative comparison with analytic works, showing a reduction of the true gap with respect to the bare mean-field gap due to fluctuations. It also provides a check of the method

⁵ Forcing a system to certain filling thus results in an inhomogeneous system, i.e., it leads to phase separation.

⁶ For $t' = 0$ the bare system is half filled for $\mu = 0$.

for the SC channel showing that the involved approximations are justified, and are better than in the AF case, as was expected.

For the repulsive Hubbard model, phase diagrams for zero and finite next nearest neighbour hopping t' are presented. For a zero t' the system is either antiferromagnetic and half-filled or superconducting. Forcing the system to certain fillings would lead to phase separation. For finite t' , Fermi surfaces with a finite AF gap and coexistence of AF and SC are found. This most interesting case is discussed in detail; the gap amplitudes for different bare interactions and dopings are presented. Effective Fermi surfaces and gap structures are shown. The momentum dependence of the gaps is generated by the method.

Finally, numerical values for the π -pair are presented, showing that this order parameter is indeed much smaller than the other gaps, justifying the assumption of its absence in the other calculations.

Appendix A provides a short pedagogical example for the RG. It is shown within a perturbation theory for nonlinear ordinary differential equations that renormalisation group equations can sum divergent terms to infinite order. The obtained approximative solutions are well behaved due to this procedure. In this framework it is easily seen that naïve perturbation theory might destroy the correct structure which is recovered by the RG technique.

Appendices B-D provide details of the derivation of the gap equations and some matrix algebra which is needed for simplifying the equations.

Chapter 2

Renormalisation Group Equations

In this chapter the renormalisation group (RG) equations will be derived. The RG will be understood as a tool to overcome divergencies of the naïve perturbation theory by resumming a subset of higher order contributions. By means of the RG effective low energy interactions will be obtained, incorporating the high energy physics. As a pedagogical toy-model it is shown in the appendix A how to apply this concept to ordinary differential equations.

The RG will respect the symmetry of the original model, and no symmetry breaking fields will be introduced, as this would complicate the equations and drastically increase the numerical effort. The symmetry breaking will be introduced effectively in the low energy model, by a mean-field ansatz, described in the next chapter. The derivation of the RG flow equations follows largely [Enss 2005].

The starting point is a normal-ordered Hamiltonian of a fermionic system

$$\mathcal{H} = H_0[a, a^\dagger] + H_I[a, a^\dagger], \quad (2.1)$$

with a free part H_0 and an interacting part H_I . From this the action $S[\psi, \bar{\psi}]$ in Grassmann-path-integral formalism follows as $S[\psi, \bar{\psi}] = S_0[\psi, \bar{\psi}] + S_I[\psi, \bar{\psi}]$, where the free part is given by

$$S_0[\psi, \bar{\psi}] = \sum_K \bar{\psi}_K C_K^{-1} \psi_K = \sum_K \bar{\psi}_K i\omega \psi_K - H_0[\psi, \bar{\psi}], \quad (2.2)$$

with the inverse propagator

$$Q_K = C_K^{-1} = (i\omega - \xi_k). \quad (2.3)$$

The bare interaction-part is given by

$$S_I = - \sum_{K_1, K_2, K'_2, K'_1} \frac{1}{4} V(K_1, K_2, K'_2, K'_1) \bar{\psi}_{K_1} \bar{\psi}_{K_2} \psi_{K'_2} \psi_{K'_1} = -H_I[\psi, \bar{\psi}] \quad (2.4)$$

K is the usual multi-index (ω_n, k, σ) of the spin, energy and momentum degrees of freedom; ψ and $\bar{\psi}$ are fields of Grassmann numbers.

One would like to calculate the partition function

$$Z[\eta, \bar{\eta}] = \frac{1}{Z_0} \int \mathcal{D}(\psi, \bar{\psi}) e^{\mathcal{S}[\psi, \bar{\psi}]} e^{-(\bar{\psi}, \eta) - (\bar{\eta}, \psi)} \quad (2.5)$$

with external fields η and $\bar{\eta}$ as it contains the physically relevant information. Z_0 is the partition function without interaction and with zero external fields, given by

$$Z_0 = \int \mathcal{D}(\psi, \bar{\psi}) e^{(\bar{\psi}, \mathbf{Q}\psi)} = \det(\mathbf{Q}). \quad (2.6)$$

The non-interacting system with external fields can be integrated, leading to

$$\begin{aligned} Z_{\text{non}}[\eta, \bar{\eta}] &= \frac{1}{Z_0} \int \mathcal{D}(\psi, \bar{\psi}) e^{(\bar{\psi}, \mathbf{Q}\psi)} e^{-(\bar{\psi}, \eta) - (\bar{\eta}, \psi)} \\ &= \frac{1}{Z_0} \int \mathcal{D}(\psi, \bar{\psi}) e^{(\bar{\psi} + \bar{\eta}\mathbf{C}^T, \mathbf{Q}(\psi + \mathbf{C}\eta))} e^{-(\bar{\psi} + \bar{\eta}\mathbf{C}^T, \eta) - (\bar{\eta}, \psi + \mathbf{C}\eta)} \\ &= e^{-(\bar{\eta}, \mathbf{C}\eta)} \frac{1}{Z_0} \int \mathcal{D}(\psi, \bar{\psi}) e^{(\bar{\psi}, \mathbf{Q}\psi)} \\ &= e^{-(\bar{\eta}, \mathbf{C}\eta)} \end{aligned} \quad (2.7)$$

where $\mathbf{C} = \mathbf{Q}^{-1}$ is the propagator. In the second line the integration variables were shifted by $\bar{\eta}\mathbf{C}^T$ and $\mathbf{C}\eta$, respectively. In the following the abbreviation

$$\int d\mu_{\mathbf{Q}}[\psi, \bar{\psi}] = \frac{1}{Z_0} \int \mathcal{D}(\psi, \bar{\psi}) e^{(\bar{\psi}, \mathbf{Q}\psi)} \quad (2.8)$$

will be used. Including the quadratic part into the measure is in the spirit of N. Wiener, who derived path integrals to do statistics over random walks.

The generating functional of the connected Green's functions is

$$\mathcal{G}[\eta, \bar{\eta}] = -\ln Z[\eta, \bar{\eta}] \quad (2.9)$$

since taking the derivative with respect to η and $\bar{\eta}$ produces the connected Green's functions. From this we obtain by rewriting

$$\begin{aligned} &\exp(-\mathcal{G}[\eta, \bar{\eta}]) \\ &= \frac{1}{Z_0} \int \mathcal{D}(\psi, \bar{\psi}) e^{\mathcal{S}_I[\psi, \bar{\psi}]} e^{(\bar{\psi}, \mathbf{Q}\psi) - (\bar{\psi}, \eta) - (\bar{\eta}, \psi)} \\ &= \frac{1}{Z_0} \int \mathcal{D}(\psi, \bar{\psi}) e^{\mathcal{S}_I[\psi, \bar{\psi}]} e^{((\bar{\psi} - \bar{\eta}\mathbf{C}^T), \mathbf{Q}(\psi - \mathbf{C}\eta)) - (\bar{\eta}, \mathbf{C}\eta)} \\ &= e^{-(\bar{\eta}, \mathbf{C}\eta)} \int d\mu_{\mathbf{Q}}[\psi, \bar{\psi}] e^{\mathcal{S}_I[\psi + \mathbf{C}\eta, \bar{\psi} + \bar{\eta}\mathbf{C}^T]} \\ &= e^{-(\bar{\eta}, \mathbf{C}\eta)} e^{-\mathcal{V}[\chi, \bar{\chi}]} \end{aligned} \quad (2.10)$$

the effective interaction

$$\mathcal{V}[\chi, \bar{\chi}] = \mathcal{G}[\eta, \bar{\eta}] - (\bar{\eta}, \mathbf{C}\eta), \quad (2.11)$$

where $\chi = \mathbf{C}\eta$ and $\bar{\chi} = \bar{\eta}\mathbf{C}^T$ have been introduced. The new variables have the effect of amputating the legs, i.e., the external bare propagators of all diagrams. The effective interaction can be formally calculated to be

$$\begin{aligned}
e^{-\mathcal{V}[\eta, \bar{\eta}]} &= \int d\mu_{\mathbf{Q}}[\psi, \bar{\psi}] \exp(S_I[\psi + \chi, \bar{\psi} + \bar{\chi}]) \\
&= \int d\mu_{\mathbf{Q}}[\psi, \bar{\psi}] \exp(S_I[\partial_{\bar{\varphi}}, \partial_{\varphi}]) e^{(\bar{\varphi}, \psi + \chi) - (\bar{\psi} + \bar{\chi}, \varphi)} \Big|_{\varphi = \bar{\varphi} = 0} \\
&= \exp(S_I[\partial_{\bar{\varphi}}, \partial_{\varphi}]) e^{(\bar{\varphi}, \chi) - (\bar{\chi}, \varphi)} \int d\mu_{\mathbf{Q}}[\psi, \bar{\psi}] e^{(\bar{\varphi}, \psi) - (\bar{\psi}, \varphi)} \Big|_{\varphi = \bar{\varphi} = 0} \\
&= \exp(S_I[\partial_{\bar{\varphi}}, \partial_{\varphi}]) e^{(\bar{\varphi}, \mathbf{C}\varphi)} e^{(\bar{\varphi}, \chi) - (\bar{\chi}, \varphi)} \Big|_{\varphi = \bar{\varphi} = 0} \\
&= e^{(\partial_{\chi}, \mathbf{C}\partial_{\bar{\chi}})} \exp(S_I[\partial_{\bar{\varphi}}, \partial_{\varphi}]) e^{(\bar{\varphi}, \chi) - (\bar{\chi}, \varphi)} \Big|_{\varphi = \bar{\varphi} = 0} \\
&= e^{(\partial_{\chi}, \mathbf{C}\partial_{\bar{\chi}})} e^{S_I[\chi, \bar{\chi}]} .
\end{aligned} \tag{2.12}$$

Expanding in the last line e^{S_I} in the bare potential and comparing order by order with \mathcal{V} as

$$\mathcal{V} = \sum_{m=0}^{\infty} \frac{1}{(m!)^2} \sum_{K_1 \dots K_m} \sum_{K'_1 \dots K'_m} V_m(K'_1 \dots K'_m; K_1 \dots K_m) \prod_{j=0}^m \bar{\chi}_{K'_j} \chi_{K_j} \tag{2.13}$$

leads to the naïve perturbation series. Observe that in (2.12) all terms χ and $\bar{\chi}$ appear in the same order, reflecting the particle conservation; therefore also the expression (2.13) has only such terms. A perturbation theory cannot break the symmetry of the underlying Hamiltonian. To produce the physically correct symmetry-broken ground state one has to break the symmetry by hand by introducing a symmetry-breaking field or by doing a self-consistent perturbation theory, in which the symmetry is broken by choosing one of several solutions, as is done in chapter 3.

Unfortunately the perturbation theory breaks down in certain cases. Consider for example the effective two-particle interaction up to second order in the bare interaction of the 2D $t - t'$ -Hubbard Model

$$\tag{2.14}$$

If the interaction is a constant in momentum space as in the Hubbard model, the terms can be expressed using the particle-particle (pp) bubble

$$\Xi(P) = \text{pp bubble} = \sum_K C(K)C(P - K) \tag{2.15}$$

and the particle-hole (ph) bubble

$$\Pi(P) = \text{ph bubble} = - \sum_K C(K)C(P + K). \tag{2.16}$$

For $T = 0$ and external momentum $p = 0$ the particle-particle bubble is always divergent. This is due to the fact that electrons are scattered from $k \rightarrow -k$, which has in the case of the inflection-symmetric FS $\xi_k = \xi_{-k}$, assumed here, a huge scattering space. This divergency leads, as long as the interaction is attractive (negative) in any channel, to a diverging susceptibility, interpreted as an instability towards a superconducting state, as the pp-bubble is closely connected to the susceptibility of the superconductor.

Again for $T = 0$, but for the momentum $p = (\pi, \pi)$, the particle-hole bubble is divergent for $\mu = 4t'$. The bare Fermi surface crosses the van Hove points at $(0, \pm\pi)$ and $(\pm\pi, 0)$, so that the divergent density of states leads to a divergent particle-hole bubble.

For a positive interaction the divergent ph bubble always lead to a divergent spin-susceptibility, which is interpreted as an instability towards an antiferromagnet (AF). However the converse is not always true. A finite susceptibility does not exclude a symmetry-broken ground state, as the AF can exhibit a first order transition, as is discussed in detail in chapter 4.¹

It is straightforward to see that higher order diagrams, which contain the particle-particle or particle-hole bubbles, diverge as strong or even more strongly, leading to more and more divergent terms in higher orders. These divergencies make the perturbation theory useless even for small coupling.

2.1 Derivation of the RG Equations

The renormalisation group (RG) is one tool to overcome this problem. A new energy scale Λ is introduced, by which the model is split into a high- and a low-energy part. Thereby scale-dependent n-point functions are defined, which become the full n-point functions in the limit $\Lambda \rightarrow 0$. The dependence of the n-point functions on this energy scale Λ is governed by the RG equations, so that solving the RG equations yields the desired n-point functions.

From different generating functionals different RG equations follow, which have different advantages and disadvantages. As an intermediate step first the Polchinski equation is derived, from which the Wick-ordered scheme, which is the most appropriate one for our purpose, straightly follows.

To derive the RG a new energy scale Λ is introduced splitting the quadratic part into

$$\begin{aligned} (\delta_\chi, C\delta_{\bar{\chi}}) &= (\delta_\chi, (D^\Lambda + C^\Lambda)\delta_{\bar{\chi}}) \\ &= (\delta_\chi, D^\Lambda\delta_{\bar{\chi}}) + (\delta_\chi, C^\Lambda\delta_{\bar{\chi}}), \end{aligned} \quad (2.17)$$

with the high and low energy propagator

$$D^\Lambda = (i\omega - \xi_k)^{-1} \chi_k^\Lambda \quad (2.18)$$

$$C^\Lambda = (i\omega - \xi_k)^{-1} (1 - \chi_k^\Lambda), \quad (2.19)$$

¹ A more detailed discussion of the divergencies of the pp and ph bubble is found in [Halboth 1999].

with the cut-off function

$$\chi_k^\Lambda = \Theta(\Lambda - |\xi_k|), \quad (2.20)$$

where the energy scale is defined according to the non-interacting system.

This regularises the perturbation theory as the divergent contributions are cut out if the propagator C^Λ is used instead of C . The dependence on the cut-off Λ can also be used to gain an effective low-energy model, as will be done in the following.

Splitting the propagator as in (2.17) and inserting this in the expression for the effective interaction (2.12)

$$\begin{aligned} e^{-\mathcal{V}[\chi, \bar{\chi}]} &= e^{(\partial_\chi, D \partial_{\bar{\chi}})} e^{S_I[\chi, \bar{\chi}]} \\ &= e^{(\partial_\chi, D^\Lambda \partial_{\bar{\chi}})} e^{(\partial_\chi, C^\Lambda \partial_{\bar{\chi}})} e^{S_I[\chi, \bar{\chi}]} \\ &\equiv e^{(\partial_\chi, D^\Lambda \partial_{\bar{\chi}})} e^{-\mathcal{V}^\Lambda[\chi, \bar{\chi}]} \end{aligned} \quad (2.21)$$

one obtains the Λ -dependent effective action $\mathcal{V}^\Lambda[\chi, \bar{\chi}]$. Rewritten as a functional integral, (2.21) reads

$$\begin{aligned} e^{-\mathcal{V}[\chi, \bar{\chi}]} &= \int d\mu_{C^{-1}}[\psi, \bar{\psi}] \exp(S_I[\psi + \chi, \bar{\psi} + \bar{\chi}]) \\ &= \int d\mu_{(D^\Lambda)^{-1}}[\psi, \bar{\psi}] \exp(-\mathcal{V}^\Lambda[\psi + \chi, \bar{\psi} + \bar{\chi}]). \end{aligned} \quad (2.22)$$

The last expression has the formal structure

$$\mathcal{V}(D^\Lambda + C^\Lambda, S_I) = \mathcal{V}(D^\Lambda, -\mathcal{V}(C^\Lambda, S_I)) \quad (2.23)$$

which is the structure of a semi-group [Salmhofer and Honerkamp 2001]. This identity can be interpreted as relating two systems, which are given by different microscopic parameters, but describing the same physics. The parameters are renormalised. It is this (semi-)group property, which gives the name *renormalisation group*. This property is exact, so that this RG is also called exact RG. However, to do calculations in non-trivial systems, approximations have to be employed.

The derivative of the effective action with respect to Λ is by its definition (2.21)

$$\begin{aligned} \partial_\Lambda \mathcal{V} &= -e^{\mathcal{V}^\Lambda} \partial_\Lambda e^{-\mathcal{V}^\Lambda} \\ &= -e^{\mathcal{V}^\Lambda} \partial_\Lambda \left(e^{(\partial_\chi, C^\Lambda \partial_{\bar{\chi}})} e^{S_I} \right) \\ &= -e^{\mathcal{V}^\Lambda} (\partial_\chi, \dot{C}^\Lambda \partial_{\bar{\chi}}) e^{-\mathcal{V}^\Lambda} \end{aligned} \quad (2.24)$$

leading to the flow equation for \mathcal{V}^Λ

$$\dot{\mathcal{V}} = \left((\partial_\chi, \dot{C}^\Lambda \partial_{\bar{\chi}}) \mathcal{V} \right) + (\partial_\chi \mathcal{V}, \dot{C}^\Lambda \partial_{\bar{\chi}} \mathcal{V}), \quad (2.25)$$

which is the Polchinski equation [Polchinski 1984].

This can be graphically presented, if one expands \mathcal{V} and compares orders, as

$$\partial_\Lambda \begin{array}{c} \vdots \\ \vdots \\ \text{---} \bullet \text{---} \\ \vdots \\ \vdots \\ V_m^\Lambda \end{array} = \begin{array}{c} \dot{C}^\Lambda \\ \text{---} \bullet \text{---} \\ \vdots \\ \vdots \\ V_{m+1}^\Lambda \end{array} + \sum_k \begin{array}{c} \vdots \\ \vdots \\ \text{---} \bullet \text{---} \\ \vdots \\ \vdots \\ V_k^\Lambda \end{array} \text{---} \dot{C}^\Lambda \text{---} \begin{array}{c} \vdots \\ \vdots \\ \text{---} \bullet \text{---} \\ \vdots \\ \vdots \\ V_{m-k+1}^\Lambda \end{array} \quad (2.26)$$

One obtains an infinite hierarchy of flow equations; leaving out the equation for the zero-leg vertex, which does not couple back to the other equations, the first three equations are explicitly:

$$\partial_\Lambda \begin{array}{c} \text{---} \bullet \text{---} \\ V_1^\Lambda \end{array} = \begin{array}{c} \dot{C}^\Lambda \\ \text{---} \bullet \text{---} \\ V_2^\Lambda \end{array} + \begin{array}{c} \text{---} \bullet \text{---} \\ V_1^\Lambda \end{array} \text{---} \dot{C}^\Lambda \text{---} \begin{array}{c} \text{---} \bullet \text{---} \\ V_1^\Lambda \end{array} \quad (2.27)$$

$$\partial_\Lambda \begin{array}{c} \text{---} \bullet \text{---} \\ V_2^\Lambda \end{array} = \begin{array}{c} \dot{C}^\Lambda \\ \text{---} \bullet \text{---} \\ V_3^\Lambda \end{array} + \begin{array}{c} \text{---} \bullet \text{---} \\ V_2^\Lambda \end{array} \text{---} \dot{C}^\Lambda \text{---} \begin{array}{c} \text{---} \bullet \text{---} \\ V_1^\Lambda \end{array} \quad (2.28)$$

$$\begin{aligned} \partial_\Lambda \begin{array}{c} \text{---} \bullet \text{---} \\ V_3^\Lambda \end{array} &= \begin{array}{c} \dot{C}^\Lambda \\ \text{---} \bullet \text{---} \\ V_4^\Lambda \end{array} + \begin{array}{c} \text{---} \bullet \text{---} \\ V_2^\Lambda \end{array} \text{---} \dot{C}^\Lambda \text{---} \begin{array}{c} \text{---} \bullet \text{---} \\ V_2^\Lambda \end{array} \\ &+ \begin{array}{c} \text{---} \bullet \text{---} \\ V_3^\Lambda \end{array} \text{---} \dot{C}^\Lambda \text{---} \begin{array}{c} \text{---} \bullet \text{---} \\ V_1^\Lambda \end{array} \quad (2.29) \end{aligned}$$

The initial condition is

$$\mathcal{V}^{\Lambda_0} = -\frac{1}{4}V, \quad (2.30)$$

with Λ_0 being the maximum of $|\xi_k|$ on the Brillouin zone.

To do any numerical calculation one has to truncate this hierarchy, i.e., set all coefficients higher than some n_0 to zero: $V_n = 0, \forall n \geq n_0$.

This scheme was used by [Zanchi and Schulz 2000],[Zanchi and Schulz 1998] for the 2D Hubbard model. However, to calculate effective two particle interactions to second order in the interaction, the authors had to incorporate the six point function V_3 ; the RHS of flow equation of V_3 , (2.29), is approximated by the term quadratic in V_2 , so that the eight-point function V_4 and the feedback due to the term $\propto V_3V_1$ is neglected. Inserting the tree term $\propto (V_2)^2$ into eq. (2.28), and closing this tree diagram by the tadpole in the equation for V_2 leads to the desired one-loop term. Due to this procedure the locality in the flow is lost and one propagator lives on energy scales above the cut-off [Zanchi and Schulz 2000]. Thus the flow history is needed to calculate the flow of an interaction. Due to this the effective couplings at a given scale Λ cannot be interpreted as an effective low energy model. To overcome this, the Wick-ordered scheme can be used.

The Wick ordered generating functional is defined as

$$\mathcal{W}^\Lambda[\chi, \bar{\chi}] = e^{(\partial_\chi, D^\Lambda \partial_{\bar{\chi}})} \mathcal{V}^\Lambda[\chi, \bar{\chi}]. \quad (2.31)$$

Graphically, this can be interpreted as adding all tadpoles to the monomials:

$$W_m^\Lambda = V_m^\Lambda + V_{m+1}^\Lambda + V_{m+2}^\Lambda + \dots \quad (2.32)$$

The flow equation in the Wick-ordered scheme is derived from

$$\begin{aligned} \partial_\Lambda \mathcal{W}^\Lambda &= (\partial_\chi, \dot{D}^\Lambda \partial_{\bar{\chi}}) e^{(\partial_\chi, D^\Lambda \partial_{\bar{\chi}})} \mathcal{V} + e^{(\partial_\chi, D^\Lambda \partial_{\bar{\chi}})} \partial_\Lambda \mathcal{V} \\ &= (\partial_\chi, \dot{D}^\Lambda \partial_{\bar{\chi}}) e^{(\partial_\chi, D^\Lambda \partial_{\bar{\chi}})} \mathcal{V} - e^{(\partial_\chi, D^\Lambda \partial_{\bar{\chi}})} (\partial_\chi, \dot{D}^\Lambda \partial_{\bar{\chi}}) \mathcal{V}^\Lambda \\ &\quad + e^{(\partial_\chi, D^\Lambda \partial_{\bar{\chi}})} (\partial_\chi \mathcal{V}^\Lambda, \dot{D}^\Lambda \partial_{\bar{\chi}} \mathcal{V}^\Lambda) \\ &= e^{(\partial_\chi, D^\Lambda \partial_{\bar{\chi}})} (\partial_\chi \mathcal{V}^\Lambda, \dot{D}^\Lambda \partial_{\bar{\chi}} \mathcal{V}^\Lambda), \end{aligned} \quad (2.33)$$

where in the second line the Polchinski equation, (2.25) was exploited, rewritten using $(\partial_\chi, \dot{C}^\Lambda \partial_{\bar{\chi}}) = -(\partial_\chi, \dot{D}^\Lambda \partial_{\bar{\chi}})$. The Laplacian can be split into

$$\begin{aligned} &(\partial_\chi, D^\Lambda \partial_{\bar{\chi}}) \\ &= (\partial_\chi^1, D^\Lambda \partial_{\bar{\chi}}^1) + (\partial_\chi^1, D^\Lambda \partial_{\bar{\chi}}^2) + (\partial_\chi^2, D^\Lambda \partial_{\bar{\chi}}^1) + (\partial_\chi^2, D^\Lambda \partial_{\bar{\chi}}^2). \end{aligned} \quad (2.34)$$

where the superscripts mark whether the derivative acts on the first or the second \mathcal{V} in (2.33). As all terms in (2.34) commute, the exponential of the

Laplacian in (2.33) can be written as a product, which permits one to rewrite the RHS of (2.33) in \mathcal{W} as

$$\begin{aligned}
& \partial_\Lambda \mathcal{W}^\Lambda \\
&= e^{(\partial_{\bar{x}}^1, D^\Lambda \partial_{\bar{x}}^2) + (\partial_{\bar{x}}^2, D^\Lambda \partial_{\bar{x}}^1)} \left(\partial_{\bar{x}} \left(e^{(\partial_{\bar{x}}, D^\Lambda \partial_{\bar{x}})} \mathcal{V}^\Lambda \right), \dot{D}^\Lambda \partial_{\bar{x}} \left(e^{(\partial_{\bar{x}}, D^\Lambda \partial_{\bar{x}})} \mathcal{V}^\Lambda \right) \right) \\
&= e^{(\partial_{\bar{x}}^1, D^\Lambda \partial_{\bar{x}}^2) + (\partial_{\bar{x}}^2, D^\Lambda \partial_{\bar{x}}^1)} \left(\partial_{\bar{x}} \mathcal{W}^\Lambda, \dot{D}^\Lambda \partial_{\bar{x}} \mathcal{W}^\Lambda \right), \tag{2.35}
\end{aligned}$$

which is the desired flow equation for the Wick-ordered functional. The flow equation has the graphical representation

This flow equation is now not only an infinite hierarchy if sorted by orders, but the right hand side of any equation contains also infinitely many terms. To do any calculations one has to truncate the hierarchy and the right hand sides.

As an advantage the flow equations contain the one loop terms quadratic in \mathcal{W}_2 without taking \mathcal{W}_3^Λ in account, and due to the Wick ordering all propagators live on energy scales $|\xi_k| < \Lambda$. One does not need the history of the flow to integrate the equations. Therefore the flowing couplings can be interpreted as an effective low-energy model at any scale Λ . The one-loop approximation of the flow of the two-particle interaction, rewritten in the one-particle-irreducible scheme [Halboth 1999], is given by

$$\begin{aligned}
& \frac{\partial}{\partial \Lambda} \Gamma^\Lambda(K'_1, K'_2; K_1, K_2) = \\
& \sum_{K, K'} \frac{\partial}{\partial \Lambda} [D^\Lambda(K) D^\Lambda(K')] \times \left[\frac{1}{2} \Gamma^\Lambda(K'_1, K'_2; K, K') \Gamma^\Lambda(K, K'; K_1, K_2) \right. \\
& \quad - \Gamma^\Lambda(K'_1, K; K_1, K') \Gamma^\Lambda(K', K'_2; K, K_2) \\
& \quad \left. + \Gamma^\Lambda(K'_2, K; K_1, K') \Gamma^\Lambda(K', K'_1; K, K_2) \right] \tag{2.36}
\end{aligned}$$

or graphically

$$\frac{\partial}{\partial \Lambda} \text{[Square Diagram]} = \text{[Ladder Diagram]} + \text{[Particle-hole Ladder Diagram]} + \text{[ZS' Diagram]} \quad (2.37)$$

The first term of the RHS is the particle-particle ladder or BCS digram, the second one is the RPA or ZS (zero sound) and the third is the ZS' digram; the ZS and ZS' diagram will be referred to as particle-hole diagrams.

The starting condition is, as $D^{\Lambda_0} = C$:

$$\mathcal{W}^{\Lambda_0} = e^{(\partial_{\chi}, C \partial_{\bar{\chi}})} S_I[\chi, \bar{\chi}] = \text{[Loop Diagram]} + \text{[Bubble Diagram]} + \text{[Crossed Diagram]} \quad (2.38)$$

2.2 Discussion of the RG Equations

In this section it will be shown that integrating the one-loop Wick equation creates structurally the parquet diagrams. This is done by taking the feedback in the RG equation of the created effective two-particle interactions only stepwise into account, i.e., approximating the RHS by an RHS with effective interaction created at a fixed higher Λ -scale. Thereby the iteration creating the parquet diagrams becomes apparent. This iteration leads to a restriction on the momenta of certain propagators, which is also not lifted if the step-size is going to zero.

In [Binz et al. 2003] it is argued that the one loop flow equations create the so called parquet diagrams [Diatlov et al. 1957], with certain restrictions on inner propagators. To see this it is helpful to replace the derivative by a (small) step in $\delta\Lambda$. The original equation is regained by setting $\delta\Lambda \rightarrow 0$.

The starting value for the effective interaction is just the bare interaction (2.38) and the crossed term:

$$\text{[Wavy Line]} \quad \text{[Crossed Diagram]} \quad (2.39)$$

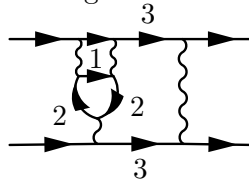
Inserting these into (2.37) and doing the step $\delta\Lambda$ we produce all the diagrams as in (2.14), where the Fermi propagators are restricted to $|\xi_k| < \Lambda_0 - \delta\Lambda = \Lambda_1$. Thus in the first step the effective iteration is given by the bare interaction plus the one loop diagrams, with restricted propagators, such as

$$\text{[Restricted Propagator Diagram]} \quad (2.40)$$

where $1 \equiv \Lambda_1$ marks the restriction on the propagator. In the next step, $\Lambda_1 - \delta\Lambda = \Lambda_2$, the newly created diagrams also have to be inserted in the RHS of the flow equation, leading to an insertion on the inner lines, giving for example


(2.41)

As the ladder diagram was created on a higher energy scale than the RPA-bubble, the energy will be restricted by the energy scale of the RPA bubble, also in the limit $\delta\Lambda \rightarrow 0$. Iterating once more we obtain, e.g.,


(2.42)

Thus by integrating the flow equation one iteratively inserts the one loop terms in all ways on the inner lines, effectively creating topologically the parquet diagram subset.

All the parquet diagrams are created; however, due to the way the diagrams are created momenta of some propagators are restricted by the momenta of others. It can be shown, that all divergencies in leading logarithmic order are correctly included [Binz et al. 2003].

Even though the leading order divergency is included correctly, i.e., summed over, divergencies can appear when integrating this flow equation, namely below a certain temperature. This is indicating the onset of a (second order) instability towards a symmetry-broken phase. This divergency is not an artefact of the perturbation theory, but has to be considered as a physical one indicating the existence of a symmetry-broken ground state.

This divergency can be due to a simple geometric-series-like sub-class, like the RPA-diagrams for the antiferromagnet; others like the SC rely (in the repulsive Hubbard model) on the creation of an attractive channel by the interplay of other diagrams to make a sub-class divergent.

This divergency can be handled in the RG scheme by introducing a finite symmetry-breaking gap, leading to extra terms in the RHS of the flow equations. In the one particle irreducible scheme the equations can be reorganised due to [Katanin 2004] so that a correct ground state can be reached [Salmhofer et al. 2004] and [Gersch et al. 2005], at least in mean-field models².

In the next section a different ansatz will be followed, namely the flow will be stop before couplings become large. Symmetry-breaking will be introduced within a mean-field framework, which is presented in chapter 3.

2.3 Integrating the RG Equation & Introducing MF

The one-loop RG equation (2.37) is so complex that it can be integrated for the given model neither analytically nor numerically. Therefore, further sim-

² First order phase transitions require a different treatment, see 4.3, and [Gersch et al. 2006].

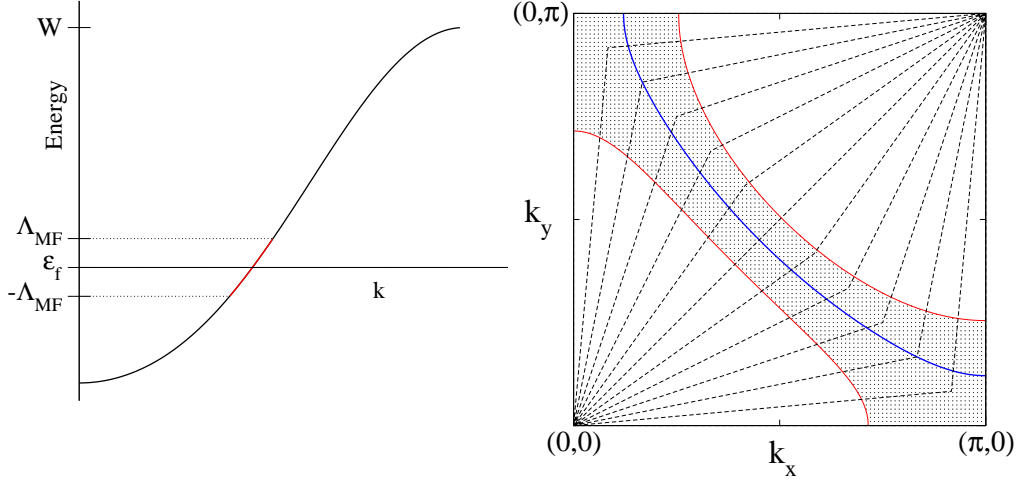


Figure 2.1: Left: The bandwidth W of the bare model and the band-width of the low-energy model Λ_{MF} . The degrees of freedom treated by the RG are given by $|\xi_k| > \Lambda_{\text{MF}}$, depicted in black, the one treated by the mean-field calculation are given by $|\xi_k| < \Lambda_{\text{MF}}$, depicted in red. Right: The restriction of the momenta by the low energy cut-off Λ_{MF} . Patches are marked by dashed lines.

plifications have to be employed. The energy dependence is usually assumed to be of minor importance, since divergences appear for $\omega = 0$ in the perturbation theory, and will thus, as in most works, be neglected. This allows one to perform the Matsubara sums analytically; the resulting Fermi functions together with the here used sharp cut-off function reduce the momentum integration to a one-dimensional integral. For $\Lambda \rightarrow 0$ the momenta are restricted to a shell close to the FS, making it reasonable to replace the momenta by momenta projected onto the FS. For large Λ the momentum dependence of the interaction is expected to be weak, since the initial interaction at $\Lambda = \Lambda_0$ is just the constant bare Hubbard U , so that the projection seems reasonable also in this case.

The dependence on the angle, i.e., parallel to the FS, cannot be neglected, since already in perturbation theory a tendency towards d-wave superconductivity is seen. To allow a numerical treatment the angular dependence is discretised. The discretisation, into so-called patches, is shown in fig. (2.1), right; the dependence of the effective interaction on *continuous* momenta is thereby replaced by a dependence on *discrete* patch numbers. The patches are chosen to be of equal area, and to be congruent under a (π, π) -translation. The latter is important for defining a spin/charge-density wave with (π, π) -modulation. Three of the outer momenta of the flow equation (2.37) are projected onto the FS, while the dashed propagator contributes for a sharp cut-off only at scale Λ . The remaining momenta are determined by momentum conservation.

The Hubbard model is spin-rotation invariant, permitting a simple parametrisation of the spin dependence [Halboth 1999]. Two decompositions are used in

this work. The singlet-triplet decomposition is given by

$$\begin{aligned} \Gamma^\Lambda \begin{pmatrix} \sigma_1 & \sigma_2 & \sigma'_2 & \sigma'_1 \\ k_1 & k_2 & k'_1 & k'_2 \end{pmatrix} &= \frac{1}{2} \Gamma_t^\Lambda(k_1, k_2, k'_1, k'_2) \left(\delta_{\sigma_1, \sigma'_1} \delta_{\sigma_2, \sigma'_2} + \delta_{\sigma_1, \sigma'_2} \delta_{\sigma_2, \sigma'_1} \right) \\ &\quad + \frac{1}{2} \Gamma_s^\Lambda(k_1, k_2, k'_1, k'_2) \left(\delta_{\sigma_1, \sigma'_1} \delta_{\sigma_2, \sigma'_2} - \delta_{\sigma_1, \sigma'_2} \delta_{\sigma_2, \sigma'_1} \right) \end{aligned} \quad (2.43)$$

and is used in the RG numerics. It is also adequate for the superconducting gap. The spin-charge decomposition

$$\begin{aligned} \Gamma^\Lambda \begin{pmatrix} \sigma_1 & \sigma_2 & \sigma'_2 & \sigma'_1 \\ k_1 & k_2 & k'_1 & k'_2 \end{pmatrix} &= \Gamma_C^\Lambda(k_1, k_2, k'_1, k'_2) \delta_{\sigma_1, \sigma'_1} \delta_{\sigma_2, \sigma'_2} \\ &\quad + \Gamma_S^\Lambda(k_1, k_2, k'_1, k'_2) \left(2\delta_{\sigma_1, \sigma'_2} \delta_{\sigma_2, \sigma'_1} - \delta_{\sigma_1, \sigma'_1} \delta_{\sigma_2, \sigma'_2} \right) \end{aligned} \quad (2.44)$$

is most suitable for the magnetic gaps, as it reveals the interpretation as a combination of a spin/charge-density-wave gap, or a spin/charge Pomeranchuk distortion, respectively, see section (3.3).

As mentioned earlier, the effective couplings diverge below a certain temperature in the limit $\Lambda \rightarrow \Lambda_c$ in one or more channels. This is interpreted as an instability towards a symmetry-broken state. The large couplings invalidate the one-loop approximation. It is difficult to separate between different instabilities if the couplings, or the associated susceptibilities, become large in more than one channel.

To circumvent this problem the RG flow can be stopped at a certain scale, for which the one-loop RG still seems to be valid, to treat the low-energy degrees of freedom $\Lambda < \Lambda_{\text{MF}}$ by another approximation, assumed to be valid in this regime. The scheme used here is an extended mean-field (MF) calculation, allowing for the coexistence of several order-parameters with arbitrary momentum-structure. The energy scale down to which the RG was utilised becomes therefore the upper cut-off or bandwidth of the low-energy model and will be called Λ_{MF} in the following, see fig. (2.1), left. The small bandwidth can be viewed as a smallness parameter which suppresses fluctuations [Feldman et al. 1993]. This is in agreement with the works of [Kuchiev and Sushkov 1996] and [Kos et al. 2004], who find in a direct calculation a suppression of the BCS gap renormalisation by the smallness of the bandwidth.

The low-energy couplings obtained by the RG can be viewed as the residual interactions between the quasi-particles. Thus, the MF approximation investigates instabilities of the RG-derived Landau-Fermi liquid.

The symmetry breaking can in principle also be included in the RG scheme. This complicates the RG equations considerably, so that so far only rather simple models were treated within this method, [Salmhofer et al. 2004] and [Gersch et al. 2005]. However, the scheme used here can be viewed as an approximation to this method, which will help to determine a reasonable low-energy scale Λ_{MF} , see chapter 6.

Chapter 3

The Mean-Field Approximation

3.1 Symmetry Breaking

Some physical systems are known to have ground states that do not have the full symmetry of the Hamiltonian. This symmetry breaking changes the physics of the system, and leads to a big variety of physical effects. In the following, the symmetry breaking will first be discussed in general, in order to proceed then to the concrete problem, which is the simultaneous breaking of different specific symmetries, which are assumed to be important in the Hubbard model.

Consider a Hamiltonian \mathcal{H} and its eigenstates Ψ_i with the energy E_i so that

$$\mathcal{H}\Psi_i = E_i\Psi_i. \quad (3.1)$$

The Hamiltonian is said to obey the symmetry specified by a symmetry-operation \mathcal{S} if and only if

$$\mathcal{S}\mathcal{H} = \mathcal{H}\mathcal{S}. \quad (3.2)$$

From this follows, due to

$$\begin{aligned} \mathcal{S}\mathcal{H}\Psi_i &= \mathcal{H}\mathcal{S}\Psi_i \\ &= E_i\mathcal{S}\Psi_i, \end{aligned} \quad (3.3)$$

that $\mathcal{S}\Psi_i$ is also an eigenvector with the same energy as Ψ_i . If the eigenvectors are non-degenerate, that is, there is only one eigenvector for a given eigenvalue, it follows that

$$\mathcal{S}\Psi_i = \Psi_i, \quad (3.4)$$

and the eigenvector has the same symmetry as the Hamiltonian. If, however, the eigenvector is degenerate iterative action of the symmetry operation on the eigenvector forms a set of eigenvectors, where the sum over all elements is again symmetric according to the symmetry-operation \mathcal{S} . A Hamiltonian can

be composed entirely of eigenvectors which do not have the symmetry of the Hamiltonian.

If a Hamiltonian has degenerate ground states they might break a symmetry. From what was said before it is clear that there is always a linear combination which is again a ground state and which does respect the symmetry. The set which has to be summed over can either be finite, as for the uniaxial ferromagnet, or infinite, as for the superconductor. In the first case the easy-axis spin symmetry, i.e., a discrete symmetry, of the Hamiltonian is broken whereas in the superconducting case the particle conservation is violated and the gauge symmetry is broken. The integration over all states, described by different phases, restores the particle conservation.

In real systems the symmetry is often truly broken. This is either due to a small field, always expected to be present in real systems, or it was broken at some earlier time and persists even when the field is removed again; a broken symmetry in a large system is expected to remain for macroscopically long time scales and even to withstand (not too big) perturbations favouring another ground state.

As an example consider a spin-density-wave ground state of a system with easy axis in z -direction. There the translational invariance in the spin channel is broken. The symmetry-breaking field h (h in z -direction) couples to

$$\sum_{\omega,k} h(\bar{\psi}_{\omega,k,\uparrow}\psi_{\omega,k+Q,\uparrow} - \bar{\psi}_{\omega,k,\downarrow}\psi_{\omega,k+Q,\downarrow}) = \sum_{\omega,k} h(n_{k,\omega\uparrow}^Q - n_{\omega,k\downarrow}^Q). \quad (3.5)$$

The external field h yields a contribution to the dispersion. The quadratic part of the action is therefore, in the Nambu formalism,

$$S_0 = \sum'_{\omega,k,\sigma} (\bar{\psi}_{\omega,k,\sigma}, \bar{\psi}_{\omega,k+Q,\sigma}) \begin{pmatrix} i\omega - \xi_k & h_\sigma \\ h_\sigma & i\omega - \xi_{k+Q} \end{pmatrix} \begin{pmatrix} \psi_{\omega,k,\sigma} \\ \psi_{\omega,k+Q,\sigma} \end{pmatrix}, \quad (3.6)$$

with $h = h_\uparrow = -h_\downarrow$.

As a function of the external field h the expected behaviour of the magnetisation $m = m_\uparrow = -m_\downarrow$, $m_\sigma = \langle \sum_{k\omega} n_{k\sigma}^Q \rangle$ is sketched in figure (3.1). Above a certain temperature T_c the magnetisation vanishes continuously for vanishing external field, while below T_c this limit produces a finite magnetisation.

The zero-field magnetisation is defined as

$$m(h=0) \equiv \lim_{h \rightarrow \pm 0} m = \pm m_0. \quad (3.7)$$

Below T_c its sign depends on the side from which zero is approached. For $T = 0$ the magnetisation is given by the magnetisation of the ground state.

The first order contribution to the self-energy is given by the Hartree diagram¹

$$\text{---} \bigcirc \Sigma \text{---} = \text{---} \bigcirc \text{---} \quad (3.8)$$

¹ A nice introduction to Feynman-diagrams in the symmetry-broken phase is given by the article [Mattuck and Johansson 1968].

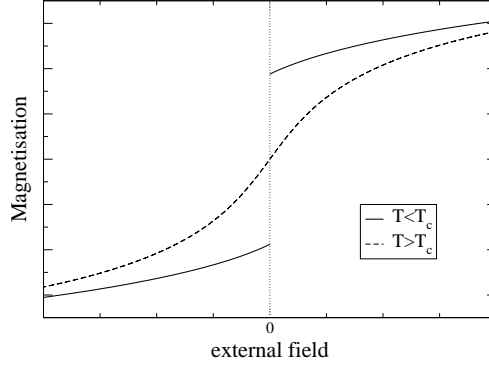


Figure 3.1: Sketch of the magnetisation as a function of the external field above and below the critical temperature. Only the thermodynamically stable state is plotted; the hysteresis is not shown.

where the propagator is the anomalous propagator. The latter is due to the magnetic field and is obtained as the off-diagonal part of the inverse of the matrix of (3.6), easily calculated with Cramer's rule. Explicitly, the anomalous part of the self-energy, being the off-diagonal part of the self-energy matrix

$$\Sigma = \begin{pmatrix} \Sigma_{\sigma}^n & \Sigma_{\sigma}^h \\ \Sigma_{\sigma}^h & \Sigma_{\sigma}^n \end{pmatrix}, \quad (3.9)$$

is obtained by closing the anomalous propagator to a loop, yielding in first order, $\Sigma_{\sigma}^h = h_{\sigma}^1 + \mathcal{O}(U^2)$,

$$h_{\sigma}^1 = U \sum_{k\omega} \frac{h_{\sigma}}{(\xi_k - i\omega)(\xi_{k+Q} - i\omega) - h_{\sigma}^2} = U m(h_{\sigma}). \quad (3.10)$$

U is the interaction of the system, assumed to be non-zero only in the spin-channel and for $Q = (\pi, \pi)$ momentum transfer. The off-diagonal part of the loop in eq. (3.8) is the bare magnetisation $m(h)$. Thus, the magnetisation with first order contribution to the self-energy is given by $m_1(h_{\sigma}) \equiv m(h_{\sigma} + h_{\sigma}^1)$. The bare magnetisation m and the first order corrected magnetisation m_1 is plotted in fig. (3.2). If the external field h vanishes, also m_1 vanishes, so that no spontaneous magnetisation remains. To any finite order this will remain true, even though the approach towards zero will become steeper and steeper. Therefore, finite order perturbation theory cannot describe spontaneous symmetry breaking.

To circumvent this one could go to infinite order in perturbation theory². One way to do this is by employing the RG. But successfully handling this problem with RG has only recently been accomplished [Salmhofer et al. 2004], [Gersch et al. 2005] and was only possible after the flow equations were reorganised by [Katanin 2004]; it is, however, rather involved already on mean-field level. Another way is a self-consistent perturbation theory demanding that the

² For MF-exact models the infinite summation can be performed analytically, see [Gaudin 1960] and [Langer 1964].

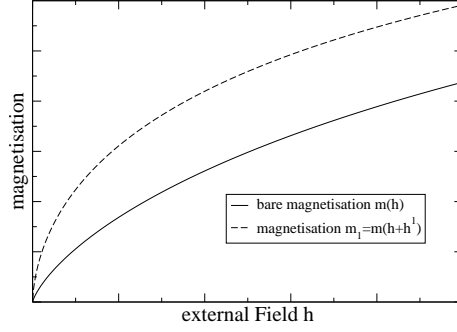


Figure 3.2: Bare magnetisation $m(h)$ and magnetisation with first-order self-energy corrections $m_1 = m(h + h_1)$ as a function of the external field for $T = 0$.

effective field $\bar{h}_\sigma = h_\sigma + Um$. This is an intuitive way to proceed, as an internal field created by a spin acts via the interaction like an external field on the other electrons, at least as long as fluctuations can be neglected. This yields a self-consistency equation

$$\bar{h}_\sigma = Um(h_\sigma + \bar{h}_\sigma) \quad (3.11)$$

for the effective field \bar{h} , and indeed sums a subclass of diagrams up to infinite order, which is seen by expanding the propagator as

$$\begin{aligned} G &= \begin{pmatrix} G_n & F \\ F & G_n \end{pmatrix} = (G_0^{-1} - \Sigma)^{-1} \\ &= G_0 - G_0 \Sigma G_0 + G_0 \Sigma G_0 \Sigma G_0 + \dots \\ &= \text{---} \text{---} \text{---} \text{---} \text{---} + \text{---} \text{---} \text{---} \text{---} \text{---} + \dots \end{aligned} \quad (3.12)$$

and inserting the result into the Hartree diagram, leading to the so-called cactus diagrams

Summing these diagrams reproduces the self-consistency equation.

Thus, a self-consistent perturbation theory can produce results which do not obey the symmetry of the Hamiltonian, in contrast to the naïve, finite order perturbation theory which cannot break the symmetry, as stated in the previous chapter.

In the next section the self-consistency equation will be derived in a slightly different manner, but from the result it will be clear that indeed it is a self-consistent first order approximation for the self energy.

3.2 Derivation of Gap Equations

In the following the gap equations will be derived. Two different methods are presented. In the functional integral formalism via a Hubbard-Stratonovich decoupling a bosonic field is introduced, which then is treated within a saddle point approximation. This ansatz naturally combines with the RG method, as it utilises also the functional integral formalism with Grassmann variables.

The operator formalism, in contrast, makes use of the Hamiltonian scheme and is thus not as natural combination with the RG; but it reveals more clearly the interpretation of the gaps as mean-fields of certain operators, and has thus a straightforward interpretation in physical terms.

3.2.1 Operator Formalism

In this section the derivation of the gap equations in the operator formalism will be sketched. Even though the derivation outlined in the next section is more general, and more natural in the RG context, this ansatz has the merit of brevity. Details can be found in appendix B. Mean-field (MF) calculations with several gaps where also done by [Kyung 2000; Murakami and Fukuyama 1998; Psaltakis and Fenton 1983; Inui et al. 1988],[Yamase and Kohno 2004]; see furthermore [Murakami 2000]; as in those papers certain form-factors of the gaps or symmetries of the dispersion were assumed, the eigenvalues of the matrix describing the part quadratic in the fermionic operators, could be easily calculated analytically. In contrast here general gap structures will be allowed, leading to a general 4th order polynomial for the eigenvalues, practically prohibiting the analytic calculation. Thus, the gap equations have to be derived without the explicit knowledge of the eigenvalues. The present scheme is more transparent and easier to handle than the one used by the cited authors. A further benefit of this derivation is that it is easy to redo the calculations for more or different gaps.

Starting by rewriting the action as a Hamiltonian, one obtains

$$\begin{aligned} \mathcal{H} &= \sum_K \xi_k a_K^\dagger a_K & (3.14) \\ &+ \sum_{K_1, K_2, K'_1, K'_2} \frac{1}{4} \Gamma^\Lambda(K_1, K_2; K'_1, K'_2) a_{K'_1}^\dagger a_{K'_2}^\dagger a_{K_2} a_{K_1}, & (3.15) \end{aligned}$$

K here being the multi-index $K = (k, \sigma)$. The interaction is zero if one of the momenta k is such that

$$|\xi_k| > \Lambda. \quad (3.16)$$

The decoupling of the quartic term is done by the mean-field approximation.

In the superconducting case it is

$$\begin{aligned}
& a_{k'_1\sigma'_1}^\dagger a_{k'_2\sigma'_2}^\dagger a_{k_2\sigma_2} a_{k_1\sigma_1} \approx \\
& \langle a_{k'_1\sigma'_1}^\dagger a_{k'_2\sigma'_2}^\dagger \rangle a_{k_2\sigma_2} a_{k_1\sigma_1} + a_{k'_1\sigma'_1}^\dagger a_{k'_2\sigma'_2}^\dagger \langle a_{k_2\sigma_2} a_{k_1\sigma_1} \rangle - \langle a_{k'_1\sigma'_1}^\dagger a_{k'_2\sigma'_2}^\dagger \rangle \langle a_{k_2\sigma_2} a_{k_1\sigma_1} \rangle
\end{aligned} \tag{3.17}$$

where terms quadratic in the fluctuations have been neglected

$$\left(a_{k'_1\sigma'_1}^\dagger a_{k'_2\sigma'_2}^\dagger - \langle a_{k'_1\sigma'_1}^\dagger a_{k'_2\sigma'_2}^\dagger \rangle \right) \left(a_{k_2\sigma_2} a_{k_1\sigma_1} - \langle a_{k_2\sigma_2} a_{k_1\sigma_1} \rangle \right) \approx 0. \tag{3.18}$$

By further restricting the momenta and spin-configurations, singlet superconductivity with zero and $Q = (\pi, \pi)$ pair-momentum $k_1 + k_2$ is chosen. The latter is referred to in the following as π -pairing.

A similar decoupling leads to the spin/charge-density wave. To determine how to group the operators, i.e., whether to group $a_{K'_1}^\dagger$ with a_{K_1} or with a_{K_2} , so that the spin rotational invariance is not destroyed by the MF decoupling, a comparison with a mean-field theory for the spin operators

$$\vec{S}\vec{S} \approx 2\langle \vec{S} \rangle \vec{S} - \langle \vec{S} \rangle \langle \vec{S} \rangle, \tag{3.19}$$

is helpful; setting the x,y-component zero after this MF decoupling, identifies unambiguously the correct terms for a spin wave in z-direction. A different grouping can lead to a wrong mean-field theory, in which the spin (charge) part of the AF gap does not couple to the spin (charge) part of the potential.

Also, a Fermi surface deformation is allowed, which will be called Pomeranchuk distortion.

By adding the various channels one arrives at the MF-Hamiltonian

$$\mathcal{H}^{\text{MF}} = E^c + \sum_{\mathbf{k}} \mathbf{a}_{\mathbf{k}}^\dagger \mathcal{M}_{\mathbf{k}} \mathbf{a}_{\mathbf{k}}. \tag{3.20}$$

Double counting appears due to the overlap of the AF and Pomeranchuk channel with the other two channels, which is negligible, since the overlap is of zero measure in the thermodynamical limit. The term

$$\begin{aligned}
E^c &= - \sum_{\mathbf{k}} \left[\langle a_{-k\downarrow} a_{k\uparrow} \rangle \Delta_{\mathbf{k}}^* + \langle a_{-k-Q\downarrow} a_{k\uparrow} \rangle \pi_{\mathbf{k}}^* \right] \\
&\quad - \sum_{k\sigma} \langle a_{k\sigma}^\dagger a_{k+Q\sigma} \rangle \mathcal{A}_{k,\sigma} / 2 - \sum_{k\sigma} \langle n_k^\sigma \rangle \delta \mu_{k\sigma} / 2 + \sum_{\mathbf{k}} \bar{\xi}_{k\downarrow}
\end{aligned} \tag{3.21}$$

will be called the c-number term. The last term is due to commuting the operators of the kinetic energy, to include it in the matrix part. The quadratic term is given by the matrix

$$\mathcal{M}_{\mathbf{k}} = \begin{pmatrix} \bar{\xi}_{k,\uparrow} & \Delta_{\mathbf{k}} & \mathcal{A}_{k,\uparrow} & \pi_{\mathbf{k}} \\ \Delta_{\mathbf{k}}^* & -\bar{\xi}_{-k,\downarrow} & \pi_{k+Q}^* & -\mathcal{A}_{-k,\downarrow}^* \\ \mathcal{A}_{k,\uparrow}^* & \pi_{k+Q} & \bar{\xi}_{k+Q,\uparrow} & \Delta_{k+Q} \\ \pi_{\mathbf{k}}^* & -\mathcal{A}_{-k,\downarrow} & \Delta_{k+Q}^* & -\bar{\xi}_{-k+Q,\downarrow} \end{pmatrix} \tag{3.22}$$

and the Nambu operators

$$\mathbf{a}_k^\dagger = (a_{k\uparrow}^\dagger, a_{-k\downarrow}, a_{k+Q\uparrow}^\dagger, a_{-k-Q\downarrow}). \quad (3.23)$$

The energy gaps in the matrix part are for the superconducting gap

$$\Delta_k = \sum_{\mathbf{k}'} V_{k,k'} \langle a_{-k'\downarrow} a_{k'\uparrow} \rangle \quad \text{with} \quad V_{kk'} = \Gamma^\Lambda \begin{pmatrix} \uparrow & \downarrow & \downarrow & \uparrow \\ k & -k & -k' & k' \end{pmatrix} \quad (3.24)$$

for the π -gap

$$\pi_k = \sum_{\mathbf{k}'} W_{k,k'} \langle a_{-k'+Q\downarrow} a_{k'\uparrow} \rangle \quad \text{with} \quad W_{kk'} = \Gamma^\Lambda \begin{pmatrix} \uparrow & \downarrow & \downarrow & \uparrow \\ k & -k-Q & -k'+Q & k' \end{pmatrix} \quad (3.25)$$

and for the spin/charge-wave-gap

$$\mathcal{A}_{k,\sigma} = \frac{1}{2} \sum_{k',\sigma'} U_{kk'}^{\sigma\sigma'} \langle a_{k'\sigma'}^\dagger a_{k'+Q\sigma'} \rangle \quad \text{with} \quad U_{kk'}^{\sigma\sigma'} = \Gamma^\Lambda \begin{pmatrix} \sigma & \sigma' & \sigma' & \sigma \\ k & k' & k'+Q & k+Q \end{pmatrix}. \quad (3.26)$$

The dispersion is

$$\bar{\xi}_{k\sigma} = \xi_k + \delta\mu_{k\sigma} \quad (3.27)$$

with the Pomeranchuk distortion

$$\delta\mu_{k\sigma} = \frac{1}{2} \sum_{k',\sigma'} f_{kk'}^{\sigma\sigma'} \langle n_{k'}^{\sigma'} \rangle \quad \text{with} \quad f_{kk'}^{\sigma\sigma'} = \Gamma^\Lambda \begin{pmatrix} \sigma & \sigma' & \sigma' & \sigma \\ k & k' & k' & k \end{pmatrix}. \quad (3.28)$$

and the bare dispersion $\xi_k = \varepsilon_k - \mu$.

The gaps have to be calculated self-consistently. The self-consistency equations can either be derived by using the definition of the gaps, re-expressing the expectation values in operators for which the matrix \mathcal{M} is diagonal, leading, as these new operators also fulfil the Fermi commutator rules, to Fermi distributions with quasi-particle energies E_k . For this procedure the explicit form of the transformation between the old and new operators has to be known. Instead one can evaluate

$$\delta\Omega = 0. \quad (3.29)$$

The variation of the grand canonical potential has to be done with respect to the different mean-fields, as the grand canonical potential has to be at a minimum with respect to all internal variational parameters. This can be evaluated without explicit knowledge of the transformation or even the eigenvalues. The resulting equations are in both cases the same.

After formally diagonalising the Hamiltonian the grand canonical potential is found to be (see B.47),

$$\Omega = E^c + (-\beta)^{-1} \sum'_{k'\alpha} \ln(1 + \exp(-\beta E_{k'}^\alpha)) \quad (3.30)$$

so that the variation leads to the expressions

$$0 = - \sum_{k'} \frac{\partial E_{k'}^c}{\partial \mathcal{F}_k} + \sum_{k'} \sum_{\alpha} \frac{\partial E_{k'}^{\alpha}}{\partial \mathcal{F}_k} f(E_{k'}^{\alpha}) \quad (3.31)$$

where \mathcal{F} denotes one of the expectation values, introduced in the MF decoupling, and the E_k^{α} represent the eigenvalues of the matrix \mathcal{M} . While the first term reproduces straight away the different gaps, more attention has to be paid to the second term. Using the characteristic polynomial

$$0 = \frac{\partial}{\partial \mathcal{F}_k} |\mathcal{M}_{k'} - \mathbf{1}E_{k'}^{\alpha}| \equiv \frac{\partial}{\partial \mathcal{F}_k} |M_{k'}^{\alpha}|, \quad (3.32)$$

the derivative of the eigenvalues can be expressed by minors of $\mathbf{M}^{\alpha} = \mathcal{M} - \mathbf{1}E^{\alpha}$,

$$\frac{\partial E_{k'}^{\alpha}}{\partial \mathcal{F}_k} = \left(\sum_l |M_{ll}^{\alpha}|(k') \right)^{-1} \sum_{i,j} \frac{\partial m_{ij}(k')}{\partial \mathcal{F}_k} (-1)^{i+j} |M_{ij}^{\alpha}|(k'), \quad (3.33)$$

where m_{ij} are the elements of \mathcal{M} . Details are found in appendix B.

The filling is calculated by the usual thermodynamic relation

$$n = - \frac{\partial \Omega}{\partial \mu}, \quad (3.34)$$

where no ambiguities appear in contrast to the HS formalism where convergence producing factors have to be introduced correctly, so that for zero-gaps the bare filling is reproduced. The reason is that the last term in the c-number term $\sum \bar{\xi}_{k\downarrow}$, (3.21), which is due to operator commutation, does the bookkeeping of the operator order.

3.2.2 Functional Integral Formalism

In this section the derivation of the mean-field equations will be sketched as the saddle-point approximation of a bosonic action, [Mühlischlegel 1962], which is obtained by means of the Hubbard-Stratonovich (HS) transformation [Stratonovich 1958; Hubbard 1959]. Details can be found in appendix C. Here, only the calculation of the SC gap equation is sketched, the calculations for the other gaps are alike.

The effective partition function is written as a Grassmann path integral

$$Z = \int \prod_K d\bar{\psi} d\psi \exp(S^{\Lambda}[\psi, \bar{\psi}]), \quad (3.35)$$

where $\bar{\psi}$ and ψ are the Grassmann fields. The Λ -dependent action is given by $S^{\Lambda} = S_0^{\Lambda} + S_I^{\Lambda}$, with the quadratic part

$$S_0^{\Lambda}[\psi, \bar{\psi}] = \sum_K \bar{\psi}_K C_K^{-1} \chi_k^{-1} \psi_K. \quad (3.36)$$

χ_k is the momentum cut-off function defined in (2.20). The interaction part is

$$S_I^\Lambda = - \sum_{K_1, K_2, K_2', K_1'} \frac{1}{4} \Gamma^\Lambda(K_1, K_2, K_2', K_1') \bar{\psi}_{K_1} \bar{\psi}_{K_2} \psi_{K_2'} \psi_{K_1'}, \quad (3.37)$$

where $K_i = (\omega_i, k_i, \sigma_i)$ are multi-indices containing the frequency, the momentum and the spin argument.

The HS transformation is performed by completing the square in the exponent, which allows to rewrite the fermion-fermion interaction as an interaction with bosonic (i.e., complex) fields depending on two momenta $\varphi \equiv \varphi(k, q)$ which can in the superconducting case be chosen to k being (half) of the relative momentum of the electrons and q the pair momentum. In the SC case the decoupling is

$$\begin{aligned} & \text{const} \times \exp \left(\frac{1}{4} \sum -\Gamma \bar{\psi}_{K_1} \bar{\psi}_{K_2} \psi_{K_2'} \psi_{K_1'} \right) \\ &= \int \mathcal{D}\varphi \exp \left(\frac{1}{4} \sum \left[-\varphi^* \Gamma \varphi + \varphi^* \Gamma \psi_{K_2'} \psi_{K_1'} + \bar{\psi}_{K_1} \bar{\psi}_{K_2} \Gamma \varphi \right] \right), \end{aligned} \quad (3.38)$$

with the potential $\Gamma = \Gamma(k, -k + q; -k' + q, k')$. The bosons can be viewed as exchange particles mediating the interaction via a Yukawa coupling term. This transformation is exact as long as all momenta are taken into account. But to reduce the computational effort usually one restricts the bosons to one or a few channels, which are assumed to be most important; for example restricting the bosons to $q = 0$ leads to the usual Cooper pairs. Due to this restriction this decoupling becomes an approximation. In the full calculation the channels of interest are the spin/charge-density wave $\mathcal{A}_{k, \sigma}$, a spin/charge Fermi-surface-distortion $\delta\mu_{k, \sigma}$ and the superconductor with zero momentum Δ_k and a pair π_k which has the pair-momentum $Q = (\pi, \pi)$; they overlap partly, resulting in double counting, but since the overlapping k -space is lower-dimensional, it is expected to be of zero measure in the thermodynamical limit. Introducing the bosons one writes the partition function

$$Z = \int \mathcal{D}\varphi \mathcal{D}\psi \mathcal{D}\bar{\psi} \exp (S[\psi, \bar{\psi}, \varphi]) \quad (3.39)$$

with a new action

$$\begin{aligned} S[\psi, \bar{\psi}, \varphi] &= S_0[\psi, \bar{\psi}] + S_I[\psi, \bar{\psi}, \varphi] \\ &= S_0[\varphi] - \sum'_{k\omega} \psi \mathcal{M} \bar{\psi}, \end{aligned} \quad (3.40)$$

which contains fermionic and bosonic degrees of freedom. The prime on the sum denotes the restriction to the magnetic BZ.

Since there is no direct interaction between the fermions any more, the fermionic integral can be performed, leading to a purely bosonic model

$$Z = \int \mathcal{D}\varphi \exp (S[\varphi]) \quad (3.41)$$

with a new, purely bosonic effective action

$$S^{\text{eff}}[\varphi] = S^c + \beta \sum'_{k,\omega} \ln \det \mathcal{M}. \quad (3.42)$$

The first term is the c-number term, being quadratic in the bosonic fields

$$\begin{aligned} S^c[\varphi] &= \sum_{\omega,k} \varphi_{\omega,k}^s \Delta^*(\omega, k) + \sum_{\omega,k} \varphi_{\omega,k}^\pi \pi_{\omega,k}^* \\ &+ \sum (\varphi_{\omega,k,\sigma}^A)^* \frac{1}{2} \mathcal{A}_{\omega,k,\sigma} + \sum_{\omega,k,\sigma} \varphi_{\omega',k',\sigma'}^\delta \frac{1}{2} \delta \mu_{\omega,k,\sigma}. \end{aligned} \quad (3.43)$$

The matrix \mathcal{M} is defined as³

$$\mathcal{M}_{k,\omega} = \begin{pmatrix} \bar{\xi}_{k,\uparrow} - i\omega & \Delta_{k,\omega} & \mathcal{A}_{k,\omega,\uparrow} & \pi_{k,\omega} \\ \Delta_{k,\omega}^* & -\bar{\xi}_{-k,\downarrow} - i\omega & \pi_{k+Q,\omega}^* & -\mathcal{A}_{-k,-\omega,\downarrow}^* \\ \mathcal{A}_{k,\omega,\uparrow}^* & \pi_{k+Q,\omega} & \bar{\xi}_{k+Q,\uparrow} - i\omega & \Delta_{k+Q,\omega} \\ \pi_{k,\omega}^* & -\mathcal{A}_{-k,-\omega,\downarrow} & \Delta_{k+Q,\omega}^* & -\bar{\xi}_{-k+Q,\downarrow} - i\omega \end{pmatrix}, \quad (3.44)$$

where, for example the SC-gap, is given by

$$\Delta_{k\omega} = T \sum_{k'\omega'} V \begin{pmatrix} \omega' & \omega \\ k' & k \end{pmatrix} \varphi(k'\omega') \quad (3.45)$$

The potential is obtained by restricting the full interaction

$$V \begin{pmatrix} \omega' & \omega \\ k' & k \end{pmatrix} = \Gamma \begin{pmatrix} \omega' & -\omega' & -\omega & \omega \\ k' & -k' & -k & k \\ \uparrow & \downarrow & \downarrow & \uparrow \end{pmatrix}. \quad (3.46)$$

The other order-parameters are defined similarly, in the appendix (C.28) (C.37) and (C.49)

Treating the integral (3.41) within a saddle-point approximation leads to equations determining the saddle point. These coupled self-consistency equations are the desired mean-field equations. In the SC case one obtains

$$\Delta_{k\omega}^* = \sum_{k'\omega'} \frac{\det(\mathcal{M}_{12}(k', \omega')) V \begin{pmatrix} \omega' & \omega \\ k' & k \end{pmatrix}}{\det \mathcal{M}(k', \omega')}. \quad (3.47)$$

The determinant \mathcal{M}_{12} is the minor of the matrix \mathcal{M} , i.e., the determinant of the matrix which is obtained by crossing out the first line and the second column of \mathcal{M} . According to Cramer's rule (D.9) the fraction of the two determinants can be interpreted as an element of the inverse matrix of \mathcal{M} . This is nothing but the anomalous SC propagator, so that in (3.47) the anomalous self-energy is given by the effective interaction which is closed by an anomalous propagator, or diagrammatically

$$\text{Diagrammatic equation (3.48)} \quad (3.48)$$

³ Here the cut-off functions are not written explicitly, cf. eq. (C.54).

This is indeed equivalent to the one loop self-consistency equation mentioned earlier.

If the potential V is frequency independent, which is the case in the numerics since the used RG scheme neglects ω -dependence, the gap will also not depend on the frequency. Then the Matsubara sum can be performed analytically, leading to

$$\Delta_k^* = - \sum_{k'} \sum_{\alpha} \frac{\det(\mathbf{M}_{12}^{\alpha}(k')) V_{k'k}}{\sum_l \det \mathbf{M}_{ll}^{\alpha}(k')} f(E_{k'}^{\alpha}). \quad (3.49)$$

where E_k^{α} are the eigenvalues of the matrix $\mathcal{M}(i\omega = 0)$, i.e., the zeros of $\det(\mathbf{M}^{\alpha}) = \det(\mathcal{M}(i\omega = E_k^{\alpha}))$. These new energies E_k^{α} stem from the fact that for $i\omega = E_k^{\alpha}$ the propagator has poles, which can be interpreted as quasi-particles energies. As the self energy has no imaginary part these quasi particles have infinite life-time, also far from the Fermi surface, as expected for a mean-field theory. Similar equations can be derived for the π -pair, the AF gap and for the Pomeranchuk distortion.

When calculating the filling, convergence creating factors carefully have to be employed. Neglecting them can lead to wrong results, even though the expressions might seem well behaved. The reason is that in the Green's functions the time-difference was set to zero throughout the calculation, instead of taking the limit at the end of the calculation. By checking that for zero gaps the correct filling is reproduced one can unambiguously find the correct factors. Similar problems are found for the Pomeranchuk distortion, since this is closely related to the filling, where the same convergence factors have to be employed.

3.3 The Gap Equations

In the following the gap equations are given. The equations contain the matrix \mathbf{M} defined as $\mathbf{M} = \mathcal{M} - E_k$ in the operator formalism, or, yielding the same, $\mathbf{M} = \mathcal{M}(i\omega = E_k)$ in HS formalism.

The equation for the singlet superconducting gap is

$$\Delta_k^* = - \sum_{k'} \sum_{\alpha} \frac{V_{kk'} |\mathbf{M}_{12}^{\alpha}(k')|}{\sum_l |\mathbf{M}_{ll}^{\alpha}(k')|} f(E_{k'}^{\alpha}). \quad (3.50)$$

Following appendix (D.3) the denominator can be interpreted as the trace of the inverse matrix of $\mathbf{M}^{\alpha}(k)$, and can be therefore re-expressed in terms of the eigenvalues E_k^{α} , yielding

$$\Delta_k^* = - \sum_{k'} \sum_{\alpha} \frac{V_{kk'} |\mathbf{M}_{12}^{\alpha}(k')|}{\prod_{i \neq \alpha} (E_{k'}^i - E_{k'}^{\alpha})} f(E_{k'}^{\alpha}). \quad (3.51)$$

With some further matrix algebra, see appendix (D.3), the gap-equation can

be re-expressed as⁴

$$\Delta_k^* = - \sum_k \sum_\alpha [V_{k'k} v_\alpha^2 (v_\alpha^1)^*] f(E_{k'}^\alpha), \quad (3.52)$$

where v_α^i is the i^{th} component of the normalised eigenvector corresponding to the eigenvalue E_k^α . This expression has (numerical) advantages, when two eigenvalues approach each other.

In singlet/triplet decomposition, eq. (2.43), the potential $V_{kk'}^\Lambda$ reads

$$V_{kk'} = \Gamma^\Lambda \begin{pmatrix} \uparrow & \downarrow & \downarrow & \uparrow \\ k & -k & -k' & k' \end{pmatrix} \quad (3.53)$$

$$= \frac{1}{2} (V_{kk'}^s + V_{kk'}^t), \quad (3.54)$$

with the symmetry $V_{k,k'}^{s/t} = \pm V_{k,-k'}^{s/t}$. If $\Delta_k = \Delta_{-k}$ is assumed, the triplet part is projected out. This is in accordance with earlier works which found a much stronger attraction in the singlet than in the triplet channel.

The equation for the π -pair is given by

$$\pi_k^* = - \sum_{k'} \sum_\alpha \frac{W_{kk'}^\Lambda |\mathbf{M}_{14}^\alpha|(k')}{\prod_{i \neq \alpha} (E_{k'}^i - E_{k'}^\alpha)} f(E_{k'}^\alpha). \quad (3.55)$$

Again, as in the SC case, the potential can be written as

$$W_{kk'} = \Gamma^\Lambda \begin{pmatrix} \uparrow & \downarrow & \downarrow & \uparrow \\ k & -k-Q & -k'+Q & k' \end{pmatrix} \quad (3.56)$$

$$= \frac{1}{2} (W_{kk'}^s + W_{kk'}^t). \quad (3.57)$$

If $\pi_k = \pm \pi_{-k+Q}$ then according to $W_{-k+Q,k'} = 1/2 (W_{kk'}^s - W_{kk'}^t)$ either the triplet or singlet part of the potential is projected out. In case of a $(\cos(k_x) - \cos(k_y))$ form-factor we have $\pi_{-k+Q} = -\pi_k$, so that only the triplet part contributes. In section (5.3.2) it is argued that indeed the π -pair is a spin-triplet pair, with zero spin projection in the z -direction, also for different form factors.

The gap equation for the AF gap is

$$\mathcal{A}_{k\sigma} = \sum_{k'} \sum_\alpha \frac{1}{2} \frac{U^\Lambda \begin{pmatrix} \sigma & \uparrow \\ k & k' \end{pmatrix} |\mathbf{M}_{13}^\alpha| - U^\Lambda \begin{pmatrix} \sigma & \downarrow \\ k & -k' \end{pmatrix} |\mathbf{M}_{42}^\alpha|}{\prod_{i \neq \alpha} (E_{k'}^i - E_{k'}^\alpha)} f(E_{k'}^\alpha). \quad (3.58)$$

The potential can be decomposed in the singlet/triplet representation, eq. (2.43),

$$U \begin{pmatrix} k & k' \\ \sigma & \sigma' \end{pmatrix} = \Gamma^\Lambda \begin{pmatrix} \sigma & \sigma' & \sigma' & \sigma \\ k & k' & k'+Q & k+Q \end{pmatrix} \quad (3.59)$$

$$= U_{k,k'}^s \frac{1}{2} (1 - \delta_{\sigma,\sigma'}) + U_{k,k'}^t \frac{1}{2} (1 + \delta_{\sigma,\sigma'}) \quad (3.60)$$

⁴ This expression is very close to the text-book calculation of the BCS theory, where it is found that $u_k v_k = \Delta/(2E_k)$ where u_k and v_k are transformation-components between new and old operators, see for example [Fetter and Walecka 1971].

and in the spin/charge representation, eq. (2.44),

$$U \begin{pmatrix} k & k' \\ \sigma & \sigma' \end{pmatrix} = U_{k,k'}^C + U_{k,k'}^S (2\delta_{\sigma,\sigma'} - 1). \quad (3.61)$$

If the latter form is inserted into the gap definition (3.26) one obtains

$$\begin{aligned} \mathcal{A}_{k,\sigma} &= \frac{1}{2} \sum_{k'} U_{k,k'}^C \left(\langle a_{k'\uparrow}^\dagger a_{k'+Q\uparrow} \rangle + \langle a_{k'\downarrow}^\dagger a_{k'+Q\downarrow} \rangle \right) \\ &\quad + \frac{1}{2} \sum_{k'} U_{k,k'}^S \sigma \left(\langle a_{k'\uparrow}^\dagger a_{k'+Q\uparrow} \rangle - \langle a_{k'\downarrow}^\dagger a_{k'+Q\downarrow} \rangle \right), \end{aligned} \quad (3.62)$$

σ being ± 1 , depending on the spin-index of the gap. As expected, U^C couples to the charge part, while U^S couples to the spin part. This makes the decomposition

$$\mathcal{A}_k^\sigma = \mathcal{C}_k + \sigma \mathcal{S}_k \quad (3.63)$$

reasonable, where \mathcal{C}_k is the charge density wave, and \mathcal{S}_k the spin density wave. For a special case relevant in the numerics the gap equation (3.58) can be simplified further. If the Pomeranchuk distortion is so that $\bar{\xi}_{k\uparrow} = \bar{\xi}_{-k\downarrow}$ and all gaps are real, if further the AF gap is of s -wave type and the π -pair and the superconducting pair have d -wave structure, the matrices \mathbf{M}_{13}^α and \mathbf{M}_{42}^α have the same value, which can be seen by direct calculation. Then the numerator of (3.58) reads, after changing the summation of the second addend $k' \rightarrow -k'$,

$$\begin{aligned} &U^\Lambda \begin{pmatrix} \sigma & \uparrow \\ k & k' \end{pmatrix} |\mathbf{M}_{13}^\alpha| - U^\Lambda \begin{pmatrix} \sigma & \downarrow \\ k & k' \end{pmatrix} |\mathbf{M}_{42}^\alpha| \\ &= |\mathbf{M}_{13}^\alpha| \left(U^\Lambda \begin{pmatrix} \sigma & \uparrow \\ k & k' \end{pmatrix} - U^\Lambda \begin{pmatrix} \sigma & \downarrow \\ k & k' \end{pmatrix} \right) \\ &= |\mathbf{M}_{13}^\alpha| U_{kk'}^S 2\sigma, \end{aligned} \quad (3.64)$$

where σ is ± 1 for up/down spin. In the third line (3.61) was used.

The gap equation for the Pomeranchuk distortion is

$$\delta\mu_{k\sigma} = \frac{1}{2} \sum_{k'} \sum_{\alpha} \frac{f_{k',k}^{\uparrow,\sigma} |M_{11}^\alpha| - f_{-k',k}^{\downarrow,\sigma} |M_{22}^\alpha|}{\prod_{l \neq \alpha} (E_{k'}^l - E_{k'}^\alpha)} f(E_{k'}^\alpha) + \sum_{k'} \frac{1}{2} f_{-k',k}^{\downarrow,\sigma}. \quad (3.65)$$

As for the AF potential the spin-charge representation

$$f_{kk'}^{\sigma\sigma'} = f_{kk'}^C + f_{kk'}^S (2\delta_{\sigma,\sigma'} - 1) \quad (3.66)$$

leads to a natural decomposition of $\delta\mu$ into

$$\delta\mu_k^\sigma = \delta\mu_k^P + \sigma \delta\mu_k^m \quad (3.67)$$

where $\delta\mu_k^P$ is for example a spin-independent Fermi surface deformation in the case of a d -wave, and $\delta\mu_k^m$ is for example a ferromagnetic gap in the case of an s -wave.

The filling is

$$n = - \sum_{k', \alpha}' \sum_m \frac{\det(\mathbf{M}_{mm}^\alpha)}{\prod_{i \neq \alpha} (E_{k'}^i - E_{k'}^\alpha)} f((-1)^{m+1} E_{k'}^\alpha), \quad (3.68)$$

where the sum still runs over the magnetic BZ, indicated by the prime. The filling is for k and $k + Q$ outside the Λ -reduced BZ, the same as for the non-interacting gas, as there all gaps are zero. The fraction in (3.68) is not unity only if the π or SC gap is non-zero, due to the mixing of particles and holes.

If there are several locally stable solutions of the gap equations, one has to compare the grand canonical potentials to distinguish globally stable solutions from meta-stable solutions. In this work $T = 0$ is always assumed; finite T is not considered since there fluctuation correction should be taken into account.

The grand canonical potential Ω is given by (3.30). In the limit $T \rightarrow 0$ the second part becomes

$$\sum_{k, \alpha; E_k^\alpha < 0} E_k^\alpha, \quad (3.69)$$

which is just the sum over the negative eigenvalues.

To rewrite the c-number term in terms of the gaps, one has to invert the gap definitions (3.24), (3.25), (3.26) and (3.28) to eliminate the expectation values (or bosonic fields), which requires some care if the interaction-matrices⁵ do not have full rank. Details can be found in the appendix (B.6). The c-number term is obtained in the form⁶

$$E^c = \sum_i \frac{\Delta_i^2}{v_i} + \sum_i \frac{\pi_i^2}{w_i} + \sum_i \frac{C_i^2}{2u_i^C} + \sum_i \frac{S_i^2}{2u_i^S} + \sum_i \frac{(\delta\mu_i^P)^2}{2f_i^C} + \sum_i \frac{(\delta\mu_i^m)^2}{2f_i^S} \quad (3.70)$$

Here v_i, w_i etc., are the non-zero eigenvalues of the interactions, and Δ_i, π_i etc., are the coefficients of the gaps decomposed in eigenvectors of the associated potentials. Combining this rewritten c-number term with (3.69) leads to the desired zero-temperature grand canonical potential as a function of the order parameters.

⁵ The interaction have finite dimension due to the discretisation in the numerical evaluation.

⁶ Where the various factors in front of the potential in the relation between the gaps and the expectation values have been absorbed into the eigenvalues of the potential.

Chapter 4

AF Mean-Field Solutions

In this chapter we discuss the mean-field equation for the case of a purely antiferromagnetic (AF) order parameter. It turns out that the structure is much richer than the structure of the mean-field theory of a superconductor, due to the possibility of Fermi surfaces even in presence of a finite AF-gap. The results presented here are important for interpreting the results of the full RG+MF calculation, given in chapter 6.

First the right hand side (RHS) of the gap equation will be discussed for $t' = 0$ and $t' \neq 0$. Then in section (4.2) the solutions of the self-consistency requirement, the corresponding filling and the corresponding grand canonical potential will be analysed. Finally the connection to the renormalisation-group equations will be made.

Some parts of the facts discussed here are known, but are scattered over the literature: [Hirsch 1985; Lin and Hirsch 1987], [Sachdev et al. 1995; Chubukov and Frenkel 1992], [Singh and Tešanović 1990], [Fazekas 2003], [Hofstetter and Vollhardt 1998] and [Langmann and Wallin 1997, 2004]. Often the authors contend themselves with studying the susceptibility, which turns out not to be sufficient in all cases. Even where such a study determines correctly the AF order it does not capture the doping dependence, since the filling strongly depends on the size of the gap.

4.1 The Right Hand Side

The gap equation for a spin/charge-density wave with modulation $Q = (\pi, \pi)$ reads

$$\mathcal{A}_{k\sigma} = - \sum'_{k'\omega'\sigma'} \frac{\mathcal{A}_{k'\sigma'} U \left(\begin{smallmatrix} k & k' \\ \sigma & \sigma' \end{smallmatrix} \right)}{|\mathbf{Q}_{k'\sigma'}(i\omega')|} \quad (4.1)$$

where the prime is marking the sum over the magnetic Brillouin zone. The inverse propagator in Nambu notation is

$$\mathbf{Q}_{k'\sigma'}(z) = \begin{pmatrix} \xi_{k'} - z & \mathcal{A}_{k'\sigma'} \\ \mathcal{A}_{k'\sigma'}^* & \xi_{k'+Q} - z \end{pmatrix}. \quad (4.2)$$

After performing the Matsubara sum, the gap equation reads

$$\mathcal{A}_{k\sigma} = \sum_{k', \alpha = \pm, \sigma'}' \frac{\mathcal{A}_{k'\sigma'} U \left(\begin{smallmatrix} k & k' \\ \sigma & \sigma' \end{smallmatrix} \right)}{E_{k'\sigma'}^\alpha - E_{k'\sigma'}^{-\alpha}} f(E_{k', \sigma'}^\alpha), \quad (4.3)$$

The eigenvalues are given by

$$E_{k\sigma}^\pm = \frac{\xi_k + \xi_{k+Q}}{2} \pm \sqrt{\frac{(\xi_k - \xi_{k+Q})^2}{4} + |\mathcal{A}_{k\sigma}|^2} \quad (4.4)$$

$$= \varepsilon_k^{t'} \pm \sqrt{(\varepsilon_k^t)^2 + (\mathcal{A}_{k\sigma})^2} - \mu \quad (4.5)$$

where we have used $\xi_k = \varepsilon_k^t + \varepsilon_k^{t'} - \mu$ with the anti-symmetric and symmetric part under (π, π) -translation:

$$\begin{aligned} \varepsilon_k^t &= -2t(\cos k_x + \cos k_y) \\ \varepsilon_k^{t'} &= -4t' \cos k_x \cos k_y. \end{aligned} \quad (4.6)$$

As ε_k^t vanishes on the umklapp-surface the gap will have the largest impact close to the umklapp-surface. There, the eigenvalues are

$$E_k^\pm \Big|_{k_{\text{umklapp}}} = \varepsilon_k^{t'} \pm |\mathcal{A}_k| - \mu \Big|_{k_{\text{umklapp}}} \quad (4.7)$$

$$= 4t' \cos^2 k_x \pm |\mathcal{A}_k| - \mu, \quad (4.8)$$

see fig. (4.6). The two branches can, as a function of k_x , have zeros even for a non-zero gap. This is in contrast to the superconducting (SC) case, where $E_k^\pm = \pm E_k$, with $E_k > 0$ if the SC gap is non-zero. An electron-pocket exists, if $E_k^+ = 0$ for some k -values; a hole-pocket exists, if $E_k^- = 0$. For $t' < 0$ the electron-pocket will be found to be around $(\pm\pi, 0)$ and $(0, \pm\pi)$, the hole-pocket will be around $(\pm\pi/2, \pm\pi/2)$.

If t' and μ are zero, i.e., in the case of perfect nesting, $E_k^\pm = \pm E_k$ and the gap equation is the same as in the SC case for an attractive U . If μ or t' are non-zero the gap-equation will structurally change, leading to a much richer behaviour compared with the SC case. Observe that μ and t' enter only via the Fermi functions, since

$$E_{k'}^\pm - E_{k'}^\mp = \pm 2\sqrt{(\varepsilon_k^t)^2 + |\mathcal{A}_{k\sigma}|^2}. \quad (4.9)$$

In the following a momentum independent AF gap $\mathcal{A}_{k\sigma} = \mathcal{A}s_\sigma$, with the spin structure $s_\uparrow = -s_\downarrow = 1$ and $T = 0$ will be assumed. The slope of the RHS of (4.1) with respect to \mathcal{A} is given by

$$\sum_{k', \omega', \sigma'}' \frac{U \left(\begin{smallmatrix} k & k' \\ \sigma & \sigma' \end{smallmatrix} \right) s_{\sigma'}}{|\mathbf{Q}_{k'\sigma'}(i\omega')|} + 2 \sum_{k', \omega', \sigma'}' \frac{(\mathcal{A})^2 s_{\sigma'} U \left(\begin{smallmatrix} k & k' \\ \sigma & \sigma' \end{smallmatrix} \right)}{|\mathbf{Q}(i\omega')_{k'\sigma'}|^2}. \quad (4.10)$$

The first term can, in the limit $\mathcal{A} \rightarrow 0$ be interpreted as the AF-bubble in the symmetric state, the second term as the anomalous contribution to the

AF-bubble in the symmetry-broken state. The spin-density-wave form-factor projects on the spin part U^S of the potential, which will be simply denoted by $U = U^S$, in the following.

After performing the ω -sum, one obtains

$$\sum'_{k',\pm} \frac{2U}{E_{k'}^{\pm} - E_{k'}^{\mp}} f(E_{k'}^{\pm}) - \sum'_{k',\pm} \frac{8U\mathcal{A}^2}{(E_{k'}^{\pm} - E_{k'}^{\mp})^3} f(E_{k'}^{\pm}) - \sum'_{k',\pm} \frac{4U\mathcal{A}^2}{(E_{k'}^{\pm} - E_{k'}^{\mp})^2} f'(E_{k'}^{\pm}). \quad (4.11)$$

The f' term is due to the second order pole of (4.10). The term with f' can be, at $T = 0$, expressed as a line integral due to $f'(x) = -\delta(x)$ as

$$\frac{1}{4\pi^2} \int dk_x |\nabla E_k^{\pm}|^{-1} \frac{U\mathcal{A}^2}{(\varepsilon_k^t)^2 + |\mathcal{A}|^2} \sqrt{1 + \left(\frac{dk_y}{dk_x}\right)^2}, \quad (4.12)$$

where k_y is on the Fermi surface. While the first two terms in (4.11) are always finite for a finite gap, these terms can become divergent due to the derivative $|\nabla E_k^{\pm}|^{-1}$.

In absence of an external field the RHS is antisymmetric with respect to the origin, therefore only the positive side will be drawn.

4.1.1 Zero Next-Nearest Neighbour Hopping

If $t' = 0$ is assumed, the eigenvalues are given by

$$E_k^{\pm} = \pm \sqrt{(\varepsilon_k^t)^2 + \mathcal{A}^2} - \mu. \quad (4.13)$$

If $|\mathcal{A}| > |\mu|$ the upper branch will be always positive, the lower always negative. Thus, the RHS does not depend on μ , which enters only via the Fermi functions. At $|\mathcal{A}| = |\mu|$ one of the branches, say E_k^- , changes the sign and the whole umklapp-surface is cut out of the integral (4.3). Thus the RHS has there a kink, see figure (4.1).

The kink is associated with the appearance of an effective Fermi-surface, found from $E_k^{\pm} = 0$ to be

$$\cos k_y = \pm \delta / (2t) - \cos k_x, \quad (4.14)$$

where $\delta = \sqrt{\mu^2 - \mathcal{A}^2} = |\varepsilon_k^t|$.

The slope of the RHS is divergent at the kink, as will be shown in the following. The term

$$\nabla E_k^- = \frac{2t\delta}{\mu} \begin{pmatrix} \sin(k_x) \\ \sin(k_y) \end{pmatrix} \quad (4.15)$$

vanishes with $\delta \rightarrow 0$. With the help of (4.14) we get from

$$\begin{aligned} \sin^2(k_x) + \sin^2(k_y) &= \sin^2(k_x) + 1 - \cos^2(k_y) \\ &= 2\sin^2(k_x) + \frac{\delta}{t} \cos^2(k_x) + \mathcal{O}(\delta^2) \end{aligned} \quad (4.16)$$

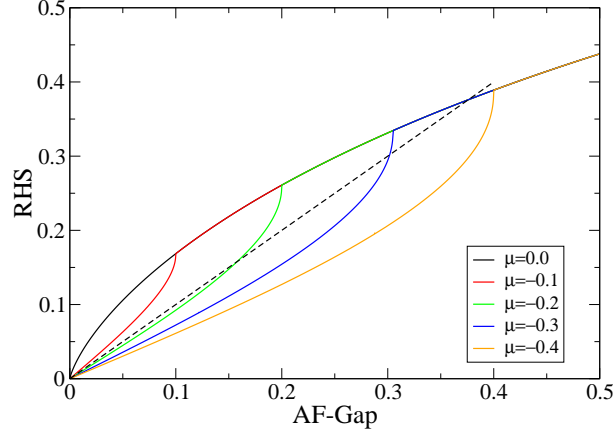


Figure 4.1: The RHS of the AF gap equation with $t' = 0$ for different μ . Due to the appearance of an effective Fermi surface the RHS has a kink at $|\mathcal{A}| = |\mu|$. Dashed line is the bisector. Coupling $U = 2.0$.

we get another zero for $\delta \rightarrow 0$ and $k_x \rightarrow 0$. The contribution to the slope (4.12) becomes

$$\int_0^{\bar{k}_x} \frac{\mu}{2t\delta} \frac{1}{\sqrt{2\sin^2(k_x) + \frac{\delta}{t}\cos^2(k_x)}} \frac{1}{4} \frac{4U\mathcal{A}^2}{\mu^2} \sqrt{1 + \left(\frac{dk_x}{dk_y}\right)^2}. \quad (4.17)$$

\bar{k}_x is the crossing point of the Fermi surface with the border of the octant. We restrict the discussion to the second octant, i.e., $k_y > k_x > 0$, and to the magnetic BZ. Due to this $0 \leq \frac{dk_x}{dk_y} \leq 1$ so that the second square root term can be neglected. The integrand becomes infinite close to $k_x \approx 0$, where $\cos k_x \approx 1$ and $\sin k_x \approx k_x$ can be employed. The integral is for $\delta \rightarrow 0$ thus dominated by

$$\frac{1}{\delta} \frac{U\mathcal{A}^2}{2t\mu} \int_0^1 dk_x \frac{1}{\sqrt{2k_x^2 + \delta/t}} \tilde{c} \quad (4.18)$$

$$\sim \frac{1}{\delta} \frac{U\mathcal{A}^2}{2t\mu} \frac{\tilde{c}}{\sqrt{2}} \left[\ln \left(k_x + \sqrt{k_x^2 + \frac{2\delta}{t}} \right) \right]_0^1 \quad (4.19)$$

$$\sim \frac{1}{\delta} \ln \delta \sim \frac{1}{\sqrt{\delta\mathcal{A}}} \ln \sqrt{\delta\mathcal{A}}, \quad (4.20)$$

divergent for $\delta \rightarrow 0$ or $\delta\mathcal{A} = (\mu - \mathcal{A}) \rightarrow 0$. The slope of one RHS is plotted in figure (4.3).

This peculiar behaviour of the RHS for $t' = 0$ leads to either fully gapped, half-filled systems, or to systems with zero gap,¹ as will be discussed in section (4.2).

[Hirsch 1985] did similar MF calculations for $t' = 0$ which he compared with Monte Carlo (MC) data. Since he utilised the susceptibility and presumably the bare filling he predicted a finite doping range with non-zero AF-gap in

¹ Forcing the system to a certain filling can thus lead to phase separation.

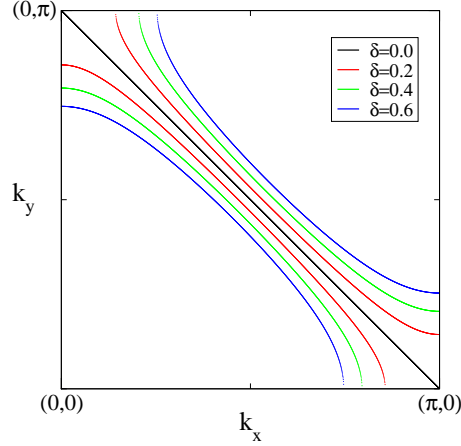


Figure 4.2: The effective Fermi-surface for $t' = 0$. The effective Fermi surfaces have the same shape as bare FSs with an effective chemical potential $\delta = \sqrt{\mu^2 - \mathcal{A}^2}$.

contradiction with his MC data. However, our MF results agree qualitatively with these MC data.

4.1.2 Finite next-nearest Neighbour Hopping

For $t' \neq 0$ the Fermi surface can cross the umklapp surface. Due to this the effective Fermi surfaces, i.e., the borders of the electron- or hole-pocket (defined by $E_k^\pm = 0$) have a more complex behaviour, and can not be described by a single parameter δ like in the case² $t' = 0$. As the structure of the effective Fermi surface determines widely the behaviour of the RHS of the gap equation, it will be discussed in the following. $t' < 0$ will always be assumed, $t' > 0$ leads to similar results.

If the gap is zero the eigenvalues reduce to:

$$E_k^\pm = \varepsilon_k^{t'} \pm |\varepsilon_k^t| - \mu. \quad (4.21)$$

As $\varepsilon_k^t < 0$ (> 0) inside (outside) the magnetic BZ, E_k^- is the free dispersion inside, E_k^+ the free (π, π) -shifted dispersion outside the magnetic BZ.

Thus, the electron/hole-pocket picture is a mere reinterpretation, see figure (4.4). If the Fermi surface crosses the umklapp surface, there is an electron- and a hole-pocket. Those pockets touch on the umklapp-surface where the bare Fermi surface crosses it. If the FS does not cross the umklapp-surface there will be either of the pockets.

If now a finite gap is introduced, the pockets separate and shrink. This can be understood by considering the dispersion on the umklapp surface, which is given by eq. (4.8) and shown in figure (4.6). The two branches are shifted by $2\mathcal{A}$ against each other, thus for a non-zero gap the pockets separate. By increasing \mathcal{A} the size of the pockets is reduced.

² The explicit expression is given by eq. (4.24).

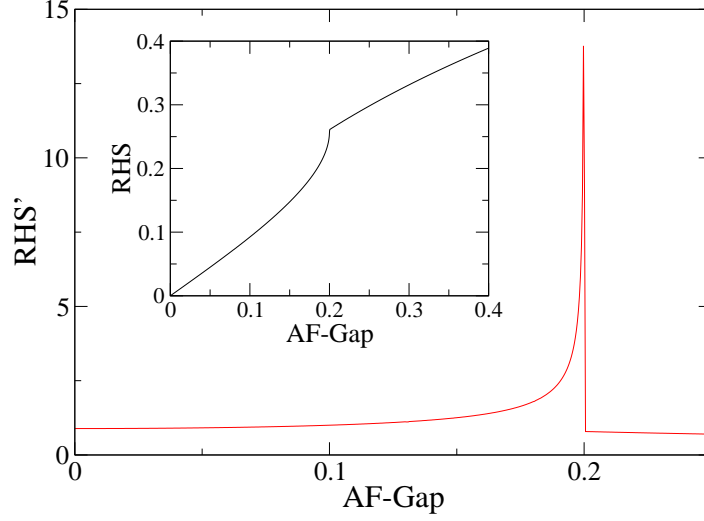


Figure 4.3: The slope of the RHS for $t' = 0$, $\mu = 0.2$. At $\mathcal{A} = |\mu|$ a divergence $\propto (1/\sqrt{|\mu| - \mathcal{A}}) \log(|\mu| - \mathcal{A})$ is found.

The value of μ and the height of the branches, given by $4t'$, determines for which gap-size the pockets vanish. For a gap of $\mathcal{A} \geq \mu - 4t'$ the electron-pocket vanishes, for $\mathcal{A} \geq -\mu$ the hole-pocket vanishes. In the following $\mu - 4t' \equiv \delta_{vH}$ describing the energy distance of the bare Fermi surface from the van Hove point will play an important rôle. To have half-filling with a finite gap both pockets have to be closed³. This is obtained, if the gap is at least $|\mathcal{A}| \geq -2t'$, for a system with $\mu = \mu_{1/2} \equiv 2t'$, see figure (4.6), right.

In the following we assume that the system is on the hole-doped side, i.e., the electron-pocket vanishes first. The electron-doped case will be discussed briefly at the end of this section.

4.1.2.1 $\delta_{vH} = 0$

The van Hove points cause a logarithmic divergence in the density of states. This leads to a well known divergence of the first term in (4.11), being identical with the RPA bubble of the symmetric system, for a vanishing gap. The divergence at $\mathcal{A} = 0$ leads, like it is generic in the SC case, to a solution for any U , see fig. (4.7).

The kink due to the opening of the hole Fermi surface in the RHS is at $|\mathcal{A}| = |\mu| = -4t'$. For larger $|t'|$ the kink will be at larger $|\mathcal{A}|$, leading to a smaller RHS close to the origin. A larger t' thus reduces the size of the gap for systems with $\mu_{vH} = 4t'$, see figure (4.8).

³ Half-filling with both, hole- and electron-pocket, which could in principle also lead to half-filling *with* Fermi surfaces, is not expected to be stable, as will be discussed later, see page 49.

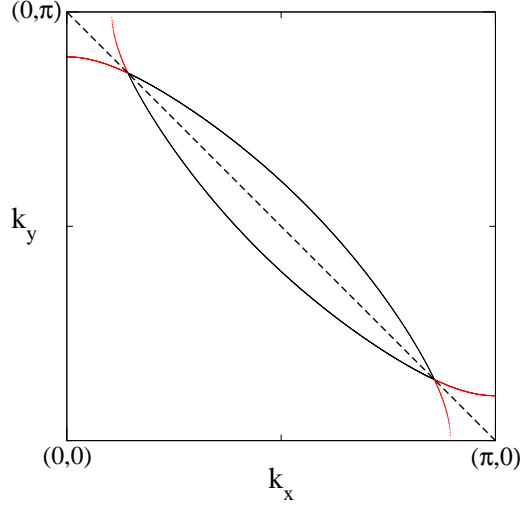


Figure 4.4: The pockets without a gap. Hole-pocket in black, electron-pocket in red. In the absence of a gap the pockets are merely a reinterpretation of the bare FS.

4.1.2.2 $\delta_{vH} > 0$

For $\mathcal{A} = \mu - 4t' = \delta_{vH}$ the electron-pocket vanishes, as stated before. To determine the jump of the slope of the RHS due to the closing of the electron-pocket consider (4.12). E_k^+ can be expanded around the van Hove points, yielding (around $(0, \pi)$)

$$E_k^+ = 4t' + |\mathcal{A}| - \mu + 2t'(-\delta_x^2 - \delta_y^2) + \mathcal{O}(\delta_{x,y}^4), \quad (4.22)$$

thus becoming a circle with radius $r^2 = (|\mathcal{A}| - \delta_{vH})/2t'$. Therefore $|\nabla E_k^+| = |4t'|r$ and the integral (4.12) can with $\varepsilon_k^t \approx 0$ be evaluated to

$$U \frac{1}{4\pi^2} \int d\delta_x \frac{1}{4t'r} \sqrt{\frac{r^2}{r^2 - \delta_x^2}} = \frac{U}{8\pi t'}, \quad (4.23)$$

i.e., it stays finite for $\mathcal{A} \nearrow \delta_{vH}$. Due to the vanishing FS a jump in the slope occurs, which is independent of μ . It is plotted in figure (4.9).

4.1.2.3 $\delta_{vH} < 0$

The situation for $\delta_{vH} < 0$ is more complex. As the bare Fermi surface does not cross the umklapp surface only a hole-like FS appears, which has a pocket-like structure only for larger gap values.

For a gap-value a little bigger than $|\delta_{vH}|$ the branch E_k^- becomes negative at the van Hove points and a second Fermi surface appears there.⁴ It unites

⁴ This is also a hole Fermi surface, and is *not* to be mixed with the electron-pocket. The states at the van Hove points are filled.

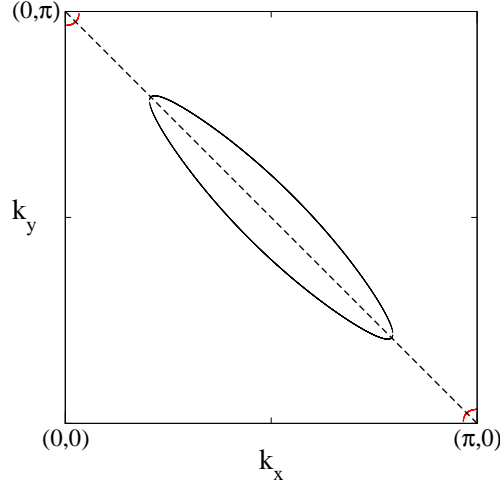


Figure 4.5: With a gap the pockets shrink; here the electron-pockets have almost vanished.

with the other FS for a larger value. This gap value is readily obtained from the expression for the Fermi surface given by⁵

$$\cos k_y = -\frac{t^2 x - t' \mu x}{t^2 - 4t'^2 x^2} \pm \sqrt{\left(\frac{t^2 x - t' \mu x}{t^2 - 4t'^2 x^2}\right)^2 + \frac{\mu^2 - \mathcal{A}^2 - 4t^2 x^2}{4(t^2 - 4t'^2 x^2)}} \quad (4.24)$$

where $x = \cos k_x$. The gap-value for which the two pockets unite is determined the vanishing of the square-root term (at $x = \cos(k_x) = 1$), which leads to

$$\mathcal{A}^2 = 4\frac{(t^2 - 4t' \mu)^2}{t^2 - 4t'^2} + \mu - 4t^2. \quad (4.25)$$

The corresponding effective Fermi surface is plotted in figure (4.10).

The dispersion around the saddle point can be approximated as

$$E_k^- = -4t' \cos \bar{k} - c_0 - \mu + \delta_y c_1 + \delta_x^2 c_2 + \delta_y^2 \tilde{c}_2 + \mathcal{O}(\delta^5) \quad (4.26)$$

where

$$\cos \bar{k} = -\frac{t^2 x - t' \mu x}{t^2 - 4t'^2 x^2} \quad (4.27)$$

is the saddle point of the effective dispersion, with the gap given by (4.25). It is clear by construction, that for the saddle point gap $c_1 = 0$, $c_2 > 0$ and $\tilde{c}_2 < 0$. From the slope of the Fermi surface, which is close to one, it is clear that c_2/\tilde{c}_2 is close to one. The contribution of the FS to the slope of the RHS obtained is given by (4.12) with

$$|\nabla E_k^-| = 2\sqrt{c_2 \delta_x^2 + \tilde{c}_2 \delta_y^2} = \text{const} \cdot \delta_x. \quad (4.28)$$

⁵ By inverting $E_k^\pm = 0$ one loses the sign of the square-root term. Thus the expression (4.24) is either the electron or hole Fermi surface, which has to be determined by evaluating the expression E_k^\pm for the obtained values (k_x, k_y) .

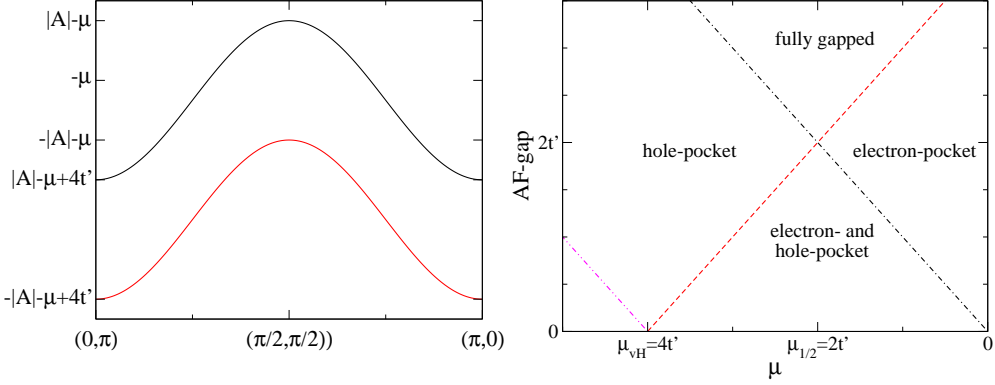


Figure 4.6: Left: The dispersion along the umklapp surface. Due to a finite gap the two branches are separated. Right: Existence of pockets as a function of μ and \mathcal{A} . The minimal gap for a fully gapped system is $\mathcal{A} = |2t'|$. The line below μ_{vH} is discussed in section (4.1.2.3).

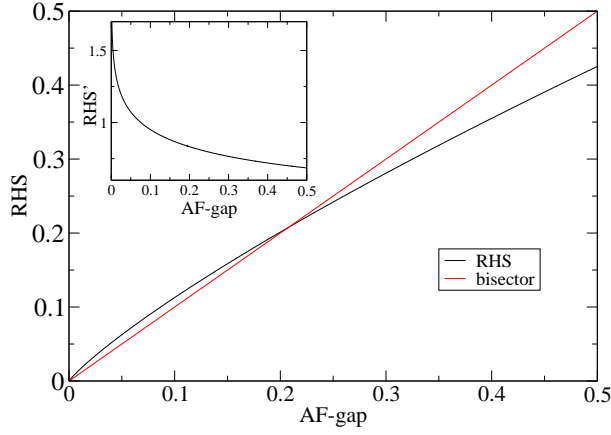


Figure 4.7: RHS for $\delta_{vH} = \mu - 4t' = 0$, and its derivative, showing the well-known logarithmic divergence at $\mathcal{A} = 0$. Parameters: $U = 2.25$, $t' = -0.2$.

The integral (4.12) can be approximated by

$$\text{const} \int_{\varepsilon}^1 d\delta_x \delta_x^{-1} \frac{1}{\mathcal{A}} \sqrt{2} \sim \ln \varepsilon \rightarrow \infty \text{ for } \varepsilon \rightarrow 0. \quad (4.29)$$

as is expected for a saddle point.

As the distance of a gap in the RHS to the saddle-point-gap, eq. (4.25), serves as an effective cut-off, also the slope of the RHS is expected to diverge logarithmically as a function of the gap. The jump in the slope of the RHS due to the opening of the second Fermi surface, and the divergence due to the saddle point for a slightly larger gap value is clearly seen in figure (4.11).

4.1.3 Electron-doped side

To have the possibility of electron-doping, the hole-pocket has to close for a smaller gap than the electron-pocket. Thus, following from the argumentation

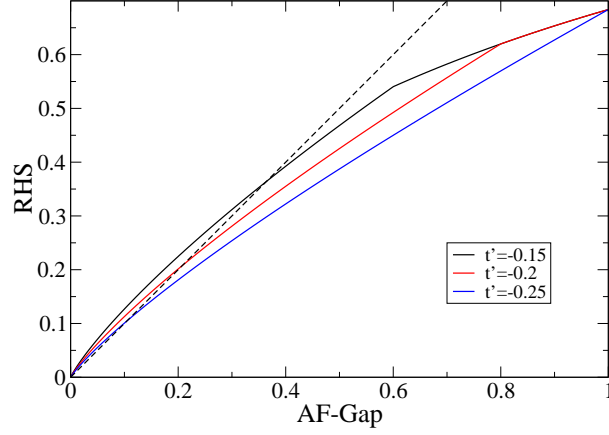


Figure 4.8: RHS for different t' with $\delta_{vH} = \mu - 4t' = 0$ and $U = 2.25$ fixed. The RHS is reduce by t' .

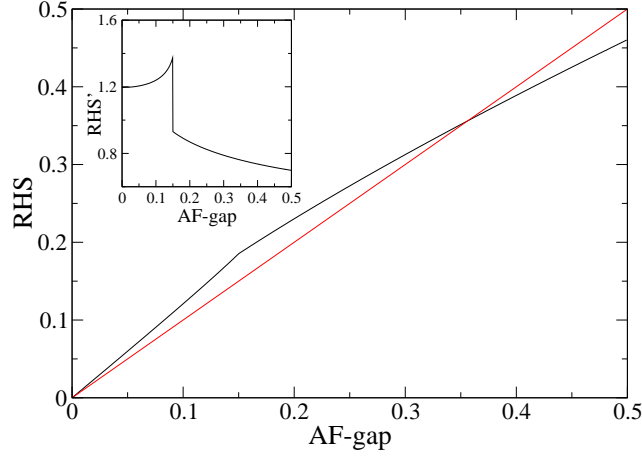


Figure 4.9: The RHS for $\delta_{vH} > 0$, and its slope in the inset, showing the finite value and the jump at $\mathcal{A} = \delta_{vH} = 0.15$. Parameter: $U = 2.25$, $t' = -0.2$.

on page 40, fig. (4.6), electron doping can only happen if $\mu > 2t'$.

The jump of the slope of the RHS at $\mathcal{A} = |\mu|$ is again calculated with (4.12). The dispersion around $(\pi/2, \pi/2)$ is given by

$$E_k^\pm = \pm|\mathcal{A}| - \mu \pm \frac{2t^2}{|\mathcal{A}|} (\delta_x^2 + \delta_y^2) + \left(-4t' \pm \frac{4t^2}{|\mathcal{A}|}\right) \delta_x \delta_y + \mathcal{O}(\delta^4), \quad (4.30)$$

which describes a general ellipse. The integration in (4.12) is thus more difficult, compared with jump at $|\mathcal{A}| = \delta_{vH}$ with circular pockets around the van Hove points; but having in mind that for $T = 0$ the Fermi function is a Heaviside function, determining the integration area as the k -values for which $E_k^\pm < 0$, the derivative Fermi function can be rewritten as the change of the pocket-size

$$\frac{1}{4\pi^2} \int dk_x dk_y \frac{U\mathcal{A}^2}{(\varepsilon_k^t)^2 + |\mathcal{A}|^2} \partial_{\mathcal{A}} A_h \Big|_{\mathcal{A}=|\mu|} \quad (4.31)$$

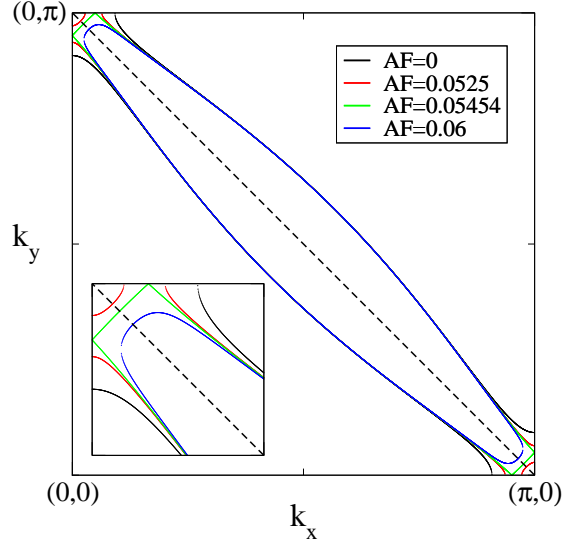


Figure 4.10: The hole-like FS for different gaps. At $\mathcal{A} = |\delta_{vH}|$ an additional hole-like FS appears at the van Hove points, which unites for larger gap values with the other FS to form a pocket. The effective Fermi surface with saddle points away from $(0, \pm\pi)$ and $(\pm\pi, 0)$ is plotted in green.

with A_h being the area of the hole-pocket. To obtain this area rewrite $E_k^- = 0$ as

$$1 - \begin{pmatrix} \delta_x \\ \delta_y \end{pmatrix} \begin{pmatrix} d & n \\ n & d \end{pmatrix} \begin{pmatrix} \delta_x \\ \delta_y \end{pmatrix} = 0 \quad (4.32)$$

with

$$d = \frac{2t^2}{\mathcal{A}} \frac{1}{\mathcal{A} + \mu} \quad \text{and} \quad n = \frac{1}{2} \frac{4t' + 4t^2/\mathcal{A}}{\mathcal{A} + \mu}. \quad (4.33)$$

The eigenvalues are $\lambda_{\pm} = d \pm n$, the main axes of the ellipse are along and perpendicular to the umklapp surface, as expected. In new coordinates the ellipse is given by $1 = x'^2 \lambda_+ + y'^2 \lambda_-$, so that the area is

$$A_h = \sqrt{\lambda_-^{-1} \lambda_+^{-1}} \pi. \quad (4.34)$$

Performing the derivative

$$\partial_{\mathcal{A}}|_{\mathcal{A}=|\mu|} A_h = |\mathcal{A}| \left((2t^2)^2 - (2t'\mathcal{A} + 2t^2)^2 \right)^{-1/2}. \quad (4.35)$$

yields, again with $\varepsilon_k^t \approx 0$, the jump

$$2 \frac{U}{4\pi} |\mu| \left((2t^2)^2 - (2t'\mu + 2t^2)^2 \right)^{-1/2}, \quad (4.36)$$

where a factor two has been introduced due to the two ellipses inside the magnetic BZ, and the gap has been set to the jump-value $\mathcal{A} = |\mu|$.

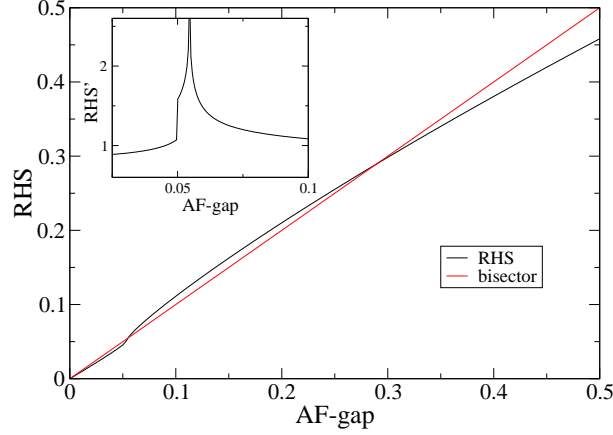


Figure 4.11: The RHS for $\delta_{vH} < 0$. The slope of the RHS in the inset, showing the finite jump at $\mathcal{A} = |\delta_{vH}| = 0.05$, and the logarithmic divergence for a slightly larger gap $\mathcal{A} \approx 0.05454$.

For typical values⁶ $|\mu| < |4t'|$ and $\mu, t' < 0$ it can be assumed $(2t'\mu)^2 \ll 8t'\mu t^2$ and the jump can be estimated to

$$\frac{U}{2\pi} \frac{\sqrt{\mu}}{\sqrt{-8t'}} \leq \frac{U}{2\pi\sqrt{2}}, \quad (4.37)$$

where in the last step again $|\mu| < |4t'|$ was used, i.e., the bare Fermi surface is above the van Hove point $\delta_{vH} > 0$; $\delta_{vH} < 0$ is not interesting, see section (4.2). Comparing this with the jump due to the electron-pocket (4.23), one gets an estimate $\sqrt{2} > 4t'$, for which the jump in the slope of the RHS is larger due to closing an electron-pocket than for a hole-pocket, which is fulfilled throughout this work.

In figure (4.12) the RHS for $\mu = -0.2$ is plotted, with the kink at $\mathcal{A} = 0.2$ for the opening hole- and $\mathcal{A} = 0.6$ for the opening electron-pocket. As a comparison the RHS for $\mu = -0.6$ is plotted having the hole-pocket and the electron-pocket kink vice versa. The smaller kink for the closing electron-pocket leads to a steeper RHS for the electron-doped systems ($\mu > 2t'$) between the kinks. Thus, the solution will depend more sensitively on U , and the free energy gain will be smaller (see section 4.2). The different jump sizes contribute strongly to the different behaviour for the electron and the hole-doped side in the phase diagram.

For $\mu > 0$ only an electron-pocket exists. Similar to the case $\delta_{vH} < 0$ the gap can create a saddle point in the effective dispersion, now at $(\pi/2, \pi/2)$, leading to a logarithmic divergence in the slope, but being very narrow, it leads to an upturn in the RHS in only such a small regime that it hardly creates new solutions, see figure (4.13).

⁶ Below $\mu_{vH} = 4t'$ no electron pocket exists for any gap.

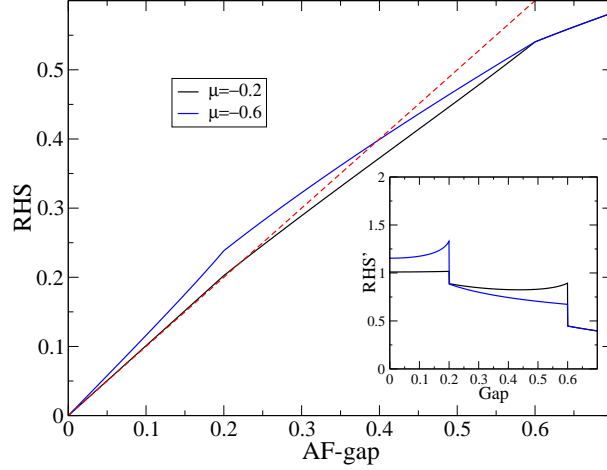


Figure 4.12: The RHS for $\mu = -0.2$ and for comparison $\mu = -0.6$. The slopes of the RHS in the inset. Due to the different jumps in the slope for vanishing electron- and hole-pocket, the gaps-sizes differ. $U = 2.0$. The steeper slope between $\mathcal{A} = 0.2$ and $\mathcal{A} = 0.6$ of the RHS for $\mu = -0.2$ leads to a stronger U dependence of the MF solution.

4.2 Solutions of the Gap Equation & Free Energies

The self-consistent solutions are given by the intersections of the bisector with the RHS. Having in general more than one crossing point, one has to choose the physically correct one. See figure (4.11) or (4.1).

The gap equation is obtained by demanding the vanishing of the derivative of the free energy⁷ with respect to expectation values $\langle a_{k\sigma}^\dagger a_{k+Q\sigma} \rangle$. Thus, the solutions are extrema of the free energy, being either a maximum or a minimum⁸. A maximum is unstable and therefore unphysical. A minimum is called metastable if it is only local, and stable if it is global. To have a free energy with a lower bound the solution with the biggest gap has to be a minimum. As minima and maxima alternate, it is easy to tell minima from maxima⁹. It is therefore clear that a solution is a (local) minimum if and only if the bisector has a bigger slope than the RHS in the crossing point.

The free energy is given by (3.30), which can be written as, if only the AF-gap is non-zero,

$$\Omega = - \sum_k \frac{\mathcal{A}^2}{2U} - T \sum_{k,\alpha=\pm}' \ln(1 + \exp(-\beta E_k^\alpha)). \quad (4.38)$$

It is $\mathcal{A} = \mathcal{A}_\uparrow = -\mathcal{A}_\downarrow$ assumed with a constant potential U . For $T \rightarrow 0$ the free

⁷ Actually the grand canonical potential Ω . Since no confusion is expected, *free energy* will be used synonymously.

⁸ Saddle points are only found for special choice of parameters, and are of little importance.

⁹ A point in which the RHS touches with the bisector is of course a saddle point of F and to be counted as a minimum and maximum at the same value.

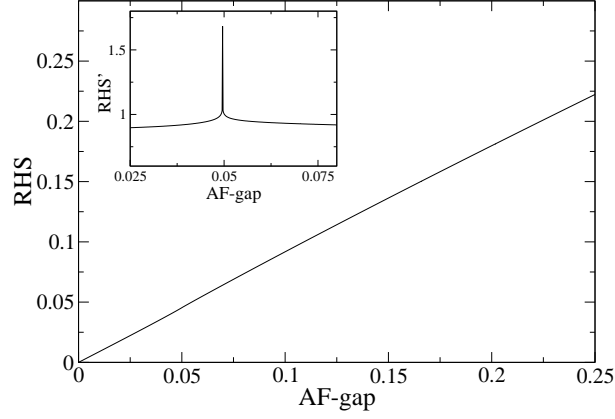


Figure 4.13: The RHS for $\mu = 0.05 > 0$. The slope of the RHS in the inset. The divergent slope is practically invisibly in the RHS plot.

energy reads

$$\Omega = - \sum_k \frac{\mathcal{A}^2}{2U} + \sum_{k,\alpha}' E_k^\alpha \Theta(-E_k^\alpha). \quad (4.39)$$

Since the gap equation is obtained by setting the derivative of the free energy to zero, the area between the bisector and the RHS gives the free energy gain.

The filling is given by

$$n = \sum_{k,\pm}' f(E_k^\pm). \quad (4.40)$$

This simple form, a sum over Fermi functions, is due to the fact that $\frac{\partial}{\partial \mu} E_k^\pm = -1$ (in contrast to the superconduction eigenvalues), since the quasi-particles have well defined charge. Calculating the filling one can plot the gap as a function of n , see figure (4.18).

If $t' = 0$ the zero solution can for a non-zero μ become meta-stable or even stable, even though a non-zero solution exists, see figure (4.14). Observe that the non-zero solution is always located at the same gap value. For the chosen potential of $U = 2.0$ the zero solution becomes globally stable for $\mu \geq 0.2484$.

For $t' = 0$ the system is either fully gapped and is therefore at half filling, or has no gap, and is therefore at the same filling as the non-interacting system. For a broad region metastable solutions exist.

If $t' \neq 0$, μ and $\delta_{vH} = \mu - 4t'$ differ, the van Hove chemical potential is $\mu_{vH} = 4t'$. For a large enough U only the non-zero solution is a minimum.

For $t' \neq 0$ systems with a finite gap away from half filling, having a FS, are possible. The solution as a function of μ is plotted in (4.17). If μ is inside the band-gap, $\mu \approx 2t'$, the solution is μ -independent, as one expects, since μ enters the gap equation only via the Fermi functions. μ outside the band gap changes the filling and the size of the gap, until the gap breaks down.

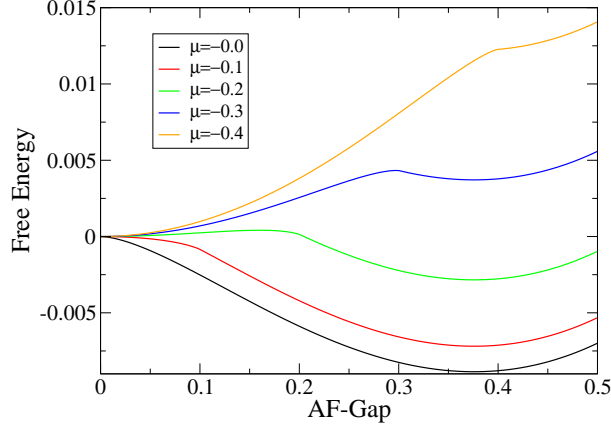


Figure 4.14: Free energy for $t' = 0$, $U = 2.0$. The position of the minimum at non-zero gap values does not change with μ , while the energy gain strongly depends on it. $F(\mathcal{A} = 0)$ is subtracted from all curves.

If a fully gapped solution ($E_k^+ > 0$ and $E_k^- < 0$) exists, that is close to $\mu = 2t'$, in general the non-zero solution is unique¹⁰, see fig. (4.15). It stays unique down to $\delta_{vH} = 0$, see again fig. (4.15). For a slightly smaller μ the zero-solution will become metastable, and for an even smaller μ the non-zero solution will disappear, see fig. (4.16). A lower bound for this is given by $-|\mathcal{A}_0| < \delta_{vH}$, where \mathcal{A}_0 is the gap at $\delta_{vH} = 0$, see fig. (4.17). This is due to the fact that the upturn of the RHS takes place at $\mathcal{A} = |\delta_{vH}|$, see section (4.1.2.3).

This behaviour of the solution as a function of μ is expected to be generic, therefore for a large enough t' the region for which metastable solutions exist is rather small, and restricted to $\mu < \mu_{vH} = 4t'$. The region of fully gapped solutions is small leading to a large region with doped finite AF solutions.

For a (meta-)stable zero-solution, the slope of the RHS for $\mathcal{A} = 0$ has to be lower than the slope of the bisector, i.e., less than one. For the values $U = 2.25$ and $t' = -0.2$ used here, metastable zero-solutions are found for $\delta_{vH} < -0.01498$. For $\delta_{vH} \approx -0.04$ the two solutions, $\mathcal{A} = 0$, $\mathcal{A} \neq 0$, have the same free energy, see fig. (4.16), while the non-symmetric solution disappears for $\delta_{vH} \approx -0.05$. In contrast to the $t' = 0$ case the location of the minimum changes with μ .

For a solution to exist at all, the slope of the RHS has to be for some gap value bigger than one, and then become smaller for a bigger gap. The behaviour away from $\delta_{vH} = 0$ is dominated by the effective Fermi surface. For a reduced slope at least one Fermi surface should close, yielding a solution with either a hole- or electron-pocket, so that no finite solutions with an electron- and a hole-pocket are expected. This argumentation is agreement with numerical findings, where also a positive curvature of the RHS was always observed for gap values which allow for a hole and an electron Fermi surface.

¹⁰Up to the sign, of course. For a gap-size very close to the break down value $\mathcal{A} = |2t'|$ a zero solution develops, because the curvature of the RHS is positive (but very small) for $\mathcal{A} < |2t'|$. But this range of metastability being tiny it does not seem relevant in most cases.

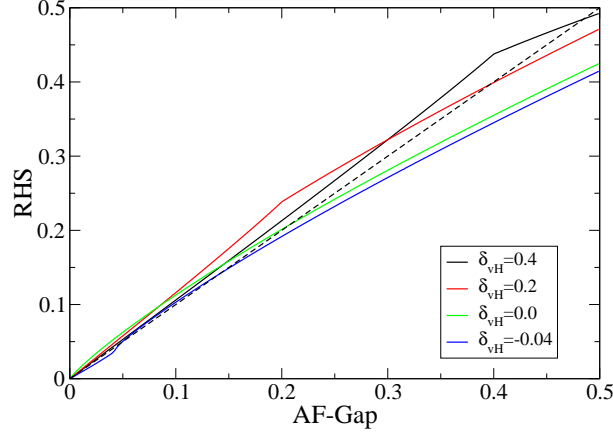


Figure 4.15: RHSs for finite $t' = -0.2$ for different chemical potentials, with hole-doped, or fully gapped solutions. All RHSs for $\delta_{vH} > 0$ are above the bisector, so that the corresponding free energies have a maximum at $\mathcal{A} = 0$. The free energies, fig. (4.16), resolve only the small range $-0.06 \leq \delta_{vH} \leq 0$. Coupling $U = 2.25$.

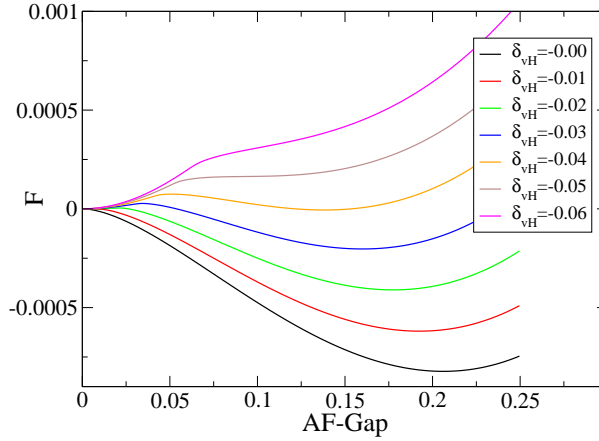


Figure 4.16: Free energy for $t' = -0.2$, $U = 2.25$. The position of the minimum and the free energy gain depends on μ . For $\delta_{vH} \approx -0.04$ the different solutions have the same free energy. Only free energies for $\delta_{vH} \leq 0$ are shown, since only there metastable states are expected.

4.3 RG and AF-Mean-Field Theory

This section aims to elucidate the relation between RG and AF-MF; this is done by introducing a cut-off in the gap equation and changing the coupling in such a way that the solution is independent of the cut-off. It is found that a RG in the symmetric phase works well for large Λ , while for smaller Λ problems appear, which are absent for a similar SC case. They are closely connected to the possibility of first order transitions, that is, they are closely connected to the existence of a FS with, and change due to, the AF gap.

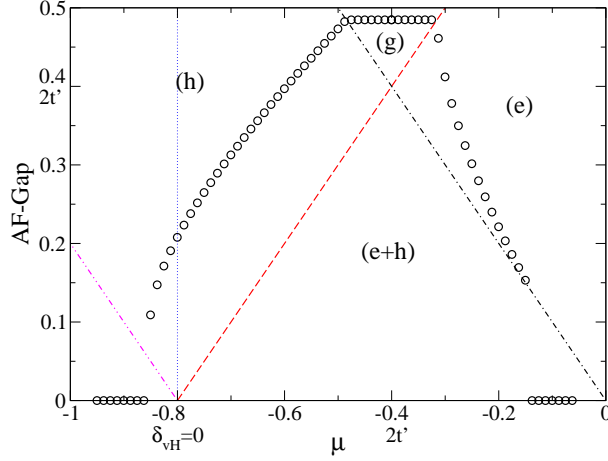


Figure 4.17: The AF gap as a function of μ , for $t' = -0.2$ and $U = 2.25$. The lines indicating the formation of effective Fermi surfaces: Hole pocket (h) in black, electron-pocket (e) in red, opening of the secondary hole-like FS in pink. With hole- and electron ($e + h$) pocket no finite solutions are expected to exist. In the fully gapped region (g) no FSs exist. The secondary hole-like FS line is a lower bound for the existence of a finite gap. In case of the existence of a finite gap, metastability with respect to a zero gap solution is not checked.

This problem is important for the interpretation of the full flows in chapter 6; it also motivated the work [Gersch et al. 2006].

Starting point is the gap equation

$$\mathcal{A} = - \sum_{k\omega} \frac{2\mathcal{A}U}{|\mathbf{Q}(i\omega)|}. \quad (4.41)$$

If the integrand becomes Λ -dependent by a (here unspecified) cut-off function, and also a Λ -dependent potential is allowed, one obtains

$$\mathcal{A} = -U^\Lambda \sum_{k\omega} \frac{2\mathcal{A}}{|\mathbf{Q}^\Lambda(i\omega)|}. \quad (4.42)$$

Demanding that the gap is non-zero and independent of Λ yields

$$0 = \dot{U}^\Lambda \sum_{k\omega} \frac{2}{|\mathbf{Q}^\Lambda(i\omega)|} - U^\Lambda \sum_{k\omega} \frac{2|\dot{\mathbf{Q}}^\Lambda(i\omega)|}{|\mathbf{Q}^\Lambda(i\omega)|^2}, \quad (4.43)$$

where the dot marks the derivative with respect to Λ . Making use of the gap equation in the first term one arrives at the flow equation

$$\dot{U}^\Lambda = (U^\Lambda)^2 \sum_{k\omega} \frac{2|\dot{\mathbf{Q}}^\Lambda(i\omega)|}{|\mathbf{Q}^\Lambda(i\omega)|^2}. \quad (4.44)$$

It describes how the potential U has to be changed with Λ , to guarantee a Λ -independent solution of the MF equation, i.e., to produce a set of physically equivalent effective models.

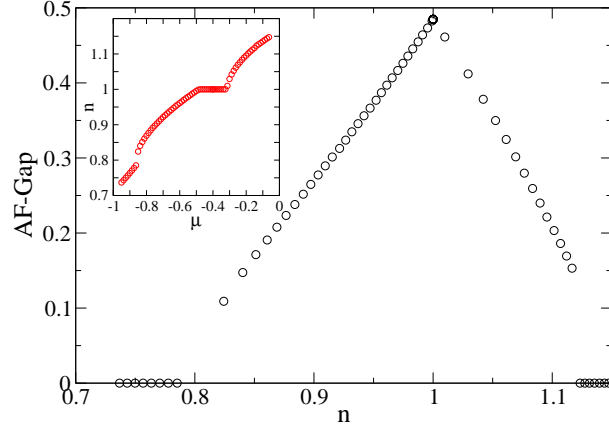


Figure 4.18: The gap as a function of the filling n , for $t' = -0.2$ and $U = 2.25$. Filling as a function of μ in the inset.

The choice of the cut-off function involves some arbitrariness. One common way is

$$\mathbf{Q}(z) = \begin{pmatrix} (\xi_{k'} - z) (\chi_k^\Lambda)^{-1} & \mathcal{A} \\ \mathcal{A} & (\xi_{k'+\pi} - z) (\chi_{k+Q}^\Lambda)^{-1} \end{pmatrix}, \quad (4.45)$$

which will be used in the following. χ_k is the usual momentum shell cut-off function (2.20).

4.3.1 Flow without Gap

If one, as an approximation, sets the gap in the flow equation (4.44) to zero one obtains

$$\dot{U}^\Lambda = - (U^\Lambda)^2 2 \sum_{k\omega} \frac{\dot{\chi}_k \chi_{k+Q} + \chi_k \dot{\chi}_{k+Q}}{(\xi_{k'} - i\omega)(\xi_{k'+Q} - i\omega)}, \quad (4.46)$$

which corresponds to the particle-hole or RPA diagram of the RG equation (2.37). It is also closely connected to the slope with respect to the gap of the RHS of the gap equation, which is the bare susceptibility.

The solution of the flow equation is given by

$$U^\Lambda = U_0 + U_0 \Pi^\Lambda U^\Lambda \quad (4.47)$$

where the scale dependent ph-bubble is $\Pi^\Lambda = \sum |\mathbf{Q}^\Lambda(i\omega)|^{-1}$ with $\mathcal{A} = 0$. The solution is easily checked by iterating the equation (4.47) to obtain the sum of all RPA diagrams. This sum fulfils (4.46), as can be seen by direct calculation. Since the potential is (trivially) separable, the solution can be rewritten as

$$U^\Lambda = \frac{U_0}{1 - U_0 \Pi^\Lambda}. \quad (4.48)$$

It is clear that the coupling diverges if the denominator vanishes. Since $\Pi^{\Lambda_0} = 0$ at the beginning of the flow, and $\Pi^{\Lambda=0}$ is the RPA diagram at the end of the flow given by the slope of the RHS at $\mathcal{A} = 0$, the ladder diverges for some scale Λ_c , if the RHS has a larger slope than the bisector, i.e., if the free energy has a (local) maximum. If the slope is smaller, i.e., the free energy has a (local) minimum, the flow produces a sharp plateau in U^Λ below a Λ_p , where no degrees of freedom are left so that k and $k+Q$ are part of the Λ reduced BZ. Observe that a non-divergent flow does not necessarily exclude a finite gap solution. Flows for different μ are shown in figure (4.19).

4.3.2 Flow with Gap

If the gap is non-zero, one obtains for a sharp cut off

$$\begin{aligned}
& \partial_\Lambda \sum_{k\omega} \frac{2}{|\mathbf{Q}^\Lambda(i\omega)|} \\
&= \sum (\dot{\chi}_k \partial_{\chi_k} + \dot{\chi}_{k+Q} \partial_{\chi_{k+Q}}) \frac{2}{|\mathbf{Q}^\Lambda(i\omega)|} \\
&= \sum \left(\dot{\chi}_k \int_0^1 d\chi_k \partial_{\chi_k} + \dot{\chi}_{k+Q} \int_0^1 d\chi_{k+Q} \partial_{\chi_{k+Q}} \right) \frac{2}{|\mathbf{Q}^\Lambda(i\omega)|} \\
&= \sum \frac{\dot{\chi}_k \chi_{k+Q}}{(\xi_{k'} - i\omega)(\xi_{k'+Q} - i\omega) - \chi_{k+Q} \mathcal{A}^2} + \frac{\chi_k \dot{\chi}_{k+Q}}{(\xi_{k'} - i\omega)(\xi_{k'+Q} - i\omega) - \chi_k \mathcal{A}^2},
\end{aligned} \tag{4.49}$$

where in the third line the Morris lemma [Morris 1994] was used

$$\int_{-\infty}^{\infty} dx \delta(x) f(\Theta(x), x) = \delta(x) \int_0^1 dt f(t, x), \tag{4.50}$$

which is just the chain rule, easily seen, if one chooses a concrete representation of the δ -function. This flow equation is exact for the mean-field model. It was derived from a MF equation with *no* external field. It does not destroy the symmetry of the free energy as only \mathcal{A}^2 enters.

By choosing a sharp cut-off χ_k^Λ , say (2.20), the domain of the integration is restricted.

4.3.3 Numerical Results

To get a quantitative understanding of the quality of approximating the flow equation by the zero gap equation (4.46), it is integrated numerically. At any scale Λ the mean-field equation is solved. The cut-off function is defined with respect to the free dispersion, i.e., $\chi_k^\Lambda = \Theta(\Lambda - |\xi_k|)$, as in the full RG. In the following $U = 2.25$ and $t' = -0.2$ is used.

The flowing coupling and the mean-field solution as a function of the cut-off are plotted in fig. (4.19). The MF solution should be constant as a function of Λ , as the low energy model should describe the same physics. For $\Lambda > 1$ this is very well fulfilled, but below a certain scale $\Lambda \approx 1$ the solution changes considerably. Thus, the zero gap approximation is not good any more.

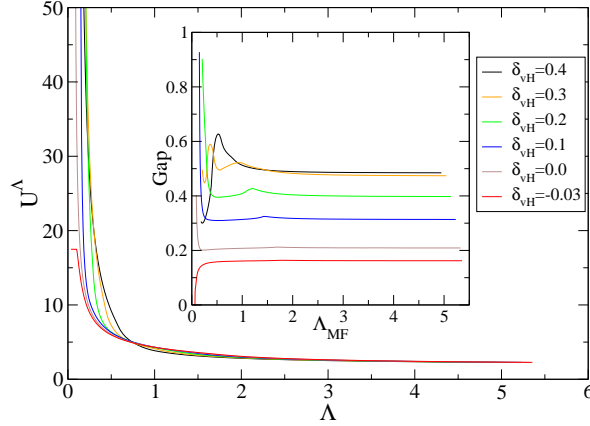


Figure 4.19: Flow of the coupling for different chemical potentials with zero gap in $\tilde{\Pi}^\Lambda$. Flow with a plateau in red. Inset: The associated gaps as a function of the scale Λ_{MF} . Parameters: $U = 2.25$, $t' = -0.2$.

To get some insight into what causes the error, the RHSs of the MF equation for the flows in fig. 4.19 with $\delta_{vH} = 0.4$ is shown for different cut-offs Λ in fig. (4.20).

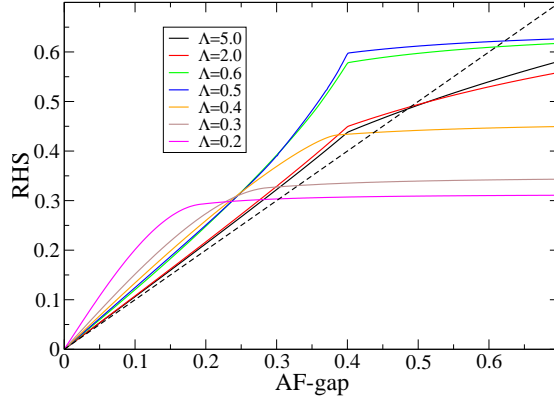


Figure 4.20: RHSs for $\delta_{vH} = 0.4$ for different cut-offs. Below $\Lambda = 0.4$ the behaviour changes qualitatively.

According to section (4.1.2.2) at $\mathcal{A} = |2t'| = 0.4$ the electron- and the hole-pocket close which should lead to a kink in the RHS. For $\Lambda > 0.4$ this is indeed the case, but for $\Lambda < 0.4$ the RHS has already saturated. The van Hove point and the point $(\pi/2, \pi/2)$ are no longer part of the effective model; thus, the kinks, which are due to the closing of the FSs close to these points, and which are essential for the solutions, disappear. Therefore, the low energy model cannot describe the correct physics. The flattening close to $\mathcal{A} = \Lambda$ results from a saturation of the integrand in the Λ -reduced BZ and is not due to the Fermi functions.

To understand why the flow equation creates non-valid low-energy models in this case, it is helpful to compare the zero-gap flow with a flow with the correct gap, which is the gap solving the mean-field equation. By construction, such a low energy model has to have the same solution as the original model. The comparison is shown in figure (4.21).

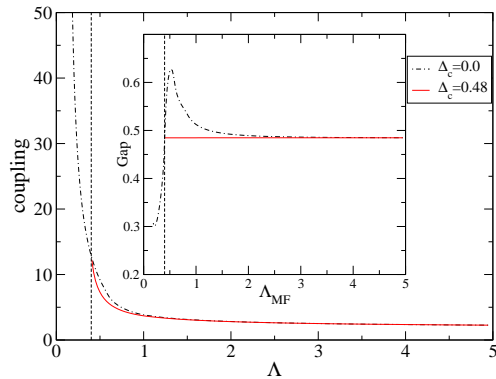


Figure 4.21: Comparison between exact and zero gap flow. The coupling of the flow with a gap is smaller for $\Lambda_{\text{MF}} > |\delta_{vH}|$ to have a sharp upturn at $\Lambda_{\text{MF}} = |\delta_{vH}|$. The coincidence of the couplings close to $\Lambda_{\text{MF}} = |\delta_{vH}|$ is accidental. Inset: The gaps of the flow with and without a gap. The first is a constant while the latter shows some deviations from the correct constant behaviour.

The gap is constant, as expected. For $\Lambda_{\text{MF}} > 0.4$ the effective coupling is smaller than before, but has a sharp upturn at $\Lambda = 0.4$, preventing the flow to smaller scales¹¹. The reason can be found in the behaviour of the factor of the RHS of the flow equation $\partial_{\Lambda}\Pi^{\Lambda}$, given by (4.49), which is plotted in fig. (4.22).

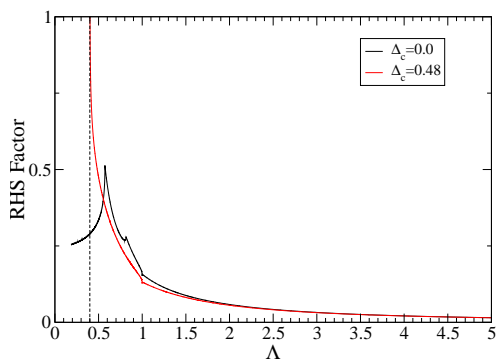


Figure 4.22: The RHS factor $\partial_{\Lambda}\Pi^{\Lambda}$ as a function of the cut-off for the exact and the zero gap flow.

The RHS factor of the zero-gap flow shows a kink at approximately $\Lambda = 1.0$, $\Lambda = 0.8$ and $\Lambda = 0.6$. While the first kink at $\Lambda = 1.0$ comes about when the

¹¹At least numerically; it was not checked if the singularity is integrable.

borders at $\xi_k = -\Lambda$ and $\xi_{k+Q} = \Lambda$ touch each other tangentially at the k_x, k_y -axes, the second and third are due to a large integrand when the integrated shell touches the Fermi surface at the bisector or, for smaller Λ , at the axis. While the kink at $\Lambda \approx 1$ remains the same for the flow with the correct gap, the other kinks disappear as the Fermi surfaces are gapped out¹².

For even smaller $\Lambda < 0.4$ the integrated shell lies partly in an area with $\xi_k < 0$ and $\xi_{k+Q} < 0$, which can be interpreted as an electron-pocket for zero gap (see section (4.1.2)). In the zero-gap case the integrand there is zero due to the cancellation of the Fermi functions, see fig. (4.23), leading to a much reduced RHS factor, and therefore a reduced feedback to the potential U^Λ .

This is in contrast to the flow with a gap. Since the electron-pocket is closed¹³ the large density of states close to the van Hove points contributes to the integrand leading to the sharp upturn of the coupling close to $\Lambda = 0.4$, fig. 4.21 and preventing the flow into non-physical regions.

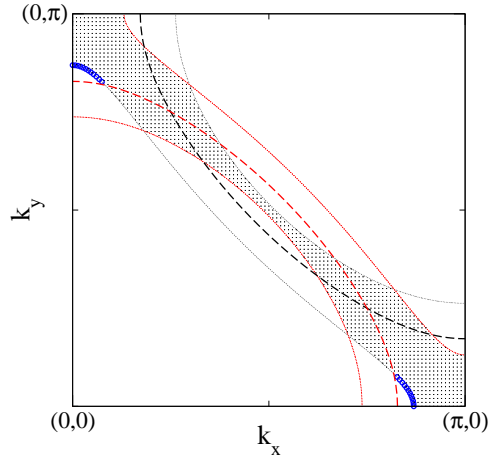


Figure 4.23: The reduced momentum space $\delta_{vH} = 0.4$ for $\Lambda = 0.5$ (shaded). Fermi surface black dashed and (π, π) -shifted Fermi surface red dashed, restriction $|\xi_k| = \Lambda$ in black, $|\xi_{k+Q}| = \Lambda$ in red. Integration region within the electron-pocket, which does not contribute to the zero-gap flow in blue.

Therefore the problem is closely related to the fact that the AF has first order transitions; an AF gap changes the Fermi surfaces strongly. Due to this degrees of freedom contribute at finite gap to the RHS which are not evaluated at zero gap, neither in the zero-field susceptibility, nor in the zero-field flow. Therefore one has to be careful not to enter this unphysical region in the full scheme.

Finally, one way to meet this problem will be suggested; it is not implemented in the full RG. The newly developed ansatz of a flow into the symmetry-broken phase with a counter term seems to be the better solution, in spite of its technical complexity [Gersch et al. 2006].

¹²This is special for the half-filled system close to $\mu = 2t'$; doped AF systems still have a FS.

¹³For all hole-doped systems with non-zero AF gap.

To correctly account for the low energy degrees of freedom, the flow has to be performed with the correct gap. But in general the solution of the low-energy model is not known. Therefore one seeks a suitable gap which can be introduced instead of the correct one into the flow equation, providing a better approximation than the zero gap. This gap will be called counter-gap. In figure (4.24) gap flows for different counter-gaps and the corresponding RHS factors are shown. One finds, that for a counter-gap $\mathcal{A}_c = 0.4 = \delta_{vH}$ only correct contributions of Fermi surfaces and, more importantly, the correct contributions of the van Hove singularities are taken into account. The too small gap in the dominator leads to a diverging gap close to the break down of a low-energy model, which is however restricted to a narrow region. Also away from half-filling for hole-doping $\mathcal{A}_c = \delta_{vH}$ seems to be a good choice, guaranteeing the correct inclusion of the van Hove points, even though the effective FSs are wrongly positioned.

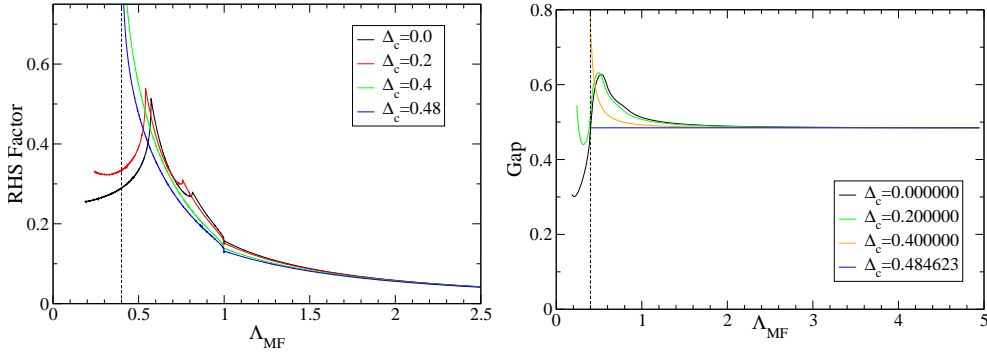


Figure 4.24: The RHS factor $\partial_{\Lambda} \Pi^{\Lambda}$ for different gaps (left). The low energy model solutions for different counter gaps. A counter gap $\mathcal{A}_c = \delta_{vH} = 0.4$ gives reasonable results (right).

The concept of a counter delta can be generalised to the electron-doped side, where $\mathcal{A}_c = -\mu$ seems to be good choice.

However, the implications in a full scheme on the couplings in other but the AF channel are difficult to estimate.

Chapter 5

SC, Pi-Pair and Coexistence

In this chapter first the basic facts for the π -gap equation and for the superconducting gap equation are stated. Then, the interplay of the AF and SC gaps and the influence on the π -pair, for the case which is relevant for the numerics is briefly discussed.

5.1 Only Pi Gap

If only the π -pair gap is non-zero the quadratic part of the mean-field Hamiltonian is described by the matrix

$$\mathbf{Q}(z) = \begin{pmatrix} \xi_{k'} & \pi_k \\ \pi_k^* & -\xi_{-k'+\pi} \end{pmatrix}. \quad (5.1)$$

Therefore the eigenvalues are

$$E_k^\pm = \varepsilon_k^t \pm \sqrt{(\varepsilon_k^{t'} - \mu)^2 + |\pi|^2}, \quad (5.2)$$

with ε_k^t ($\varepsilon_k^{t'}$) being the t (t') dependent part of the bare dispersion, see page 36. If in the case of perfect nesting $t' = \mu = 0$, (5.2) simplifies to

$$E_k^\pm = \varepsilon_k^t \pm |\pi|, \quad (5.3)$$

i.e., the square root part vanishes, so that E_k^\pm become identical for vanishing gap values in the case $t' = 0$. The Fermi functions therefore cancel in a wide k -range yielding a π -gap equation that has a finite, nearly constant slope for a small π -gap. This is in contrast to the eigenvalues in the SC case $E_k^\pm = \pm E_k$, eq. (5.5). There only one of the Fermi functions contributes for $T = 0$, and consequently the pole in the integrand leads to a diverging slope at $\Delta = 0$.

The gap equation reads

$$\pi^* = - \sum_{k,\alpha=\pm} \frac{W_{kk'}\pi^*}{\alpha\sqrt{(\varepsilon_k^{t'} - \mu)^2 + |\pi|^2}} f(E_k^\alpha). \quad (5.4)$$

As for the SC case a potential is attractive if $W_{kk'}$ is in some channel negative.

The RHS is plotted in fig. (5.1). The slope of the RHS at $\pi = 0$ is not enhanced, so that no self sub-stained solution is found for a reasonable potential.

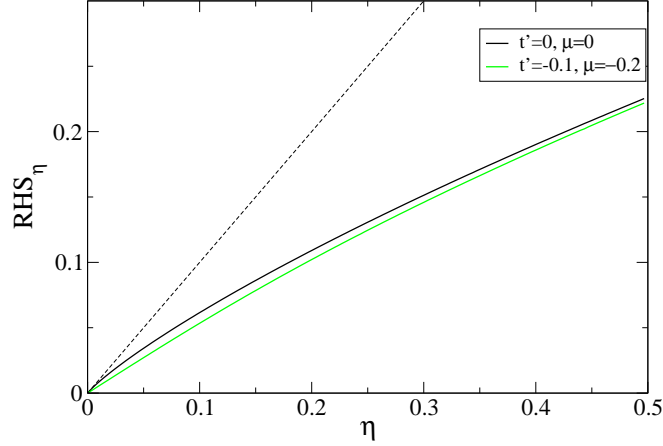


Figure 5.1: RHS of the π -pair equation for $W = -2$. A finite not too big t' and μ does not affect the qualitative behaviour.

5.2 Only SC Gap

The MF solutions of the superconductor are discussed in detail in the literature, [Fetter and Walecka 1971], [Annett 2004]. This discussion will not be repeated here. For completeness here the facts most important for this work will be summarised. The behaviour is mostly determined by the main properties of the bare Fermi surface and the interaction.

The eigenvalues are

$$E_k^\pm = \pm \sqrt{(\xi_k)^2 + |\Delta_k|^2}. \quad (5.5)$$

As both branches are non-zero for a non-zero gap no Fermi surface exists. A typical RHS is plotted in fig. 5.2, black curve (AF=0). The slope of the RHS at $\Delta = 0$ is infinite, due to the fact that the particle-particle bubble is always divergent for $T = 0$, as long as $\xi_k = \xi_{-k}$.¹ This leads to a solution for arbitrarily small interaction. At $T = 0$ this solution is, for a k -independent potential with negligible radial dependence,

$$\Delta_0 = \frac{\omega}{\sinh(1/V D(\varepsilon_F))} \approx 2\omega e^{-1/V D(\varepsilon_F)} \quad (5.6)$$

where ω is the bandwidth of the interaction, in BCS superconductors often identified with the Debye frequency. In the second step it was assumed that the interaction V is small. $D(\varepsilon_F)$ is the density of states at the Fermi level. The critical temperature has a simple connection with the zero temperature gap Δ_0 ²

$$T_c = \Delta_0/1.76. \quad (5.7)$$

The transitions are always second order as a function of temperature.

¹This is nearly always the case, as this is implied by the time reversal symmetry.

²This changes if the interaction is strongly peaked or suppressed at the Fermi level.

The simple behaviour of the SC gap is in contrast to the AF mean-field solutions, where no so simple relations for the gap at zero temperature or the critical temperature can be given.

The combination with the RG will prove to work much better than for the AF gap, cf. sec. 4.3. The important degrees of freedom for the SC gap are those close to the FS, which would only be treated by the RG and therefore not be part of the low energy model for $\Lambda \rightarrow 0$; but since the MF calculation is done well above the divergence scale Λ_c , the low energy model contains always the essential degrees of freedom for the SC gap, see page 68.

5.3 Coexistence

5.3.1 SC and AF

Of special interest is the case of a d-wave superconductor and an s-wave antiferromagnet. This is on the one hand based on the experimental fact that these order parameters are important in high- T_c materials, which is the motivation for these calculations. On the other hand, evidence was found in earlier RG based works for the Hubbard model, that the couplings in the s-AF and d-SC channel and the corresponding susceptibilities are strongly enhanced towards low scales Λ . Therefore in the numerics for the repulsive HM a d-wave superconductor, $\Delta_k = -\Delta_{\bar{k}}$, and an s-wave antiferromagnet, $\mathcal{A}_{k,\sigma} = \mathcal{A}_{\bar{k},\sigma}$, $\mathcal{A}_{k,\uparrow} = -\mathcal{A}_{k,\downarrow} \equiv \mathcal{A}_k$ will be assumed, where \bar{k} is k rotated by 90 degrees. Otherwise the gap structure will not be fixed so that in the first octant of the BZ the values are not assumed to have a certain structure. Assuming the d-wave SC and s-wave AF, and further, that the π -gap is negligible it is straightforward to see that the eigenvalues, given by

$$\left| \begin{pmatrix} \xi_k - E_k & \Delta_k & \mathcal{A}_k & \\ \Delta_k^* & -\xi_{-k} - E_k & & \mathcal{A}_{-k}^* \\ \mathcal{A}_k^* & & \xi_{k+Q} - E_k & \Delta_{k+Q} \\ & \mathcal{A}_{-k} & \Delta_{k+Q}^* & -\xi_{-k+Q} - E_k \end{pmatrix} \right| = 0, \quad (5.8)$$

also have an s-wave structure, as the characteristic polynomial contains only even powers of Δ .

In the following the influence of the SC gap on the AF gap and vice versa is investigated. The naïve expectation is that the appearance of one of the order parameters suppresses the other one. This is usually, but not always, the case.

In fig. 5.2 the RHS of the SC gap equation for $t' = \mu = 0$ is plotted. The larger the AF gap is the more the SC RHS is reduced. The slope of the RHS is finite for any finite AF gap, reflecting the fact that, for the parameters chosen here, the FS is fully gapped by an arbitrarily small AF gap.

For a finite $t' = -0.2$ and a chemical potential $\mu = 4t' + \delta_{vH} = 4t' - 0.05$ (below $\mu_{vH} = 4t'$) the SC RHS is first increased and then decreased by the presence of a AF gap, see fig. 5.3. The maximal increase is found for $\mathcal{A} \approx |\delta_{vH}|$. It is shown in sec. 4.1.2.3, that the effective FS can be enlarged by the AF gap for $\delta_{vH} < 0$, being largest at $\mathcal{A} \approx |\delta_{vH}|$. Therefore, the RHS increase with the AF gap is attributed to the larger FS.

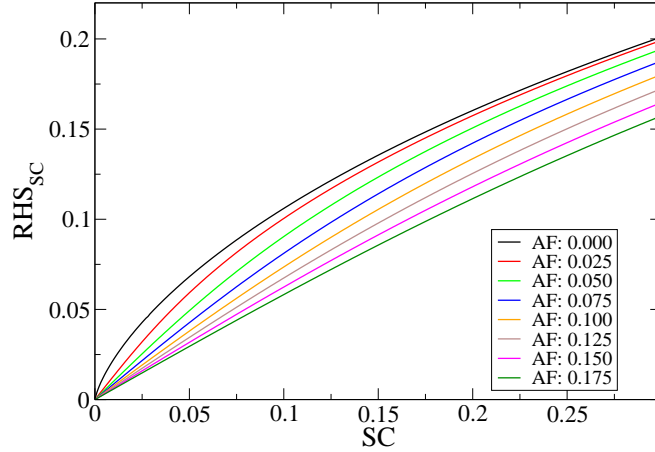


Figure 5.2: The RHS of the SC gap equation for $t' = 0$ and $\mu = 0$ with various AF gaps present. An AF gap reduces the RHS.

Above the van Hove chemical potential μ_{vH} the expected behaviour is found, see fig. 5.4, namely a reduction by the AF gap. The slope seems to be finite, even though an infinite slope is expected; for all AF gaps in the plot pocket-like FSs are open, albeit rather small and around $(\pi/2, \pi/2)$, where the d-wave interaction is weak, so that this infinite slope is presumably invisible due to the restricted numerical resolution.

The change of the AF RHS with the SC gap can be derived from the change of the SC gap with the AF gap. Remembering that the gap equations are derivatives of the free energy and that the c-number term of the Hamiltonian contains no mixed terms of the AF and SC gap one immediately sees

$$\partial_{\Delta} \text{RHS}_{\mathcal{A}} = \partial_{\Delta} \partial_{\mathcal{A}} F = \partial_{\mathcal{A}} \text{RHS}_{\Delta}. \quad (5.9)$$

Thus, an increase of the SC RHS for a certain AF gap value implies that the AF RHS is also increased at this certain AF value by a finite SC gap.

In fig. 5.5 an AF RHS for $t' = 0$ and $\mu = -0.2$ is shown. For $\mathcal{A} > |\mu|$ the RHS is decreased by an SC gap, whereas for some smaller value the AF RHS is increased. There the FS is strongly increased by the AF gap, which would also lead to a strong increase of the SC RHS.

For a finite $t' = -0.2$ and below the van Hove chemical potential $\delta_{vH} = -0.05$ a similar behaviour is found. For $\mathcal{A} < |\delta_{vH}|$ the RHS is increased, while for $\mathcal{A} > |\delta_{vH}|$ the RHS is decreased by the SC gap. This is in agreement with the corresponding SC RHS, fig. 5.3, where for a small AF gap an increase was found, which became smaller for $\mathcal{A} > |\delta_{vH}|$.

As the AF RHS becomes more smooth in the presence of a SC gap the jump as a function of μ in the AF gap can be reduced. This depends of course on the chosen parameters. It was found numerically that the first order transition of the AF gap can be changed to a continuous transition.

If the bare FS is above the van Hove points the AF RHS, fig. 5.3.1, is reduced everywhere. This again is compatible with the SC RHS, shown in fig. 5.4.

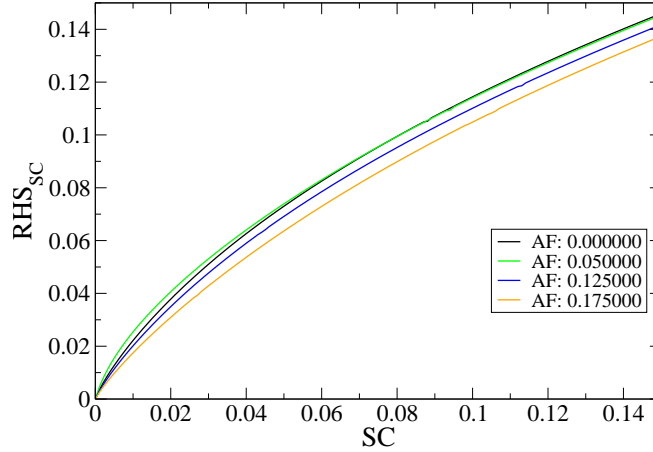


Figure 5.3: The RHS of the SC gap equation with finite $t' = -0.2$ and a bare Fermi surface below the van Hove points $\delta_{vH} = \mu - 4t' = -0.051$ with various AF gaps. A small AF gap $\mathcal{A} \approx |\delta_{vH}|$ increases the RHS, while it is reduced for bigger AF gaps. This is attributed to the change of the effective FSs due to the AF gap.

5.3.2 Interplay with the Pi-pair

As discussed in section 5.1 the π -pair needs a very big attraction to have a self-consistent non-zero solution. Such a potential is not created in the RG flow, as the relevant scattering is unimportant. But as pointed out by [Kyung 2000] a π -gap can be created by the coexistence of the SC and AF gap. If we neglect the π -pair on the RHS in its MF equation, the minor $\det \mathbf{M}_{14}$ is given by

$$\det \mathbf{M}_{14} = \left| \begin{pmatrix} \Delta_k^* & -\xi_{-k} - E_k & & \\ \mathcal{A}_k^* & & \xi_{k+Q} - E_k & \\ & -\mathcal{A}_{-k} & & -\Delta_k^* \end{pmatrix} \right|. \quad (5.10)$$

Since the EVs have s-wave symmetry, the minor has d-wave symmetry. Therefore, the π -pair will be assumed to have d-wave symmetry, as the superconductor. If all spins of the π -pair RHS are flipped, the RHS remains the same; the singlet SC gap and the pure spin-density-wave AF gap changes sign, $\Delta_k \rightarrow -\Delta_k$ and $\mathcal{A}_k \rightarrow -\mathcal{A}_k$, so that the sign drops out in product of both gaps. Therefore, the π -pair, created by the other two gaps, is a triplet gap.

If the potential were strictly zero, the only solution for the π -pair would also be strictly zero, as was already mentioned by [Psaltakis and Fenton 1983]; this is *not* in contradiction to the findings of [Kyung 2000], as there the expectation value $\langle a_{-k-Q\downarrow} a_{k\uparrow} \rangle$ is discussed, while here the focus is on the mean-field or gap

$$\pi_k = 4 \sum_{\mathbf{k}'} W_{k,k'}^\Lambda \langle a_{-k'+Q\downarrow} a_{k'\uparrow} \rangle. \quad (5.11)$$

The issue is the feedback of the π -pair on the other order parameters, and it is the gap which couples back to the MF equations, not the expectation

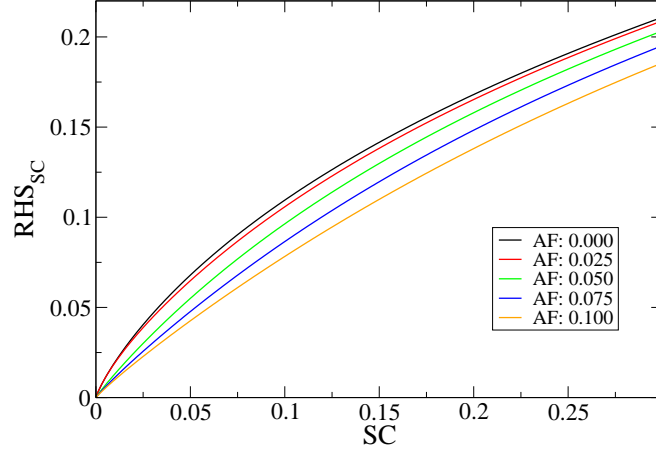


Figure 5.4: The RHS of the SC gap equation with $t' = -0.2$ and a bare FS above the van Hove points $\delta_{vH} = \mu - 4t' = 0.1$ with various AF gaps. Since the FS is reduced by the AF Gap the SC-RHS is also reduced.

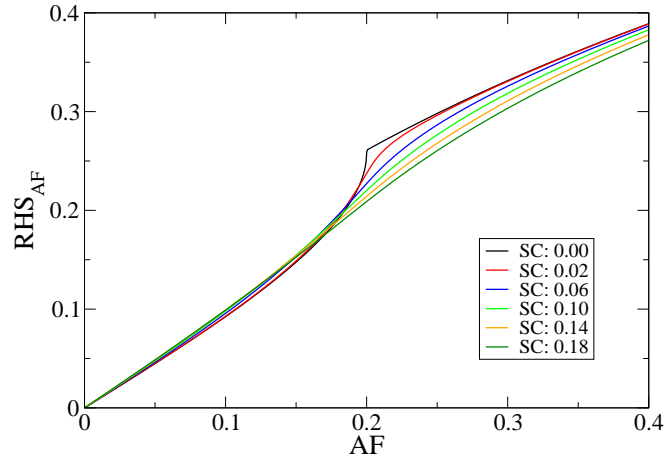


Figure 5.5: The RHS of the AF gap equation for $t' = 0$ and $\delta_{vH} = \mu = -0.2$. The AF-RHS is reduced by the SC gap well below and increased well above μ .

values. The strength of the potential is therefore crucial; it will be found to be numerically of little importance, see section 6.2.4.

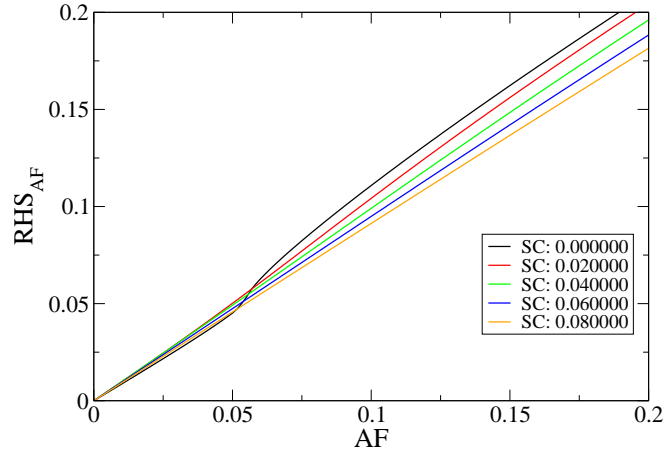


Figure 5.6: The RHS of the AF gap equation for $t' = -0.2$ and $\delta_{vH} = -0.051$. Due to the increase for small and decrease for big \mathcal{A} values due to Δ the AF-RHS becomes smoother.

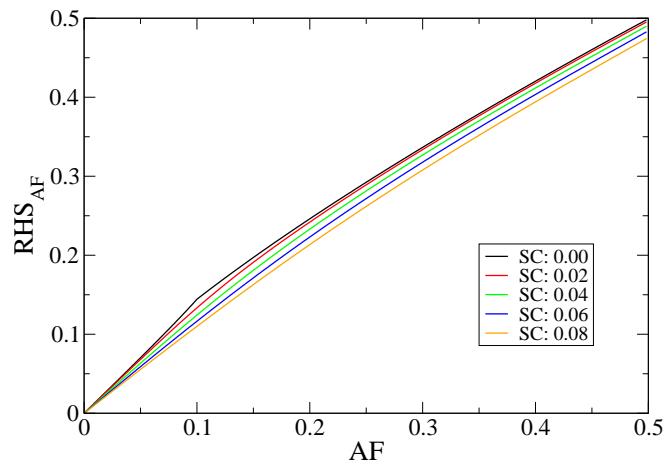


Figure 5.7: The RHS of the AF gap equation for $t' = -0.2$ and $\delta_{vH} = 0.1$. The AF-RHS is decreased everywhere due the SC gap.

Chapter 6

Numerical Results

In this chapter numerical results for the two-dimensional Hubbard model (HM) from the combination of functional renormalisation group and mean-field calculation are presented. As a function of the energy scale Λ_{MF} , at which the RG is stopped, different effective low-energy models are derived, which are then handled within the mean-field approximation. The results thus in general depend on the energy scale Λ_{MF} . Therefore, one has to find a suitable criterion to choose the solution.

One could hope that in a certain cut-off range the result does not, or only very weakly, depend on the scale. At such scales the approximation involved in the one loop RG and the mean-field approximation balance, i.e., the reduction of phase space by the cut-off function is compensated by an appropriate increase in the couplings, leading to a constant solution as a function of Λ_{MF} , a plateau. This is the case if the RG flow is mainly driven by one of the diagrams, which is connected to the susceptibility of the dominant MF solution. Naïvely one expects this behaviour to be the usual one, as the susceptibility growing most strongly is often interpreted as indicator for the dominant symmetry breaking.

If, however, several diagrams contribute down to low scales, or if the dominant MF solution is different from the most strongly growing susceptibility, no such plateau is expected. There, another stop criterion is needed. In the following, if not stated differently, the ratio between the largest gap value, Δ , and the low-energy scale Λ is utilised. The motivation is twofold: on the one hand it seems unphysical that a low-energy model creates energy scales which are larger than those it contains initially. On the other hand one can view the scheme used here as an approximation to an RG with symmetry-breaking, that is an RG with flow equations for gaps and anomalous interactions. There, the creation of a finite gap effectively serves as cut-off on the propagators, leading to a saturation of the flow. This can be modeled by stopping the flow at a scale $\Lambda_{\text{MF}} = \Delta \cdot c$, where the constant is $c \gtrsim 1$.

The so-called critical scale Λ_c at which the flow diverges in a certain channel is sometimes interpreted as the scale for the dominant gap. As the AF gap can have meta-stable zero solutions, this does not seem reliable; in this case the flow stays finite, even though a finite gap is the correct solution. It was found that this scale cannot be used as a reasonable stop criterion. As discussed in

section 4.3, it is possible to flow into unphysical low-energy models, which one has to bear in mind when analysing certain flows. It seems that these invalid low-energy models lead to a Λ_c which cannot be taken as the scale for the physical gap.

All numerical values in this chapter are given in units of the hopping t .

6.1 Attractive Hubbard model

Although the main focus of this work is on the repulsive Hubbard models, it is also interesting to study the attractive case $U < 0$. In this model an instability toward an s-wave superconductor already appears in a simple mean-field calculation. It is known that mean-field calculations have a tendency to overestimate the size of order parameters, or even predict phases which do not exist in the exact solution. This is due to the fact that fluctuations, which are not included in the MF calculations, usually reduce order parameters or even destroy the symmetry breaking. The reduction of the gap was shown in a $1/d$ expansion by [van Dongen 1991], in the 2D-Hubbard model by [Martín-Rodero and Flores 1992] and for a continuum model by [Kuchiev and Sushkov 1996].

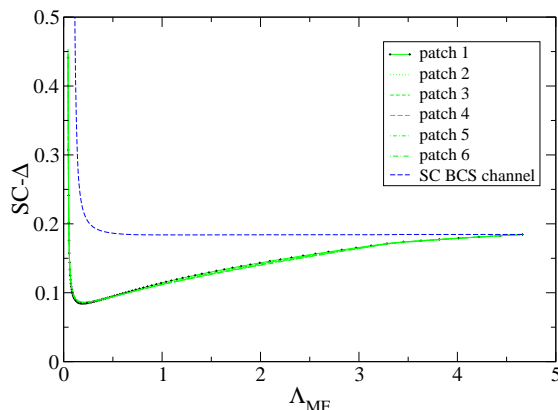


Figure 6.1: The SC s-wave gap as a function of the MF cut-off. Parameters $U = 1.5$, $t' = -0.1$, $n \sim 1$. Patch is referring to the BZ discretisation, depicted in fig. (2.1).

In fig. (6.1) a typical flow is shown. At $\Lambda = \Lambda_0 \approx 4.66$ no states are integrated out by the RG. Therefore the MF solution is the solution for the bare model. Treating high energy degrees of freedom by the RG leads to a reduction of the gap. As this reduction is due to the two particle-hole diagrams, it is interpreted as a ph-fluctuation renormalisation of the gap.

If these ph-contributions are suppressed, the change of phase space is compensated by the changed interaction, also shown in fig. (6.1). This can be used to check the numerics, as well as the quality of some of the approximations. Observe that for the SC case these approximations are much better than for the AF case presented in section 4.3. This is because the two involved particles of the SC vertex are either both at the FS or away from it, while in the AF

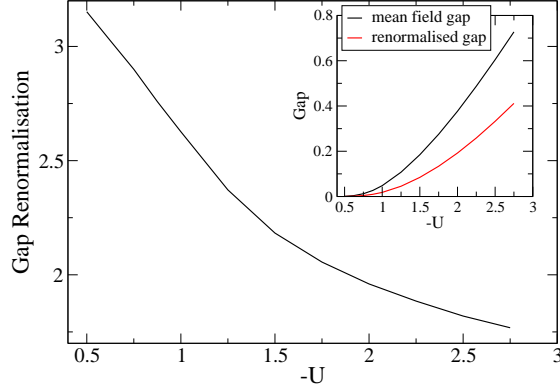


Figure 6.2: The gap renormalisation $\Delta_{\text{MF}}/\Delta_{\text{min}}$ for $t' = -0.1$ and $n \approx 1$ ($\delta_{vH} \approx 0.1388$).

case, involving momenta k and $k + Q$, this is only true in special cases. The essential degrees of freedom for the AF-MF calculations are (parts of) the umklapp surface, which might not be part of the low energy model well above Λ_c , see sec. (4.3) for details. The essential degrees for the SC case are the states close to the FS, which are only integrated by the RG in the limit $\Lambda \rightarrow 0$, which is not reached.

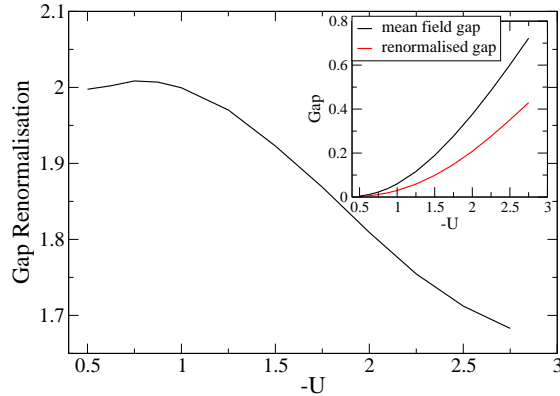


Figure 6.3: The gap renormalisation $\Delta_{\text{MF}}/\Delta_{\text{min}}$ for $t' = 0$ and $\mu = 0$.

The most physical solution is assumed to be the minimal gap. There the fluctuations had the strongest impact, while the increase for lower Λ is due to the breakdown of the symmetric RG flow; there the approximation of the full flow by a flow in the symmetric state breaks down.

In figures (6.2)-(6.4) the gap renormalisation, defined as the ratio between the MF gap of the bare model and the minimal gap from the RG and MF combination is shown. In fig. (6.2) the gap renormalisation increases steadily with decreasing bare interaction, while in fig. (6.3) the gap renormalisation saturates around $U \approx -1.0$; for the parameters $t' = \mu = 0$ used here, the bare FS includes the van Hove points leading to a strong \log^2 -divergency in the

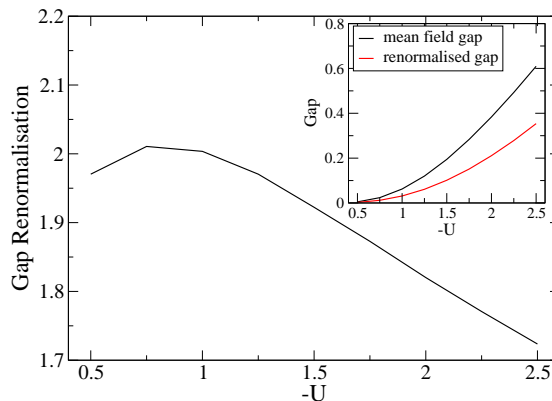


Figure 6.4: The gap renormalisation $\Delta_{\text{MF}}/\Delta_{\text{min}}$ for $t' = -0.1$ and $\delta_{vH} = \mu - 4t' = 0$.

pp-diagram. The closeness to the van Hove points seems to lead to the saturation at this scale of U , as the gap renormalisation for finite $t' = -0.1$, again with a bare FS including the van Hove points, shows the same saturation, see fig. (6.4).

It was not investigated, whether this saturation is an artefact of the calculations or of physical origin. But it seems probable that the strong divergency of the pp-bubble leads to a larger divergency scale Λ_c ; this effect becomes larger for smaller U , since there the RG integration gets closer to the vH points. Therefore this saturation might be an artefact of the minimal-gap stop criterion.

6.2 Repulsive Hubbard Model

In the following the repulsive Hubbard model, $U > 0$, is discussed. The dominant instabilities over a wide range of parameters are an s-wave antiferromagnet and a d-wave superconductor [Zanchi and Schulz 2000; Honerkamp et al. 2001; Halboth and Metzner 2000]. First calculations where only one of the gaps is allowed, are presented. Then the interplay of both is shown. In section 6.2.4 the numerical results for the pi-pairing will be shortly discussed.

The stop criterion is the relation between the maximal gap value and the cut-off Λ . It is always chosen to be $\Lambda/\Delta = 2.0$, which seems reasonable in all cases. The dependence on this ratio is discussed at the end of the chapter.

6.2.1 Only Superconducting Gap

The flow equation (2.37) produces an attraction for a d-wave superconductor from the purely repulsive HM. A sizable attraction develops only at low scales. Two plots are presented in fig. (6.5). While in the first case (left) a flattening is seen before the gap diverges, although this flattening is not perfect, in the second case no such feature appears. In the first case the bare FS is well away from the van Hove points, whereas in the second case the FS is closer to the

van Hove points leading to a contribution of all diagrams of the flow equation down to very low energy scales. Therefore, no regime of flattening is found.

Usually for smaller initial U bigger ranges of compensation, or plateaus are found, as Λ_c becomes much smaller, meaning that the ph diagrams do not contribute any more well before the flow diverges.

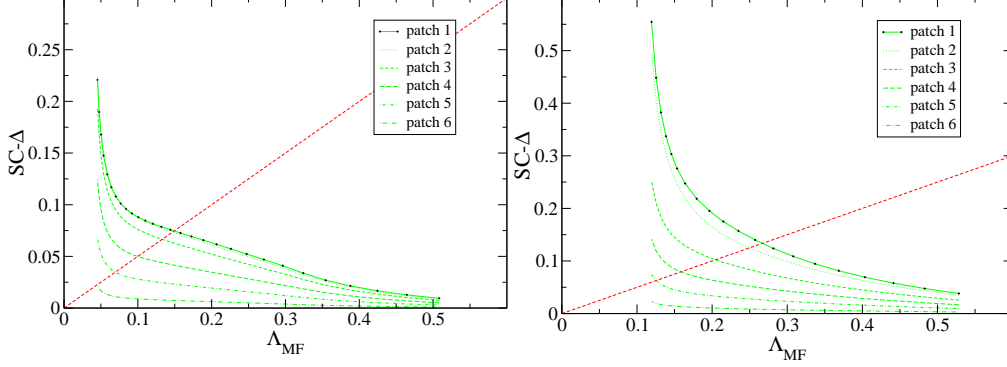


Figure 6.5: The SC gap as a function of the MF bandwidth Λ_{MF} for two different μ . The red line depicts the used stop criterion. $U=2.5$, $t' = -0.2$, $\mu = -0.477$ (left) and $\mu = -0.687$ (right).

As a plateau can not always be identified, and even in these cases some arbitrariness would be introduced in determining the exact position, the ratio of the cut-off and the maximal gap value, that is the maximal value of the SC-gap as a function of k , is used as a stop criterion. The criterion is depicted as a dashed red line in the graphs. By this procedure the SC gap as a function of μ is obtained, shown in fig. (6.6), left.

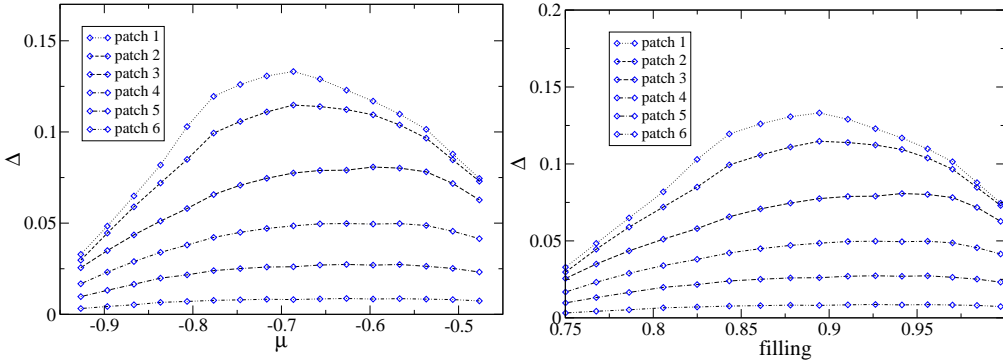


Figure 6.6: The superconducting gap as a function of the chemical potential (left), and as a function of the filling (right), if no AF gap is allowed. $U = 2.5$, $t' = -0.2$.

The superconductor has, as a function of the chemical potential, a dome-like structure, with a maximum close to, but not exactly at $\mu_{vH} = 4t' = -0.8$. While the scattering phase space is largest exactly at the van Hove filling, the d -wave attraction increases for a little larger chemical potential, leading to a small shift of the maximum.

In fig. (6.6), right, the SC gap is plotted as function of the filling. As a Fermi surface exists even at half filling, due to the lack of the AF gap, it is not surprising that there also a finite SC gap is found.

6.2.2 Only Antiferromagnetic Gap

The Hubbard model produces an s-wave AF already on the mean-field level. Similarly to the attractive HM ($U < 0$), the gap gets renormalised by fluctuations. In contrast to the SC the AF can have first order transitions as a function of the interaction, see chapter 4. Additionally, certain peculiarities can arise when combined with an RG scheme, see sec. (4.3), which make the validity of the here used method at very low scales Λ_{MF} doubtful.

In fig. (6.7) the dependence of the AF-gap on the mean-field cut-off Λ_{MF} at $\delta_{vH} = \mu - 4t' = 0$ is shown. Since the AF-gap equation has a solution for arbitrarily small interaction at μ_{vH} , thus being similar¹ to the SC case with attractive U , a comparable behaviour is expected. Indeed the gap gets first renormalised, then saturates, and finally diverges at a low energy scale Λ_c .

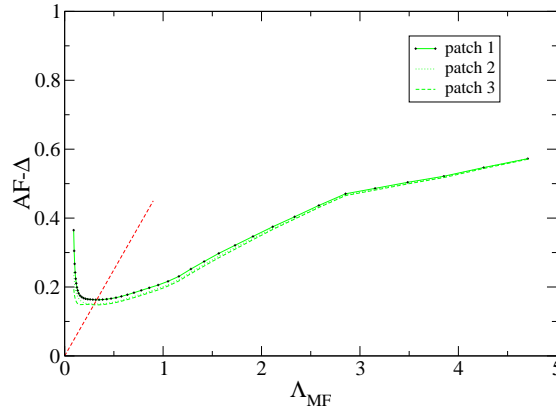


Figure 6.7: The AF gap as a function of MF band-width Λ_{MF} at $\delta_{vH} = \mu - 4t' = 0$. $U = 2.5$, $t' = -0.15$. The scale dependence is similar to the SC case for the attractive HM.

For $\mu < \mu_{vH}$ the AF gap can discontinuously jump to zero if the potential is below a certain value. In fig. (6.8) a run for $\delta_{vH} = -0.04 < 0$ is shown, where at a scale $\Lambda \approx 0.3$ the potential is so strongly renormalised, that the gap breaks down. For Λ scales little larger than this point the non-zero solution is metastable with respect to the zero solution, but this appears only in a tiny region for the here chosen U and t' , therefore no attention is paid to this fact here.

If the potential is large enough, the AF is expected to show maximal gap values much above $\mu_{vH} = 4t'$ around $\mu = 2t'$, where the electron and hole pocket close for the same gap value $\mathcal{A} = |2t'|$. A solution is only found if

¹ But not the same. Due to the existence of the FS the Fermi functions effectively reduce the integration area of the RHS, reducing the AF-gap compared with an SC-gap for the same interaction strength.

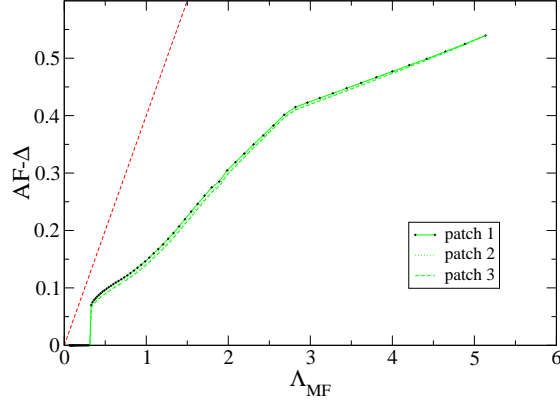


Figure 6.8: The AF gap for μ below $\mu_{vH} = 4t'$. The first order transition as a function of the interaction causes an abrupt break down of the gap. $U = 2.5$, $t' = -0.15$, $\mu = -0.64$.

the gap is larger than $|2t'|$, leading to a fully gapped, and therefore half-filled system, see section 4.2 for details. A run close to this point, leading already to a half-filled system, is shown in fig. (6.9). A plateau is forming around $\Lambda \approx 0.75$. For smaller $\Lambda < 0.5$ the gap breaks down to a much smaller value, which is due to the creation of the unphysical low-energy model, in which parts of the BZ, essential for the MF calculation, are integrated out. This is possible because of the very different Fermi surface topology of the ungapped and the gapped system. This problem is discussed in detail in section 4.3 within a MF-exact model. Therefore the plateau around $\Lambda \approx 0.75$ has to be considered as the renormalised, physical solution.

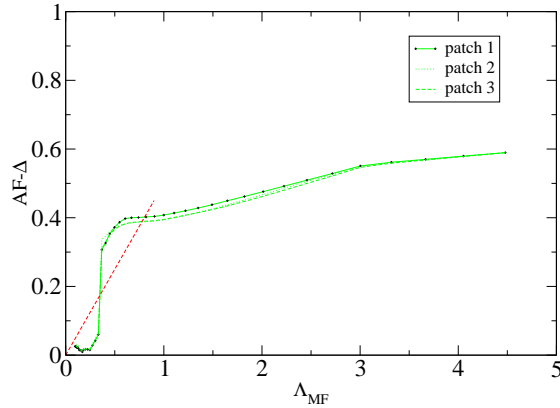


Figure 6.9: The AF gap close to $\mu = 2t'$ where half filling is forced by an existing gap, by fully gapping the system. $U = 2.5$, $t' = -0.15$, $\mu = -0.35$.

If the potential U was not strong enough, the gap would break down, or be zero already in MF theory, since the minimal AF gap is there $\mathcal{A} > |2t'|$. In this case the frustration due to t' would lead to a half-filled system without an AF gap, in contrast to the naïve expectation, and only in an (unsymmetric) region

around μ_{vH} AF solutions would be found.

Applying the stop criterion $\Lambda_{MF}/\mathcal{A} = \text{const}$ enables one again to plot the gap as a function of the chemical potential. This is shown in fig. (6.10). The

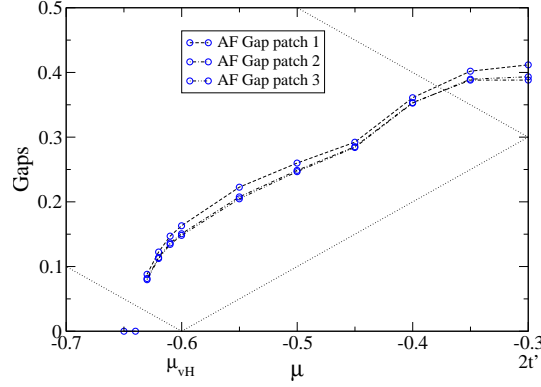


Figure 6.10: The AF gap as a function of μ Parameters: $U = 2.5$, $t' = -0.15$, 3 patches. Thin, dotted lines mark the AF values for which effective Fermi surfaces appear. Gap values larger than both lines correspond to fully gapped, half-filled systems, below one line a pocket opens (here a hole pocket); no non-zero solution is stable below both lines.

result is qualitatively similar to the unrenormalised MF calculation shown in fig. (4.17), with a reduced U . Observe however that the solution is not strictly constant around $\mu = 2t' = -0.3$. Changing μ should have no influence on the solution as μ is within the gap of a fully gapped system. The slight dependence is most likely due to the stop criterion, as it leads to effective low-energy models which include different degrees of freedom, as Λ is defined with respect to the FS, which is shifted by μ . Two systems for which the gap breaks down before the stop criterion is reached are included as zero solutions; they show that here again a jump in the AF order parameter occurs at a certain value $\delta_{vH} \approx -0.035$.

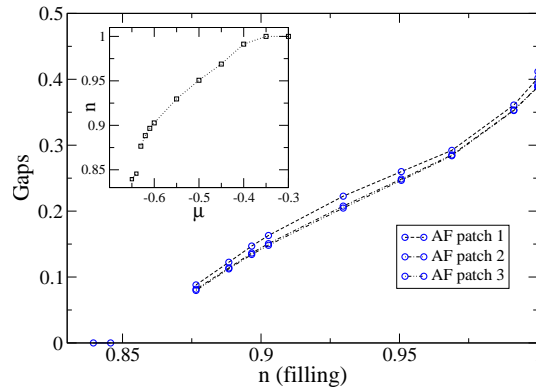


Figure 6.11: The AF gap as a function of the filling, $U = 2.5$, $t' = -0.15$. The inset shows the jump in the filling due to the jump in the AF gap value for a certain μ .

The gap versus the filling is plotted in fig. (6.11). Again it is very similar to the pure MF calculation with slightly reduced U , see fig. (4.18). The jump of the AF order parameter leads to a jump in the density, which is illustrated in the inset.

6.2.3 Interplay of both Gaps

In the following results are presented, where an SC-d-wave-gap and an AF-s-wave-gap are both allowed. Only the hole-doped side will be considered. The electron-doped side leads to difficulties, which are discussed in section (6.2.5).

If a large AF order parameter gaps out the FS completely, or reduces the FS to a small pocket around² $(\pi/2, \pi/2)$, the SC gap will be zero or exponentially small. Therefore it is expected to find SC solutions only close to or below $\mu_{vH} = 4t'$, where the effective FS is extended, leading to a reduced AF gap, so that the SC gap can coexist with, or even suppress the AF gap. If the AF breaks down, an SC gap has to be created, as for any small potential a SC is created if an FS exists; the RG creates an attractive interaction in the d -channel from the purely repulsive electron-electron interaction, albeit it might be small.

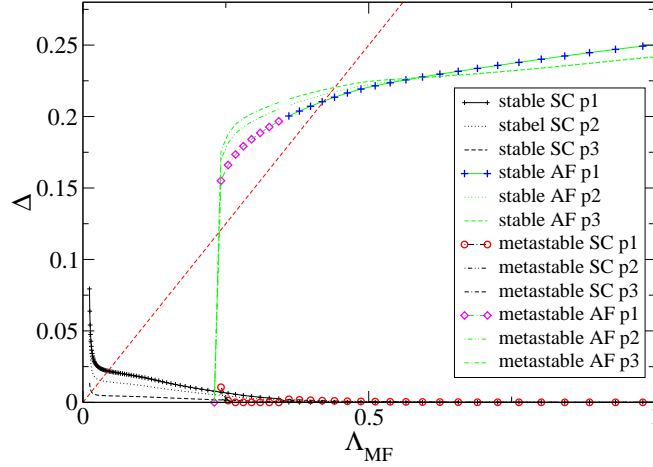


Figure 6.12: Cut-off dependence of the AF and SC gap. Comparing the free energy (not shown here) of the finite AF solution with the free energy of a pure SC solution determines the stable one. For large Λ_{MF} the finite AF solution is preferred, while at $\Lambda_{MF} \approx 0.35$ the AF zero-gap solution has lower free energy. The SC has inverse behaviour, being suppressed by the AF. Abbreviation 'p' stands for 'patch'. Parameters $t' = 0$, $U = 2.0$, $\mu = -0.13$.

6.2.3.1 Zero Next-Nearest Neighbour Hopping

Fig. (6.12) shows the Λ_{MF} dependence of the AF and SC for $t' = 0$. The system is fully gapped as long as the AF gap is present, therefore no SC appears, while an SC gap builds up for Λ_{MF} -values, where the AF gap is zero. It is shown in

² As it is expected for the hole-doped case, see chapter 4.

section (4.1.1) that for $t' = 0$ there is a big range of μ where AF metastable solutions exist; corresponding free energies are plotted in fig. (4.14). Thus the free energy of the AF solution is compared with the pure SC solution, leading to a range where the AF is metastable, see again fig. (6.12). It is not checked, from which scale on the zero AF solution metastably exists, since the focus is on the stable solution. It is assumed that the SC gap is too small to destabilise the zero AF solution, i.e., to change the minimum with respect to the AF gap of free energy at $\mathcal{A} = 0$ to a maximum, which is in principle possible, see section (5.3.1).

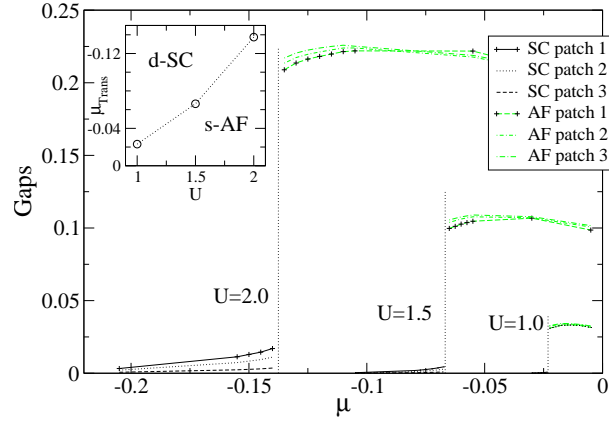


Figure 6.13: Gap sizes and transition- μ for $t' = 0$. The phase diagram in the inset. Dotted lines depict change from pure AF to pure SC solutions.

Depending on the scale where the AF gap breaks down, the stop criterion leads either to a pure SC or a pure AF solution. The phase diagram and the gap sizes are shown in fig. (6.13); there is always a sharp μ for which the system changes from the SC to the AF state, as no coexistence is found. The SC gap becomes very small for small U , so that for $U = 1.0$ the SC gap is practically invisible.

6.2.3.2 Finite next-nearest Neighbour Hopping

The results change qualitatively for a finite t' . Now the SC and the AF gap can coexist. A typical Λ_{MF} -dependence of the gaps is shown in fig. (6.14). The nonzero AF gap, coexisting with an SC gap, is nearly always the stable solution, and only in a very narrow range a pure SC state is preferred. Therefore further on a nonzero AF gap will be chosen, if it exists at all, and no check of metastability of the solution with a finite AF gap with respect to a pure SC state will be performed.

In fig. (6.15) the corresponding phase diagram is presented. For a medium-sized bare interaction of $U = 2.0$ coexistence is found close to $\mu_{vH} = 4t'$, for lower μ the superconductor wins³. AF dominates going towards $\mu_{1/2} = 2t'$,

³ Here a finite AF solution with a FS is considered to be a pure AF already if the SC is numerically zero (at least 10^{-3} smaller than the AF).

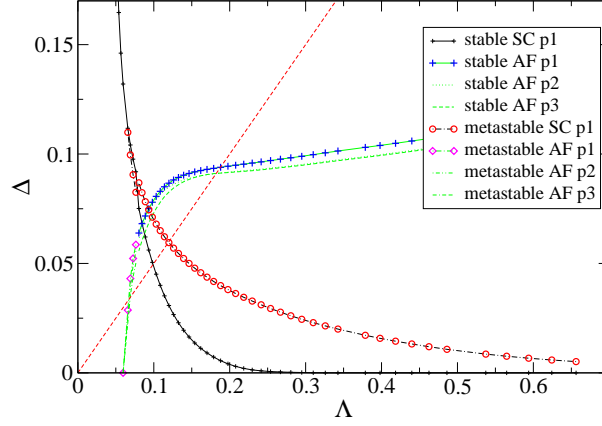


Figure 6.14: Λ_{MF} dependence of the AF and SC gap for finite $t' = -0.1$, $U = 2.0$, $\mu = -0.401$, and comparison with a pure SC state. The free energy determines which of the solutions is stable and which is metastable. Only the anti-nodal SC gap value is shown.

at which half filling is forced, if a AF gap exists, see page 40. At $\mu_{1/2}$ for an AF solution the frustration by t' is too strong so that the SC takes over again. However, analysing the corresponding RG+MF-run, one can see that the AF gap is close to survive for $\mu = \mu_{1/2}$.

For larger $U = 2.5$ the situation resembles the $t' = 0$ case, having less or no coexistence, and an abrupt change from the AF to the SC dominated system.

For smaller U the AF range is reduced more and more; first the frustration of the AF gap due to t' becomes too big at $\mu_{1/2}$, where the AF system was fully gapped and therefore half-filled. For even smaller U the range where the AF is destroyed is growing towards μ_{vH} until the superconductor gap is the only one over the whole range of μ .

At $\mu_{vH} = 4t'$ the pp and the ph bubble diverge, which is interpreted as competing instabilities of SC and AF type. This point is therefore of special interest and is studied in the following. The corresponding plot is presented in fig. (6.16). At a given U for small t' the AF wins, as expected. There the system is close to half filling, leading to no or only a small FS. For intermediate t' a coexistence region is found, while for big t' the superconductor wins. This is in qualitative agreement with earlier findings, based on flows of susceptibilities [Halboth and Metzner 2000]. The numerical values do not fit perfectly, which was expected because they depend on the exact stop ratio in this scheme, and on the break size⁴ of the susceptibilities in the other. However the methods should be most comparable for μ_{vH} , since there not first order transition is expected, making the susceptibility a reasonable indicator⁵.

The possibility of having a doped AF and the coexistence with the SC due

⁴ The large but finite size of the susceptibilities which determines the divergence scale Λ_c in the numerics; the true divergence point can of course not be determined numerically.

⁵ It is, however, not guaranteed that a stronger divergence of the susceptibility necessarily leads to a larger free energy gain of the symmetry-broken state.

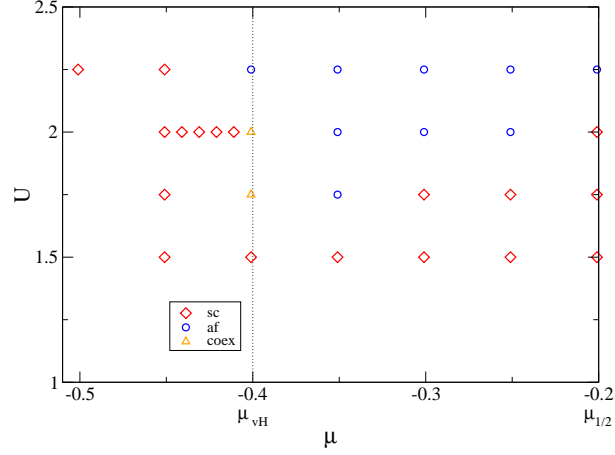


Figure 6.15: The phase-diagram for finite $t' = -0.1$. For large U it resembles the $t' = 0$ case, while for lower U the AF is frustrated, and destroyed starting at $\mu_{1/2} = 2t'$, leading to a superconducting system. For moderate U a range of coexistence is found.

to a finite t' seems to be the most interesting case and is examined in more detail in the following. If the interaction is strong enough to create an AF gap $\mathcal{A} \gtrsim |2t'|$ at $\mu = 2t'$ half filling solutions are possible, providing a guideline for the parameters U and t' . The first three sets of data are discussed with a bare interaction of $U = 2.5$ and with different $t' = -0.2, -0.15, -0.11$, to understand how in detail the gaps depend on the next nearest neighbour hopping. Then a system with $t' = -0.11$ but a smaller $U = 2.25$ is presented. For higher U or lower U the system is similar to $t' = 0$ or always superconducting, respectively.

For $U = 2.5$ and $t' = -0.15$, fig. (6.17), the AF gap at $\mu = \mu_{1/2} = -0.3$ is $\mathcal{A} \approx 0.42$. Therefore, the system is fully gapped and half-filled. The SC gap is numerically zero, and is expected to be truly zero due to lack of a FS. Towards the van Hove chemical potential $\mu_{vH} = 4t' = -0.6$ the AF solution crosses the line depicting the appearance of a FS. The AF gap size is therefore reduced, but stays finite. The SC gap is numerically still zero, even though a tiny value is expected, as in the presence of a FS a finite attraction always creates a SC gap. However the FS being small, and close to the points $(\pi/2, \pi/2)$, see fig. (6.21), the SC gap is strongly suppressed.

Close to μ_{vH} the AF gap is strongly reduced and a sizeable SC gap appears, which becomes bigger than the AF gap for an even smaller chemical potential. For an even lower μ the AF gap is truly zero.

In fig. (6.18) the same data is plotted as a function of the filling and, for comparison, the results of the calculations where only SC or only AF is allowed. As expected, the AF gap is maximal at half filling. The AF gap has the same size as in the only-AF calculation, while the SC gap, being finite in the only-SC calculation, is now suppressed to zero. At the point where the superconductor wins over the AF a jump in the filling is found. This is, as in the pure AF case, due to the jump in the AF gap, which strongly changes the filling.

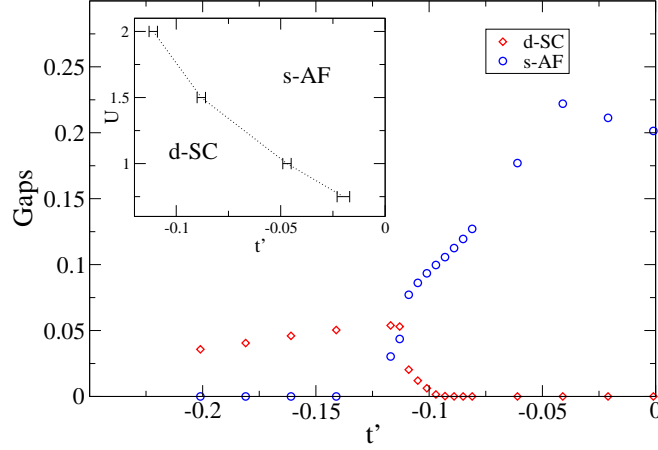


Figure 6.16: The phase diagram at $\delta_{vH} = 0$. For small t' the AF dominates, while for large t' the system is purely superconducting, in contrast to $t' = 0$ a coexistence region is found. Phase-diagram in the inset, line marking the cross-over.

For three different choices of μ , or fillings, the gap structure and the effective FSs are shown in figures (6.19)-(6.21). In the numerics only the angular part of the k -dependence was taken into account. The angle is measured with respect to one crystal axis. In fig. (6.19) a doping with zero AF gap and finite SC gap is chosen, the d-wave gap structure is clearly visible. The k -dependence is generated by the RG, and is not assumed to have a special form. Frequently, in previous calculations a special form, for example $\Delta(\cos k_x - \cos k_y)$, was assumed. The effective (gapped) Fermi surface is identical to the bare one.

For a μ close to half filling, fig. (6.21), the SC gap is numerically zero. The AF gap has s-wave-structure, with a slight enhancement at the crystal axes. The FS is a small hole pocket around $(\pi/2, \pi/2)$. The smallness of the FS and the weak d-wave potential for the SC around the nodal points lead to a strong suppression of the SC gap.

In the coexistence region, fig. (6.20), the FS has extended to be of nearly the same size as the bare one. However, the small part at the van Hove points between hot spots and the crystal axis is not part of it. Due to this big FS which is also closer to the van Hove points than the one in fig. (6.21) a finite SC gap is possible. The enhancement of the AF gap at the crystal axis is stronger than in fig. (6.21).

For a comparison, now two further sets of data are discussed, having the same bare potential $U = 2.5$, but a larger $t' = -0.2$ and a smaller $t' = -0.11$.

For smaller $t' = -0.11$ the data are shown in fig. (6.22) and fig. (6.23). The maximal values of the AF gap are obtained close to $\mu = \mu_{1/2} = 2t' = -0.22$, for half filling. It has the approximately same value as the half-filled AF value in the $t' = -0.2$ case. This is in agreement with the pure mean-field calculation of chapter 4, where it was found that the AF half-filling solution, if it exists, is independent of t' . It is also expected to be independent of μ for a fully gapped

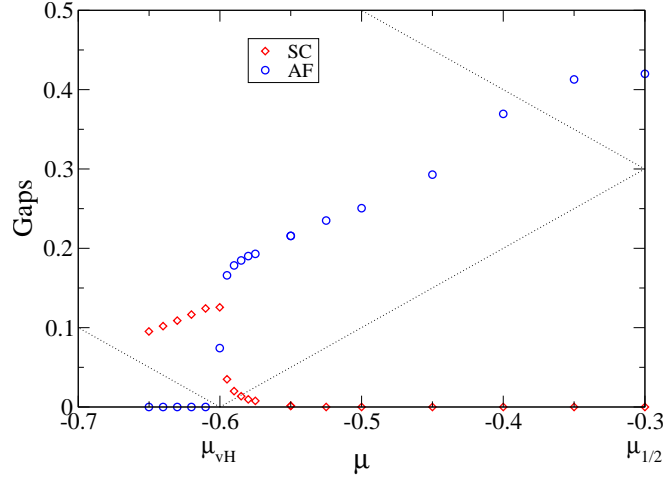


Figure 6.17: Gaps as a function of μ for $U = 2.5$, $t' = -0.15$, $\Lambda_{\text{MF}}/\Delta = 2.0$. Lines for which FSs disappear due to the AF gap are depicted. Coexistence is found close to $\mu_{vH} = 4t'$.

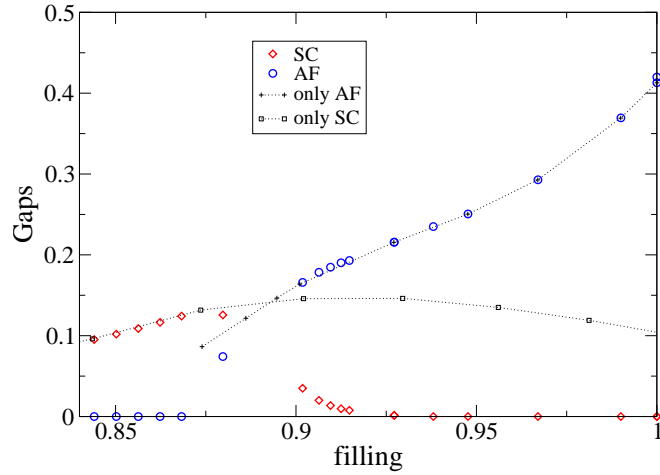


Figure 6.18: Gaps as a function of the filling for $U = 2.5$, $t' = -0.15$. $\Lambda_{\text{MF}}/\Delta = 2.0$. Towards half filling the AF dominates, while for strong doping the SC wins. Coexistence is found in the cross-over region. The AF gap value at half filling is not unique, since a slight μ -dependence of the half filled solution was found, see fig. 6.17. For comparison results from calculations where only the SC gap or only the AF gap was allowed are shown.

system, which is not fulfilled very well here. This problem was already discussed in sec. (6.2.2), and is stronger here, since the gapped μ -range is rather large.

Since the region (as a function of μ) of the half-filled system is larger, the region of the doped AF is smaller, and in contrast to the $t' = -0.15$ case the AF is still dominant at $\mu_{vH} = -0.44$ leading to a smaller range of coexistence.

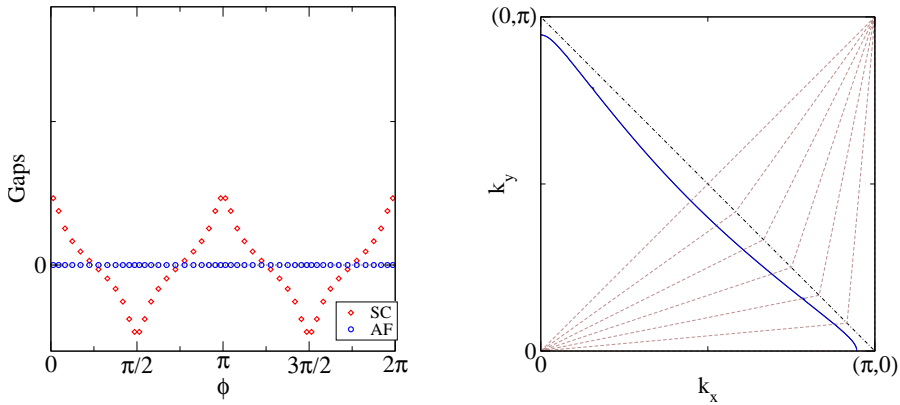


Figure 6.19: The gap structure as a function of the angle with respect to a crystal axis for strong doping $n = 0.8623$, $\mu = -0.6201$ (left); the effective (gapped) Fermi surface is on-top of the bare FS (right). The AF gap is zero resulting in a system with a pure SC order parameter. Patches are depicted by thin dashed lines.

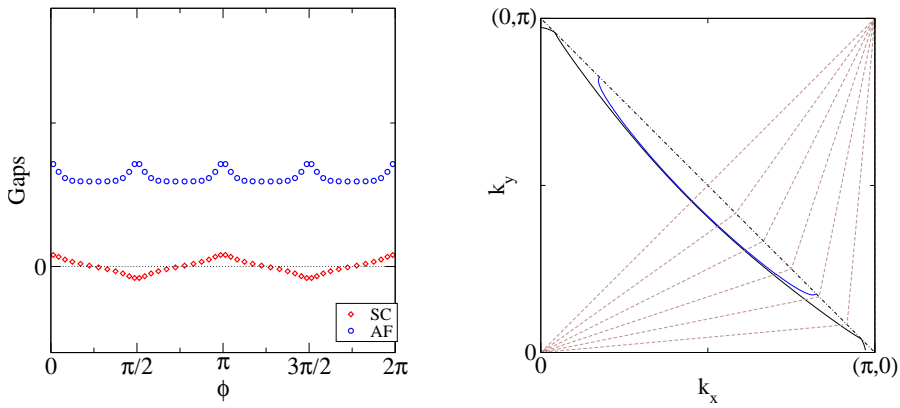


Figure 6.20: The Gap structure and the Fermi surfaces at $\mu = -0.59$, $n = 0.9063$, AF and SC coexist.

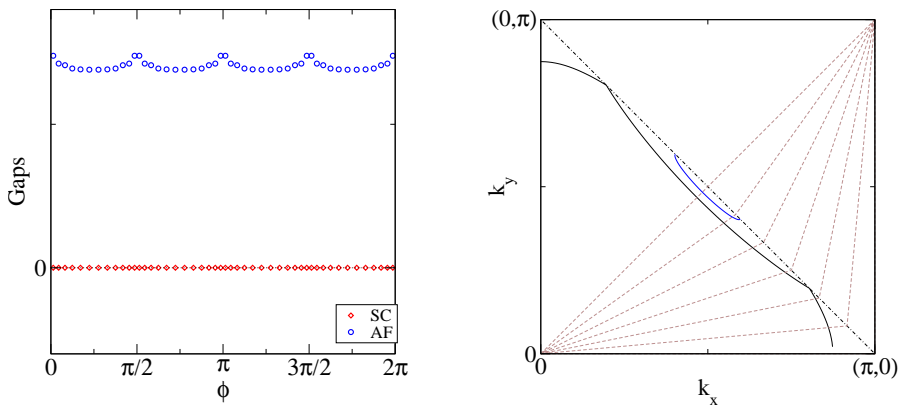


Figure 6.21: The Gap structure and the Fermi surfaces at $\mu = -0.4$, $n = 0.99$. Close to half filling the AF dominates and the SC gap is numerically zero.

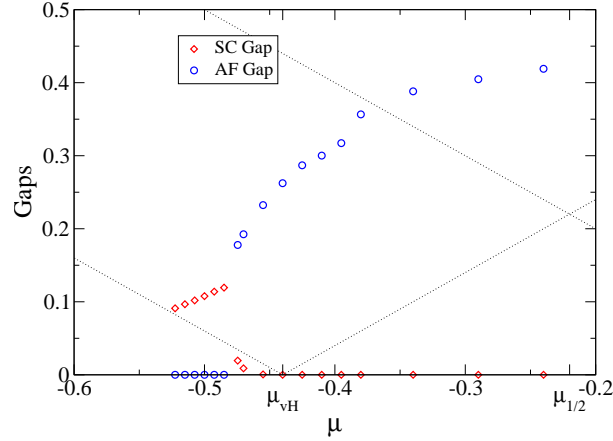


Figure 6.22: Gaps as a function of μ , for a smaller $t' = -0.11$ than before (fig. 6.17). The fully gapped region becomes larger, while the doped region becomes smaller. Solutions at μ_{vH} are closer to half filling so that there the AF gap still dominates. Parameters: $U = 2.5$, $\Lambda/\Delta = 2.0$.

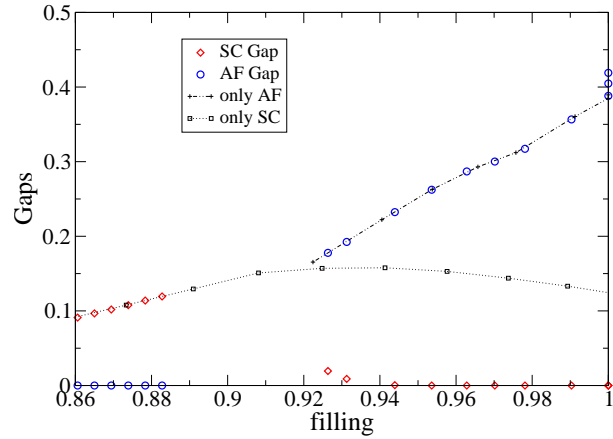


Figure 6.23: Gaps as a function of the filling for $U = 2.5$, $t' = -0.11$, $\Lambda/\Delta = 2.0$. The half-filled AF gap is not unique due to the μ -dependence of the fully gapped solution.

This becomes clear if one compares with the $t' = 0$ case, fig. (6.13). There, a jump from the AF fully gapped, half-filled system to a pure SC state was found; in a finite region around $\mu = 0 \equiv \mu_{vH}$ the AF is the only solution. The solution for $t' \rightarrow 0$ should more and more resemble the $t' = 0$ case.

For the larger $t' = -0.2$ the coexistence region grows and is shifted to higher μ , being situated now well above the van Hove chemical potential μ_{vH} , see fig. (6.24). The jump of the AF gap in the coexistence region is much smaller, and therefore also the jump in the filling. The magnetic frustration due to the diagonal hopping t' is now so strong, that for $\mu = \mu_{1/2} = 2t'$ the interaction renormalisation leads to a break-down of the AF gap, so that even

at half filling a superconductor is found. Surprisingly, for a finite doping the AF gap is still finite. Fluctuations might change this since the free energy gain of this solution close to the value for which an electron pocket opens is rather small, see chapter 4.

If the bare interaction is reduced while keeping t' fixed, the range with a non-zero AF gap is further and further reduced, until the AF gap is zero everywhere leading to a superconducting ground-state for any doping.

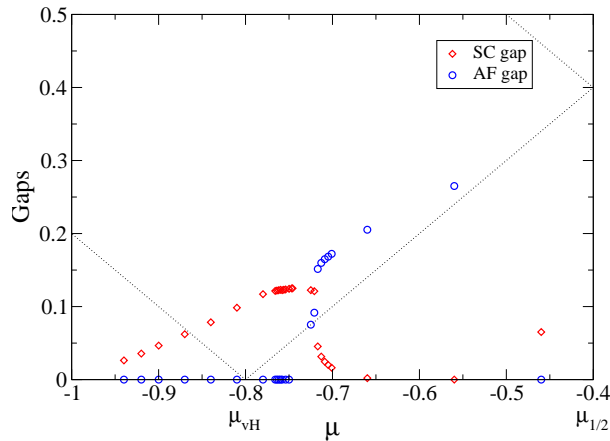


Figure 6.24: Gaps as a function of μ for $U = 2.5$, $t' = -0.2$. The frustration due to t' becomes too big close to $\mu_{1/2}$.

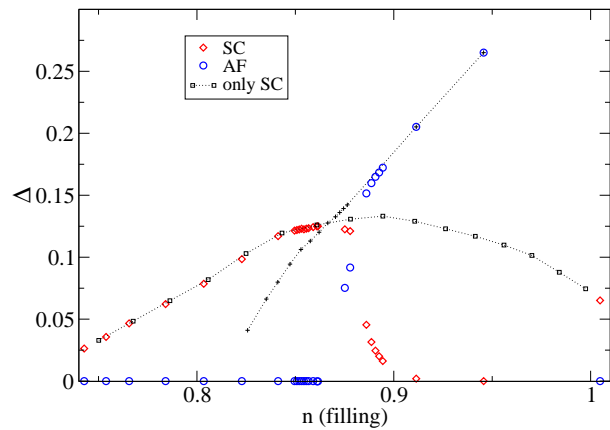


Figure 6.25: Gaps as a function of the filling. $U = 2.5$, $t' = -0.2$. At half filling the AF gap is zero yielding a SC ground state.

If for $t' = -0.11$ the bare potential is reduced from $U = 2.5$ to $U = 2.25$, figures (6.26) and (6.27), the half-filled μ -range becomes smaller, and the range of the doped AF bigger; also the relative jump of the AF gap in the coexistence region becomes smaller. Qualitatively the plot resembles the diagram for $U = 2.5$ and $t' = -0.15$.

The jump of the AF gap from a finite to a different but also finite value

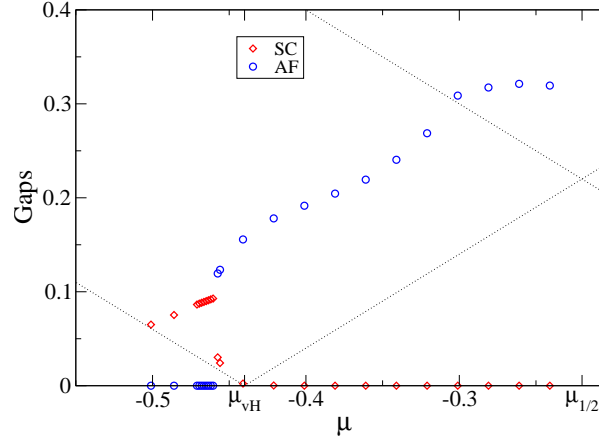


Figure 6.26: Gaps as a function of μ . $U = 2.25$, $t' = -0.11$, $\Lambda/\Delta = 2.0$.

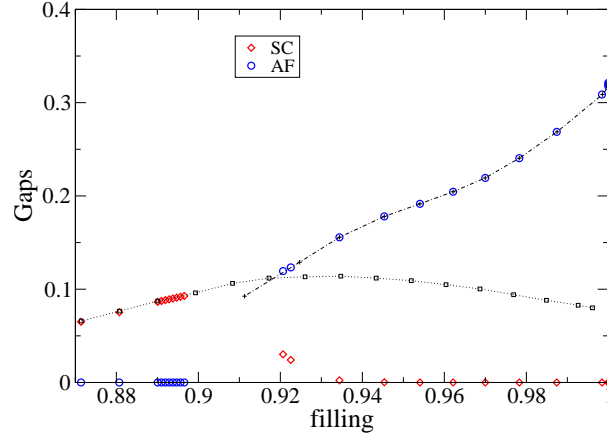


Figure 6.27: Gaps as a function of the filling. $U = 2.25$, $t' = -0.11$, $\Lambda/\Delta = 2.0$

close to $\mu_{vH} = 4t'$ is surprising (see fig. 6.17, fig. 6.18). It is due to the fact that the AF gap for the two calculations breaks away at a finite Λ_{MF} -scale, so that the stop criterion in one of the calculations is reached due to the AF gap and in the other, where the AF gap breaks away for slightly larger Λ_{MF} , due to the SC gap. Typically the SC gap is smaller at this scale. This leads to a jump in the scale Λ_{MF} , down to which the RG is employed and thus to a jump in the AF gap. Therefore, the way the jump is created is closely connected to the stop criterion, and might therefore well be an artefact of the method.

The jump of the AF gap from a finite value to zero, seen before in the pure AF case, is not always observable any more if a SC gap is allowed. It is possible that the inclusion of the SC gap changes, for suitable values of the potential, the AF transition to a continuous one, see section 5.3.1. It is, however, difficult to resolve this area well, because the numerics is very involved there; the RHS of the AF gap has nearly the same slope as the bisector (similar to a RHS at the critical point) leading to very bad convergence of the self consistency equation.

The dependence on the stop ratio is shown in fig. (6.28). It can be seen that the overall picture does not change much. The strongest change is in the μ value, for which the crossover between AF and SC is found. The amplitude of the SC gap changes moderately. If plotted against the filling the AF gap does hardly change, as the AF gap size strongly determines the filling.

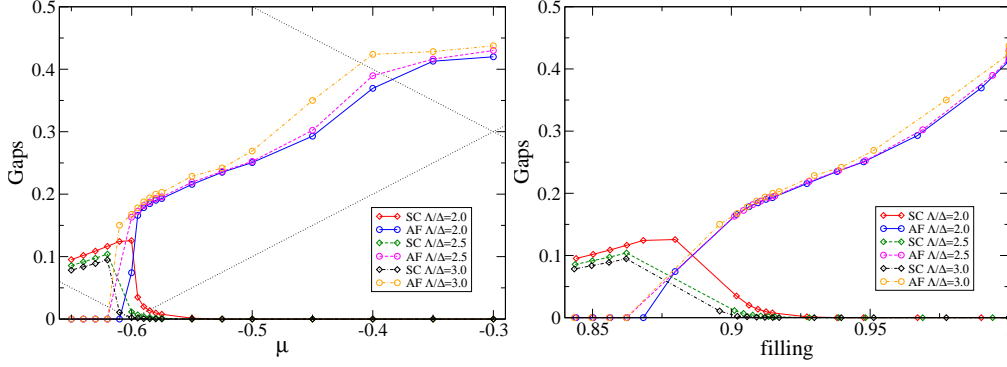


Figure 6.28: Dependence on the stop ratio Λ/Δ . Qualitatively the results change only slightly.

The value $\Lambda_{\text{MF}}/\Delta = 2.0$ used here proved to work well in all cases for a bare coupling of $U \approx 2$. The gaps are at or close to a plateau, if it exists. The energy cut-off Λ_{MF} of the systems where the AF gap dominated were well above the cut-off of the invalid low-energy model discussed in section 4.3.

6.2.4 The Pi-pairing

It was found in section 5.1 that the pi-pair needs a big attractive potential to have a self consistent non-zero solution. No strong attractive interaction is created by the RG, but instead a repulsive d-wave component is found, see

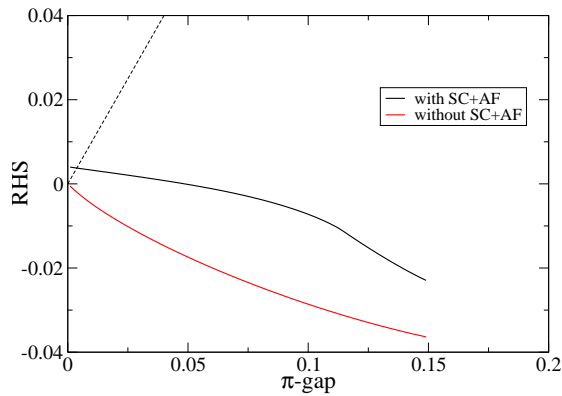


Figure 6.29: The RHS of the d-wave pi-pair, with and without other gaps, see text. Since the RHS is negative for positive π -gap values the interaction is repulsive.

fig. (6.29). Following [Kyung 2000] it was mentioned in section 5.3.2 that a

π -gap is created if the SC and the AF coexist. The RHS of the pi-pair in presence of a finite s-wave-AF and d-wave-SC gap is also shown in fig. (6.29); the gap sizes are taken to be the same as in the system depicted in fig. (6.30) at $\Lambda = 0.2485$, where the two gaps are of similar size, and the biggest effect on the RHS of the pi-pair is expected. The RHS is indeed nonzero at zero π -gap.

The self-consistent solution, given by the crossing point with the bisecting line, is of the same order as the zero gap value, but is difficult to reach by iteration, since the slope of the RHS is negative. Therefore, the self-consistent solution is replaced by the value of the RHS at $\pi = 0$, i.e., by the non-self-consistent or direct value. The direct value of the π -gap for one run is plotted

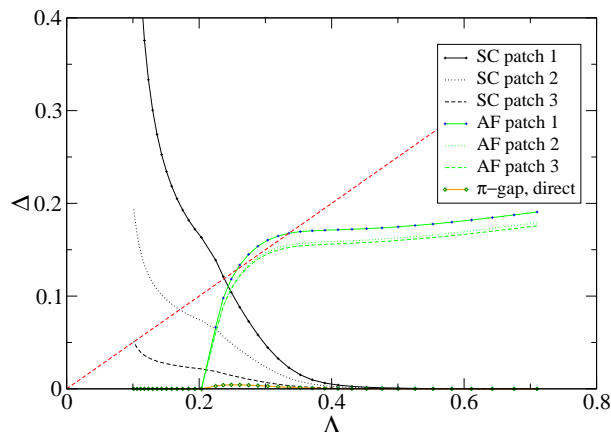


Figure 6.30: A coexistence run with the pi-pair, calculated non-self-consistent.

in fig. (6.30). It is indeed biggest close to $\Lambda = 0.2485$, where it is $\pi \approx 0.004$, which is two orders of magnitude smaller than the other gaps. It is therefore neglected in the other calculations. This finding is in agreement with findings for the $t - J$ model of [Yamase and Kohno 2004].

6.2.5 Electron-doped Side

All data presented so far were for hole doped systems. Here, some results for the electron-doped side are presented. The stop criterion plays an essential rôle for determining which degrees of freedom are treated by the RG and which are treated within the MF approximation. Unfortunately, no satisfactory criterion was found for the electron doped side.

It was discussed in section (4.1.3) that the solutions of the AF mean-field equation for $\mu > 2t'$, where the electron-doping is possible, differ from the side ($\mu < 2t'$, $t' < 0$), where the hole-doping is possible. Going away from the half-filled state the AF solution decays faster on the electron-doped (e-doped) side than on the hole doped (h-doped) side as a function of μ , see fig. (4.17), which finds its reason in the different properties of the electron and the hole pockets. Furthermore, while on the h-doped side a $\mu = \mu_{vH} = 4t'$ exists for which for an arbitrarily small interaction an AF solution is found, nothing comparable exists on the e-doped side.

Most importantly, for the e-doped side the gap's dependence on the interaction is much stronger than on the h-doped side, see again section (4.1.3) and fig. (4.12).

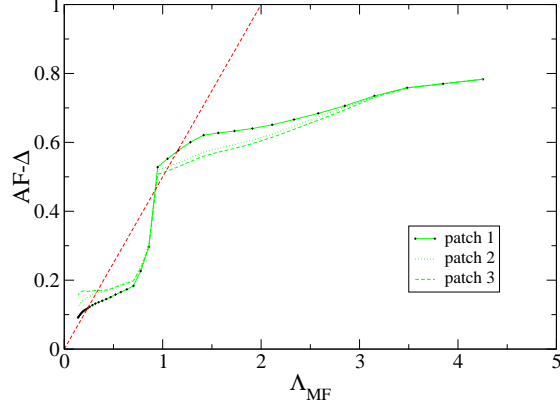


Figure 6.31: The AF gap for electron doping $\mu > 2t'$ as a function of the MF bandwidth Λ_{MF} . The red dashed line shows the standard stop criterion. It does not allow entering the doped regime for a big range of μ , due to the long persistency followed by a rapid change of the gap. Parameters: $U = 2.9$, $t' = -0.15$ and $\mu = -0.1$.

In fig. (6.31) the AF gap's dependence on Λ_{MF} is shown. For large scales the gap is only slightly renormalised; at a scale $\Lambda_{\text{MF}} \approx 1$ the gap value allows the appearance of an electron pocket, leading to a much more sensitive dependence on the renormalised interaction, resulting in a strong renormalisation in a small range of Λ_{MF} . At even lower scales the gap changes only slightly with Λ_{MF} and saturates to a much smaller gap-value.

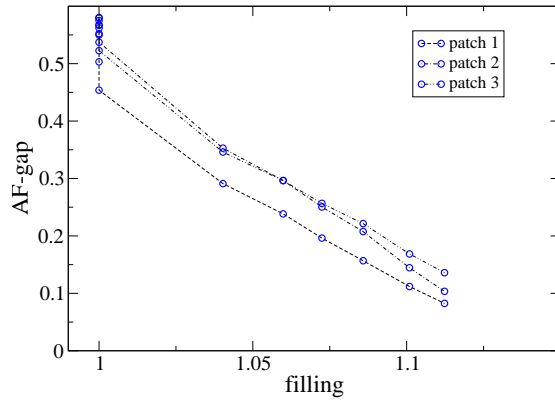


Figure 6.32: The AF gap as a function of the filling on electron doped side. The stop criterion differs from the one used before, see text. $U = 2.9$, $t' = -0.15$.

Due to this behaviour the stop criterion, being the ratio of gap and Λ_{MF} used in part before, causes jumps of the gap as a function of μ , which have to be considered as artefacts. No satisfactory criterion was found. These jumps

are similar to the jumps from a finite to a different finite AF-value discussed on page 84, but are much bigger here. In section (4.3) it was argued that unphysical low-energy models are created on the e-doped side for $\Lambda_{\text{MF}} \leq |\mu|$. A stop criterion $\Lambda_{\text{MF}} = c \cdot |\mu|$, $c > 1$, might produce reasonable results over a wide range, but it surely fails, if a finite solution is expected at $\mu = 0$. In fig. (6.32) this criterion, with $c = 2.0$, is used. The result resembles the result from the pure AF mean-field calculation. However, a very strong ambiguity at half filling is found. For the chosen parameters no gap was found at $\mu = 0$ already for large Λ_{MF} . Being unable to find a satisfactory stop criterion, a systematic investigation of the e-doped side was impossible.

Chapter 7

Conclusions and Outlook

In this thesis a new method to gain insight into the symmetry-broken phase of systems with competing instabilities, namely a combination of a functional renormalisation group (RG) and an extended mean-field (MF) calculation, was investigated. The ground state phase diagram, the gap amplitudes as well as gap form-factors were computed for the two dimensional Hubbard model at weak to intermediate couplings.

In contrast to earlier fermionic functional RG methods a controlled step *into* the symmetry-broken phase was made. While in older schemes the instability towards a certain order parameter had to be read off from growing couplings or susceptibilities, here the order parameters could be calculated. The scheme used here is more controlled, since it was possible to stay with the RG in a regime where the couplings are still of moderate size. Large couplings invalidate the one-loop approximation usually made. It also became clear that a large coupling or susceptibility does not guarantee a large gap or a large free energy gain. Furthermore, coexistence of the antiferromagnet and superconductor could be investigated. Also the gap dependence of the filling, which can strongly deviate from the filling of the bare system, could be determined. This can for example lead to a finite range of the chemical potential μ where the filling is constant.

The functional RG allowing for gaps and anomalous vertices, which might be an alternative, leads to considerably larger analytical and numerical effort, so that only simple models have been treated so far.

A new derivation of coupled mean-field equations was presented. Although not being the first one, the procedure used here has several advantages over the former ones. Most importantly the derivation is very general and can easily be adapted to other problems. This is due to the fact that only little use of the specific gaps or the model used here was made. In spite of their generality the derivations are easier and more transparent than the former derivations.

To be able to understand combined RG+MF calculations a detailed understanding of the pure antiferromagnetic (AF) mean-field theory was necessary. A transparent picture emerged. The effective Fermi surfaces (FS) determine most features, so that understanding the FS is the key to understanding the AF gap solutions. The possibility of metastable phases and a strong dependence of the filling on the gap was found. These two facts are often not taken into

account in similar works which only consider the susceptibility and therefore arrive sometimes at misleading results.

The first-order transition or even only the proximity to a first order transition was found to be problematic for this RG+MF scheme, and is expected to affect also other methods based on susceptibilities. The problem was discussed in detail for a purely AF model.

Some analytical insight into the interplay of SC and AF was presented. Unexpected at first sight, but clear after the discussion of the effective FSs of the pure AF mean-field theory, the AF gap does not always reduce an SC gap, but can as well increase it. Since the gap equations are not independent, but are connected as derivatives of the grand canonical potential, similar behaviour is found for the AF gap equation.

Several extensions to the scheme presented here are promising.

The numerical treatment of ferromagnetic order and Pomeranchuk distortion might elucidate their importance in the Hubbard model. Especially a Pomeranchuk distortion with d -wave symmetry has been analysed in recent years [Halboth and Metzner 2000; Neumayr and Metzner 2003; Yamase et al. 2005]. In certain regions the charge density wave might play an important rôle. Thus, investigating further order parameters or form factors, partly already implemented in the numerics or easy to implement within a short time, might be rewarding.

Gap structures have been calculated. Some experimental features result from details of the momentum dependence, such as the heat-conductivity of the d -wave-SC state, [Durst and Lee 2000]. A detailed study of the gap-structure might give some new insight into experimental data, [Sutherland et al. 2003; Sun et al. 2006].

Further discussion of the interplay of the antiferromagnetic and superconducting gap seems very interesting. Especially the fact that below the van Hove chemical potential $\mu_{vH} = 4t'$ the presence of one gap can increase another gap is unexpected and, therefore, worth to be investigated further. Even if no self-consistent solution is found for gap sizes which increase each other, a remnant of this effect could still show up in calculations including fluctuations.

The mean field-equation for the AF gap was discussed in detail. Since all main features of the bare MF calculation survive in the combined method, a detailed comparison with experimental data could elucidate whether the obtained results are accidentally similar to high- T_c materials, or catch some of the true physics. Three facts come into mind: first, the pocket structure, which should be seen for example in ARPES, second, the very existence of the Fermi surfaces, leading to a metallic state where the conductivity could be strongly suppressed by impurities and third, the effective band structure.

The criterion for determining the energy-scale Λ_{MF} down to which the RG was employed and where the MF method started leads to some problems. Therefore, redoing this method with another cut-off scheme, like a cut-off in the Matsubara frequency or a temperature cut-off might improve the situation strongly, since there the phase-space of the AF would not be reduced so drastically by the cut-off (compared with the phase-space of the superconductor)

away from perfect nesting. This alone would however not be sufficient to cure the problems connected with the proximity to a first-order transition.

A better understanding how to handle order parameters which can in principle exhibit first-order transitions is needed. Some progress was already made by using counter terms [Gersch et al. 2006].

Appendix A

Analogy of the RG in ODE Theory

In this section perturbation theory in ordinary differential equations is shown to provide a simple, but instructive example for the RG. As an example the anharmonic oscillator is treated by the RG. It is stressed, however, that the scheme is much more general [Chen et al. 1996].

A.1 Stating the Problem

Consider an ordinary differential equation (ODE)

$$\dot{y}_\epsilon(t) = f_\epsilon(t, y_\epsilon(t)) \quad (\text{A.1})$$

where ϵ is some small parameter, and the solution for $\epsilon = 0$

$$\dot{y}_0(t) = f_0(t, y_0(t)) \quad (\text{A.2})$$

is supposed to be known. One might try to systematically get a solution by expanding $y_\epsilon(t)$ in a series of functions

$$y_\epsilon(t) = \sum_{n=0}^{\infty} \epsilon^n y_n(t). \quad (\text{A.3})$$

The ansatz is local in ϵ , i.e., valid for small ϵ , if the series is approximated by the first terms, but global in t .

As an example consider the anharmonic oscillator

$$\ddot{y}(t) + y(t) + \epsilon y^3(t) = 0. \quad (\text{A.4})$$

Inserting the ansatz (A.3) into this ODE and sorting by the order in ϵ one obtains

$$\ddot{y}_0(t) + y_0(t) = 0 \quad (\text{A.5})$$

$$\ddot{y}_1(t) + y_1(t) = -y_0^3(t) \quad (\text{A.6})$$

...

The general zero-order solution is of course

$$y_0(t) = A \cos(t + \Theta), \quad (\text{A.7})$$

from which the first order equation is found to be, using a trigonometric identity

$$\ddot{y}_1(t) + y_1(t) = -y_0^3(t) = -A^3 \left(\frac{1}{4} \cos(3t + 3\Theta) + \frac{3}{4} \cos(t + \Theta) \right). \quad (\text{A.8})$$

The solution is

$$y_1(t) = \text{H.S.} + \frac{A^3}{32} \cos(3t + 3\Theta) - \frac{3A^3}{8} t \sin(t + \Theta), \quad (\text{A.9})$$

where the H.S. stands for the homogeneous solution. While the first term is just an oscillation due to and with the same frequency as the first term of the inhomogeneity (A.8), the second term's amplitude grows linearly with t . This is because the second term in (A.8) is in resonance with the homogeneous equation. Such a term is called secular. The solution up to first order by (A.3) is

$$\begin{aligned} y_\epsilon(t) = & A \cos(t + \Theta) + \epsilon \text{H.S.} + \epsilon \frac{A^3}{32} \cos(3t + 3\Theta) - \epsilon t \frac{3A^3}{8} \sin(t + \Theta) \\ & + \mathcal{O}(\epsilon^2) \end{aligned} \quad (\text{A.10})$$

As long as $\epsilon \ll 1$ and $t \ll 1$ this appears to be a reliable perturbation expansion, as the correction to the unperturbed solution is small. If $\epsilon \ll 1$ but $t \propto 1/\epsilon$ the secular term becomes of order one, so that the first order correction is of the same size as the zeroth order and naïve perturbation theory breaks down. It is straight-forward to show, that this secular term leads in second order to a term which is growing with t^2 , and in general in n^{th} order a term growing like t^n is found. The structure is

$$\begin{aligned} y(t) = & f_0 \\ & + \epsilon f_1^0 + \epsilon t f_1^1 \\ & + \epsilon^2 f_2^0 + \epsilon^2 t f_2^1 + \epsilon^2 t^2 f_2^2 \\ & \vdots \quad \quad \quad \vdots \quad \quad \quad \vdots \quad \quad \quad \ddots \end{aligned}$$

where the functions f_i^j are of order one. For $t \propto 1/\epsilon$ one has therefore to sum over all terms $\epsilon^n t^n f_n^n \propto 1$, to regain a small parameter¹.

Thus, even though a global ansatz in t was inserted the solution is only valid for small t , meaning it is local in t .

This problem is well known. It is due to the fact, that the strict ϵ -expansion destroys the correct structure of the solution. It can be handled in several ways. The terms can be summed by hand, which is possible in this special case, but impossible in general. A counter term can be introduced, which is tuned in

¹ A divergence is not necessary to have a non-valid perturbation series. If for example the unperturbed solution of an ODE was e^{-t} , terms like $t^n e^{-t}$ would be secular and lead to terms of order one for any fixed t .

such a way that the resonant, secular term is cancelled. This again works only for a restricted set of problems. A more general ansatz is the multiple-scale analysis, which is sometimes not trivial to carry out [Bender and Orszag 1999]. Also a Z-factor RG can be employed which seems the most general and handy method, see [Chen et al. 1996]. In the following an RG scheme will be derived, following the spirit of the exact RG.

A.2 Deriving the RG equations

If the RHS of (A.1) is t -independent, any solution fulfils²

$$y(t + s, y(0)) = y(t, y(s, y(0))) \quad (\text{A.11})$$

$$y(0, y(0)) = y(0), \quad (\text{A.12})$$

which is also called the flow axiom, where the first argument is the time, the second the initial value. It states simply, that a solution at a certain time $t + s$ and for an initial value $y(0)$ can be rewritten as the solution with the value reached at time s as the initial value and flow for only the residual time t .

The approximate solution breaks the flow axiom, which is not easy to see directly. We will argue at the end, that this is the case.

With the flow axiom a solution for a time t can be rewritten as

$$y(t, y(0)) = y(t - \tau, y(\tau, y(0))). \quad (\text{A.13})$$

This equation takes the rôle of the semi-group property of the exact RG (2.23). Taking the derivative with respect to τ one obtains, as the left hand side is independent of τ ,

$$\partial_\tau y(t - \tau, y(\tau, y(0))) = 0. \quad (\text{A.14})$$

The dependence on the initial value is given by the integration constants, which are $n - 1$ for an ODE of order n . Thus the equation (A.14) gives a system of $n - 1$ equations for the integration constants as a function of τ . This resembles strongly functional RG where the dependence of various quantities on some parameter, usually the cut-off, is transformed into a dependence of the action, which is determined by the model and considered to be given by constants, like the (bare) mass or the (bare) interaction.

After solving (A.14) τ can be chosen. For any τ we gain a good approximation local in $t - \tau$, touching the global solution at τ . One can thus consider the global solution as the envelope of those local solutions [Kunihiro and Tsumura 2005].

If τ is set to t the time dependence is completely shifted to the time dependence of the constants:

$$y^{\text{ren}}(t) = y(0, y(t, y(0))). \quad (\text{A.15})$$

² To be strict the RHS has to fulfil the Lipschitz condition. Otherwise the solution is not unique, and the flow axiom is not generally valid. As in physics determinism is usually assumed we will not worry about this.

This fulfils by construction the flow axiom (A.11).

a) As a very first example consider the *harmonic* oscillator

$$y(t) = A \cos(\omega t + \Theta). \quad (\text{A.16})$$

The flow equation is derived from

$$\partial_\tau A \cos(\omega(t - \tau) + \Theta) = 0 \quad (\text{A.17})$$

to be

$$\dot{A} \cos(\omega(t - \tau) + \Theta) + (-\omega + \dot{\Theta}) \sin(\omega(t - \tau) + \Theta) = 0, \quad (\text{A.18})$$

where the dot marks the derivative with respect to τ . Therefore,

$$\dot{A} = 0 \quad (\text{A.19})$$

$$\dot{\Theta} = \omega, \quad (\text{A.20})$$

and from this $A = \text{const} = A_0$, and $\Theta = \omega\tau + \Theta_0$. Inserting this and using (A.15)

$$\begin{aligned} y^{\text{ren}}(t) &= A(\tau) \cos(\omega(t - \tau) + \Theta(\tau))|_{\tau=t} \\ &= A_0 \cos(\omega t + \Theta_0), \end{aligned} \quad (\text{A.21})$$

which is of course the original, exact solution.

b) The perturbative solution of the *anharmonic* oscillator is

$$y(t) = A \cos(t + \Theta) + \epsilon \frac{A^3}{32} \cos(3t + 3\Theta) - \epsilon A^3 \frac{3}{8} t \sin(t + \Theta) + \mathcal{O}(\epsilon^2), \quad (\text{A.22})$$

where the homogeneous solution in first order has been absorbed into the zeroth order by appropriate redefinition of the constants.

From this we derive the RG equations by

$$\begin{aligned} &\partial_\tau y(t - \tau, y(\tau, y(0))) \\ &= \dot{A} \cos(t - \tau + \Theta) - A \sin(t - \tau + \Theta)(-1 + -\epsilon A^2 \frac{3}{8} + \dot{\Theta}) \\ &\quad + \frac{\epsilon}{32} 3A^2 \dot{A} \cos(3(t - \tau + \Theta)) - \frac{\epsilon}{32} A^3 \sin(3(t - \tau + \Theta)) 3(-1 + \dot{\Theta}) \\ &\quad - \epsilon 3A^2 \dot{A} \frac{3}{8} (t - \tau) \sin(t - \tau + \Theta) - \epsilon A^3 \frac{3}{8} (t - \tau) \cos(t - \tau + \Theta)(-1 + \dot{\Theta}) + \mathcal{O}(\epsilon^2) \\ &= 0 \end{aligned} \quad (\text{A.23})$$

as

$$\dot{A} = 0 + \mathcal{O}(\epsilon^2) \quad (\text{A.24})$$

$$\dot{\Theta} = 1 + \epsilon A^2 \frac{3}{8} + \mathcal{O}(\epsilon^2), \quad (\text{A.25})$$

where $\dot{\Theta} - 1 = \mathcal{O}(\epsilon)$ has been used. Integrating equations (A.24),(A.25) leads to

$$A = A_0 + \mathcal{O}(\epsilon^2) \quad (\text{A.26})$$

$$\Theta = \Theta_0 + \tau \left(1 + \epsilon A^2 \frac{3}{8} \right) + \mathcal{O}(\epsilon^2). \quad (\text{A.27})$$

It is no surprise that the amplitude does not change with time. It reflects the conservation of energy, as the perturbation is non-dissipative.

The renormalised function is thus

$$\begin{aligned} y^{\text{ren}}(t) &= y(0, y(t, y(0))) \\ &= A(t) \cos(\Theta(t)) + \epsilon \frac{A(t)^3}{32} \cos(3\Theta(t)) - \epsilon A(t)^3 \frac{3}{8} (0) \sin(\Theta(t)) + \mathcal{O}(\epsilon^2) \\ &= A_0 \cos \left(t \left(1 + \epsilon A_0^2 \frac{3}{8} \right) + \Theta_0 \right) + \epsilon \frac{A_0^3}{32} \cos \left(3t \left(1 + \epsilon A_0^2 \frac{3}{8} \right) + 3\Theta_0 \right) \end{aligned} \quad (\text{A.28})$$

Obviously the flow axiom is full-filled, since a shift in the time t can be absorbed into Θ_0 .

Choosing the initial values as $y(0) = 1$, $\dot{y}(0) = 0$ one obtains

$$y(t) = \cos(t\omega) + \epsilon \frac{1}{32} (\cos(3t\omega) - \cos(t\omega)) \quad (\text{A.29})$$

with the changed frequency $\omega = 1 + \epsilon 3/8$. This is the desired correct structure, a frequency-shift, which is destroyed by the strict ϵ -expansion. The secular terms can be reproduced by expanding the cosine-functions in ϵ . It can be shown that this frequency-shift sums up all terms $\epsilon^n t^n f_n^n$. Observe that the frequency shift (A.27) is different for different amplitudes, likewise the shape of the oscillation is, given by (A.28).

It was stated above, that the naïve perturbation result breaks the flow axiom; forcing the solution to fulfil the flow axiom, led to the RG equations; since the obtained solution after solving the RG equations is different, (A.10) did not fulfil the flow axiom.

In general not every the zero order of a perturbation theory is a good starting point for this ODE-RG. It has to have as many integration constants as the full equation, otherwise the RG cannot, in general, reproduce the full solution. The equations (3.7)-(3.10) in [Chen et al. 1996] are therefore of doubtful value, and are not an example for the Wilson RG as claimed.

For other properties of the field theoretical RG examples can be found; for example oscillators with limit cycles, as the Rayleigh-oscillator, approaching a subspace in the long time limit, are examples for irrelevant variables, as used by [Polchinski 1984] to prove renormalisability. In this case less RG equations are needed to describe the physics than naïvely expected, as it is the case in field theory, where a finite number of equations is enough, instead of infinitely many.

Appendix B

Gap Equations in Operator Formalism

In this section the derivation of the mean-field equations in the operator formalism will be presented in detail.

Starting-point is the Hamilton-operator

$$\begin{aligned} \mathcal{H} &= \sum_{k,\sigma} \xi_k a_{k,\sigma}^\dagger a_{k,\sigma} \\ &+ \sum_{K'_1, K'_2, K_1, K_2} \frac{1}{4} \Gamma^\Lambda(K_1, K_2; K'_2, K'_1) a_{K'_1}^\dagger a_{K'_2}^\dagger a_{K_2} a_{K_1} \end{aligned} \quad (\text{B.1})$$

where $\xi_k = \epsilon_k - \mu$ is the free dispersion, and $K = (\sigma, k)$ is the usual multi-index.

The restriction to the low energy BZ is by restriction of the interaction

$$\Gamma^\Lambda(K'_1, K'_2; K_2, K_1) = \Gamma(K'_1, K'_2; K_2, K_1) \Theta^\Lambda(k'_1, k'_2, k_2, k_1) \quad (\text{B.2})$$

where $\Theta^\Lambda(k_1, \dots, k_n) = \Theta^\Lambda(k_1) \cdots \Theta^\Lambda(k_n)$ and $\Theta^\Lambda(k) = \Theta(\Lambda - |\xi_k|)$ is the usual cut-off function (2.20).

B.1 Antiferromagnetism

The spin/charge-density wave gap with modulation $Q = (\pi, \pi)$ and spin projection in the z -direction will be derived. It will be referred to simply as AF-gap.

To be able apply the mean-field approximation in the AF-channel one has to regroup the operators first, as the AF mean-field is built from a creation and an annihilation operator. It is a priori not clear whether one should group the creation operator $a_{K_1}^\dagger$ with $a_{K'_1}$ or $a_{K'_2}$, or even regroup the operators in a certain representation of the potential. Comparison with the MF calculation for the z -component of the spin operators $\vec{S} \sim \vec{\sigma}$ shows that the naive grouping $K_1 \leftrightarrow K'_1, K_2 \leftrightarrow K'_2$ is the correct one. Regrouping leads to

$$\begin{aligned} &\sum \Gamma^\Lambda(K'_1, K'_2; K_2, K_1) a_{K'_1}^\dagger a_{K'_2}^\dagger a_{K_2} a_{K_1} \\ &= \sum \Gamma^\Lambda(K'_1, K'_2; K_2, K_1) \left(a_{K'_1}^\dagger a_{K_1} a_{K'_2}^\dagger a_{K_2} - a_{K'_1}^\dagger a_{K_2} \delta_{K_1, K'_2} \right). \end{aligned} \quad (\text{B.3})$$

The second term leads to a contribution to the kinetic energy

$$-\sum \Gamma^\Lambda(K'_1, K'_2; K_2, K_1) a_{K'_1}^\dagger a_{K_2} \delta_{K_1, K'_2} = -\sum_K a_K^\dagger a_K \sum_{K'} \Gamma^\Lambda(K, K'; K, K') \quad (\text{B.4})$$

which will be neglected.

The first term of (B.3) leads in the MF decoupling to

$$\begin{aligned} & a_{K'_1}^\dagger a_{K_1} a_{K'_2}^\dagger a_{K_2} \\ \rightarrow & -\langle a_{K'_1}^\dagger a_{K_1} \rangle \langle a_{K'_2}^\dagger a_{K_2} \rangle + \langle a_{K'_1}^\dagger a_{K_1} \rangle a_{K'_2}^\dagger a_{K_2} + a_{K'_1}^\dagger a_{K_1} \langle a_{K'_2}^\dagger a_{K_2} \rangle \end{aligned} \quad (\text{B.5})$$

and with the restriction to the z -spin-projection and modulation $Q = (\pi, \pi)$

$$\langle a_{k'_1 \sigma'_1}^\dagger a_{k_1 \sigma_1} \rangle = \delta_{k'_1, k_1 + Q} \delta_{\sigma'_1, \sigma_1} \langle a_{k'_1 \sigma_1}^\dagger a_{k'_1 + Q \sigma_1} \rangle \quad (\text{B.6})$$

to

$$-\sum_{k\sigma} \mathcal{F}_{k\sigma} \frac{1}{2} \mathcal{A}_{k,\sigma} + \sum_{k\sigma} a_{k\sigma}^\dagger a_{k+Q\sigma} \mathcal{A}_{k,\sigma}, \quad (\text{B.7})$$

where the AF gap

$$\mathcal{A}_{k,\sigma} = \frac{1}{2} \sum_{k',\sigma'} U^\Lambda \begin{pmatrix} \sigma & \sigma' \\ k & k' \end{pmatrix} \mathcal{F}_{k'\sigma'} \quad (\text{B.8})$$

was introduced. The potential is defined as

$$U^\Lambda \begin{pmatrix} \sigma & \sigma' \\ k & k' \end{pmatrix} = \Gamma^\Lambda \begin{pmatrix} \sigma & \sigma' & \sigma' & \sigma \\ k & k' & k'+Q & k+Q \end{pmatrix} \quad (\text{B.9})$$

$$= U^\Lambda \begin{pmatrix} \sigma & \sigma' \\ k+Q & k'+Q \end{pmatrix} \quad (\text{B.10})$$

The expectation value is

$$\mathcal{F}_{k\sigma} = \langle a_{k\sigma}^\dagger a_{k+Q\sigma} \rangle = \mathcal{F}_{k+Q\sigma}^*. \quad (\text{B.11})$$

It follows immediately that

$$\mathcal{A}_{k+Q\sigma} = \mathcal{A}_{k\sigma}^*. \quad (\text{B.12})$$

In order to rewrite the result as a Nambu matrix the magnetic BZ is introduced with the help of

$$\sum_k f(k) = \sum'_k (f(k) + f(k+Q)), \quad (\text{B.13})$$

where the prime signals the sum over the magnetic (half) BZ. Therefore we get the magnetic contribution

$$\sum'_k \left(a_{k\uparrow}^\dagger a_{k+Q\uparrow} \mathcal{A}_{k\uparrow} + a_{k+Q\uparrow}^\dagger a_{k\uparrow} \mathcal{A}_{k\uparrow}^* \right) \quad (\text{B.14})$$

$$+ \sum'_k \left(a_{-k\downarrow}^\dagger a_{-k-Q\downarrow} \mathcal{A}_{-k\downarrow} + a_{-k-Q\downarrow}^\dagger a_{-k\downarrow} \mathcal{A}_{-k\downarrow}^* \right) \quad (\text{B.15})$$

The second sum runs over $-k$ instead of k which will prove to be helpful later.

B.2 Superconductivity and the π -Pairing

The contribution to the Hamiltonian of the singlet superconducting pair (SC) with zero centre of mass momentum and with centre of mass momentum $Q = (\pi, \pi)$ will be derived. The latter will be called π -pair.

The procedure in SC case is

$$\frac{1}{4} \sum_{K'_1, K'_2, K_1, K_2} \Gamma^\Lambda(K'_1, K'_2; K_2, K_1) \times \left(-\langle a_{K'_1}^\dagger a_{K'_2}^\dagger \rangle \langle a_{K_2} a_{K_1} \rangle + a_{K'_1}^\dagger a_{K'_2}^\dagger \langle a_{K_2} a_{K_1} \rangle + a_{K_2} a_{K_1} \langle a_{K'_1}^\dagger a_{K'_2}^\dagger \rangle \right). \quad (\text{B.16})$$

The restriction to spin singlets and to zero pair momentum and Q pair momentum is formalised

$$\langle a_{k_2 \sigma_2} a_{k_1 \sigma_1} \rangle = \delta_{\sigma_1, -\sigma_2} \delta_{k_1 + k_2} \langle a_{-k_1, -\sigma_1} a_{k_1 \sigma_1} \rangle + \delta_{\sigma_1, -\sigma_2} \delta_{k_1 + k_2 + Q} \langle a_{-k_1 + Q, -\sigma_1} a_{k_1 \sigma_1} \rangle,$$

which leads in (B.16) after performing the spin sums to

$$\begin{aligned} & - \sum_k (\mathcal{F}_k^o)^* \Delta_k - \sum_k (\mathcal{F}_k^\pi)^* \pi_k \\ & + \sum_k a_{k\uparrow}^\dagger a_{-k\downarrow}^\dagger \Delta_k + \sum_k a_{k\uparrow}^\dagger a_{-k-Q\downarrow}^\dagger \pi_k \\ & + \sum_k a_{-k\downarrow} a_{k\uparrow} \Delta_k^* + \sum_k a_{-k-Q\downarrow} a_{k\uparrow} \pi_k^* \end{aligned} \quad (\text{B.17})$$

where the SC pair field is $\mathcal{F}_k^o = \langle a_{-k, \downarrow} a_{k, \uparrow} \rangle$ and the π -pair field is $\mathcal{F}_k^\pi = \langle a_{-k-Q, \downarrow} a_{k, \uparrow} \rangle$ and the associated gaps

$$\Delta_k = \sum_{\mathbf{k}'} V_{k, \mathbf{k}'} \mathcal{F}_{\mathbf{k}'}^o \quad (\text{B.18})$$

and

$$\pi_k = \sum_{\mathbf{k}'} W_{k, \mathbf{k}'} \mathcal{F}_{\mathbf{k}'}^\pi \quad (\text{B.19})$$

have been introduced. The potentials are given by

$$V_{k, k'}^\Lambda = \Gamma^\Lambda \begin{pmatrix} \uparrow & \downarrow & \downarrow & \uparrow \\ k & -k & -k' & k' \end{pmatrix} \quad (\text{B.20})$$

and

$$W_{k, k'}^\Lambda = \Gamma^\Lambda \begin{pmatrix} \uparrow & \downarrow & \downarrow & \uparrow \\ k & -k-Q & -k'+Q & k' \end{pmatrix} \quad (\text{B.21})$$

The restriction of the sums containing quadratic terms in the operators of (B.17) to the magnetic BZ is again accomplished by using (B.13), leading for the Cooper pair to

$$\sum_k' \left(a_{k\uparrow}^\dagger a_{-k\downarrow}^\dagger \Delta_k + a_{k+Q\uparrow}^\dagger a_{-k-Q\downarrow}^\dagger \Delta_{k+Q} \right) \quad (\text{B.22})$$

$$+ \sum_k' \left(a_{-k\downarrow} a_{k\uparrow} \Delta_k^* + a_{-k-Q\downarrow} a_{k+Q\uparrow} \Delta_{k+Q}^* \right) \quad (\text{B.23})$$

and for the π pair to

$$\begin{aligned} & \sum_k' \left(a_{k\uparrow}^\dagger a_{-k-Q\downarrow}^\dagger \pi_k + a_{k+Q\uparrow}^\dagger a_{-k\downarrow}^\dagger \pi_{k+Q} \right) \\ & + \sum_k' \left(a_{-k-Q\downarrow} a_{k\uparrow} (\pi_k)^* + a_{-k\downarrow} a_{k+Q\uparrow} (\pi_{k+Q})^* \right). \end{aligned} \quad (\text{B.24})$$

B.3 The Pomeranchuk and Magnetic Gap

The Pomeranchuk and magnetic gap is the spin and charge wave with $q = 0$ modulation. It is thus closely related to the spin and charge wave, derived in the section (B.1).

The Pomeranchuk and magnetic gap is due to forward scattering processes of the form

$$\sum_{kk',\sigma\sigma'} n_k^\sigma f_{kk'}^{\sigma\sigma'} n_{k'}^{\sigma'} \quad (\text{B.25})$$

where $n_k^\sigma = a_{k\sigma}^\dagger a_{k\sigma}$. The scattering potential is therefore given by¹

$$f_{kk'}^{\sigma\sigma'} = \Gamma^\Lambda \left(\begin{matrix} \sigma & \sigma' & \sigma' & \sigma \\ k & k' & k' & k \end{matrix} \right) \quad (\text{B.26})$$

The mean field decoupling (3.17) of (B.25) leads to

$$\sum_{k\sigma} \delta\mu_{k\sigma} n_k^\sigma - \frac{1}{2} \sum_{k\sigma} \delta\mu_{k\sigma} \langle n_k^\sigma \rangle, \quad (\text{B.27})$$

where the Pomeranchuk gap

$$\delta\mu_{k\sigma} = \sum_{k'\sigma'} \frac{1}{2} f_{kk'}^{\sigma\sigma'} \langle n_{k'}^{\sigma'} \rangle \quad (\text{B.28})$$

was introduced. The first term of (B.27) has the form of a k - and σ -dependent chemical potential, and can therefore be absorbed into the dispersion

$$\bar{\xi}_{k\sigma} = \xi_k + \delta\mu_{k\sigma}, \quad (\text{B.29})$$

which becomes spin dependent. The second term of (B.27) is a contribution to the c-number term.

B.4 The Mean-Field Hamiltonian

The mean-field Hamiltonian is given by the sum of the different channels. While the SC and π pairs are disjoint, as the AF pair and the Pomeranchuk pair are, the first two overlaps with the other two, that is, there are scattering terms which belong to the AF or Pomeranchuk channel and the SC or π channel. As the dimension of the overlap is one dimension lower than the dimension of

¹ The cut-off Λ will not be written explicitly in the following.

potentials, it is expected to be of zero measure. If the potential diverged in the relevant subspace, this approach would have to be reconsidered.

$$\begin{aligned} \mathcal{H}^{\text{MF}} &= - \sum_{\mathbf{k}} [\mathcal{F}_k^o \Delta_k^* + \mathcal{F}_k^\pi \pi_k^*] - \sum_{k\sigma} \mathcal{F}_{k,\sigma} \mathcal{A}_{k,\sigma} / 2 - \sum_{k\sigma} \langle n_k^\sigma \rangle \delta\mu_{k\sigma} / 2 + \sum_{\mathbf{k}} \bar{\xi}_{k\downarrow} \\ &\quad + \sum_{\mathbf{k}}' a_k^\dagger \mathcal{M}_k a_k \end{aligned} \quad (\text{B.30})$$

$$\equiv E^c + \sum_{\mathbf{k}}' a_k^\dagger \mathcal{M}_k a_k \quad (\text{B.31})$$

with the Nambu operator $a_k^\dagger = (a_{k\uparrow}^\dagger, a_{-k\downarrow}, a_{k+Q\uparrow}^\dagger, a_{-k-Q\downarrow})$ and

$$\mathcal{M} = \begin{pmatrix} \bar{\xi}_{k\uparrow} & \Delta_k & \mathcal{A}_{k,\uparrow} & \pi_k \\ \Delta_k^* & -\bar{\xi}_{k\downarrow} & \pi_{k+Q}^* & -\mathcal{A}_{-k,\downarrow}^* \\ \mathcal{A}_{k,\uparrow}^* & \pi_{k+Q} & \bar{\xi}_{k+Q,\uparrow} & \Delta_{k+Q} \\ \pi_k^* & -\mathcal{A}_{-k,\downarrow} & \Delta_{k+Q}^* & -\bar{\xi}_{k+Q,\downarrow} \end{pmatrix}. \quad (\text{B.32})$$

Observe that due to the definition of the potential the gaps are only non-zero if $\chi^\Lambda(k)$ is non-zero in the SC case and $\chi^\Lambda(k)\chi^\Lambda(k+Q)$ is nonzero in the AF and π case. The last term in the c-number term is due to the commutation of $a_{-k\downarrow} a_{-k\downarrow}^\dagger$ and $a_{-k-Q\downarrow} a_{-k-Q\downarrow}^\dagger$ respectively, necessary to obtain the matrix form. The effective dispersion is due to the Pomeranchuk gap

$$\bar{\xi}_{k\sigma} = \xi_k + \delta\mu_{k\sigma} \quad (\text{B.33})$$

where

$$\xi_k = \varepsilon_k - \mu \quad (\text{B.34})$$

is just the free dispersion, and where the last term from (B.4) was neglected.

The gap functions are defined as

$$\Delta_k = \sum_{\mathbf{k}'} V_{k,k'}^\Lambda \mathcal{F}_{k'}^o, \quad \mathcal{F}_{k'}^o = \langle a_{-k'\downarrow} a_{k'\uparrow} \rangle \quad (\text{B.35})$$

for the SC singlet,

$$\pi_k = \sum_{\mathbf{k}'} W_{k,k'}^\Lambda \mathcal{F}_{k'}^\pi, \quad \mathcal{F}_{k'}^\pi = \langle a_{-k'+Q\downarrow} a_{k'\uparrow} \rangle \quad (\text{B.36})$$

for the π pairing and

$$\begin{aligned} \mathcal{A}_{k,\sigma} &= \frac{1}{2} \sum_{k',\sigma'} U^\Lambda \begin{pmatrix} \sigma & \sigma' \\ k & k' \end{pmatrix} \mathcal{F}_{k'\sigma'} \\ \mathcal{F}_{k',\sigma} &= \langle a_{k'\sigma}^\dagger a_{k'+Q\sigma} \rangle \end{aligned} \quad (\text{B.37})$$

for the spin/charge-density-wave. The Pomeranchuk gap is

$$\delta\mu_{k\sigma} = \sum_{k'\sigma'} \frac{1}{2} f_{kk'}^{\sigma\sigma'} \langle n_{k'}^{\sigma'} \rangle. \quad (\text{B.38})$$

B.5 Gap Equations

First the general procedure will be sketched. Then the gap equations will be derived.

The derivative of the grand canonical potential has to vanish

$$\frac{\partial}{\partial \mathcal{F}_k} \Omega = 0, \quad (\text{B.39})$$

where \mathcal{F}_k is one of the expectation values

$$\mathcal{F}_{k'}^o = \langle a_{-k',\downarrow} a_{k',\uparrow} \rangle, \quad \mathcal{F}_{k'}^\pi = \langle a_{-k'-Q,\downarrow} a_{k',\uparrow} \rangle, \quad \mathcal{F}_{k\sigma} = \langle a_{k\sigma}^\dagger a_{k+Q\sigma} \rangle, \quad \langle n_{k'}^{\sigma'} \rangle, \quad (\text{B.40})$$

here considered as variational parameters. Alternatively one could vary the gaps, but this complicates the derivation a little bit, as one would have to invert the various potentials in the c-number term, which might be of low rank, so that it seems on first sight not well defined.

(B.39) can also be shown by direct calculation

$$\frac{\partial}{\partial \mathcal{F}_k} \Omega = \left\langle \frac{\partial \mathcal{H}}{\partial \mathcal{F}_k} \right\rangle \quad (\text{B.41})$$

$$= - \sum_{\mathbf{k}'} \delta_{\mathbf{k}-\mathbf{k}'} \Delta_{k'} + \sum_{\mathbf{k}'}' \left\langle \frac{\partial}{\partial \mathcal{F}_k} \left(\underline{a}_{k'}^\dagger \mathcal{M}_{\underline{a}_{k'}} \right) \right\rangle \quad (\text{B.42})$$

$$= -\Delta_k + \Delta_k = 0. \quad (\text{B.43})$$

Here Δ_k is the gap functions corresponding to one of the expectation values (B.40).

Since the matrix is hermitian it can be diagonalised²:

$$\sum_{\mathbf{k}}' \underline{a}_{\mathbf{k}}^\dagger \mathcal{M}_{\underline{a}_{\mathbf{k}}} = \sum_{\mathbf{k}}' \underline{\alpha}_{\mathbf{k}}^\dagger \mathcal{D}_{\mathbf{k}} \underline{\alpha}_{\mathbf{k}} \quad (\text{B.44})$$

where $\underline{\alpha}_{\mathbf{k}}^\dagger = (\alpha_{k,1}^\dagger, \alpha_{k,2}^\dagger, \alpha_{k,3}^\dagger, \alpha_{k,4}^\dagger)$ is the new Nambu operator and \mathcal{D} a diagonal matrix³

$$\mathcal{D}_{\mathbf{k}} = \begin{pmatrix} E_{\mathbf{k}}^{(1)} & & & \\ & E_{\mathbf{k}}^{(2)} & & \\ & & E_{\mathbf{k}}^{(3)} & \\ & & & E_{\mathbf{k}}^{(4)} \end{pmatrix}. \quad (\text{B.45})$$

Therefore (B.31) becomes

$$\begin{aligned} \mathcal{H}^{\text{MF}} &= E^c + \sum_{\mathbf{k}}' \underline{\alpha}_{\mathbf{k}}^\dagger \mathcal{D}_{\mathbf{k}} \underline{\alpha}_{\mathbf{k}} \\ &= E^c + \sum_{k\alpha}' E_k^\alpha \hat{n}_k^\alpha, \end{aligned} \quad (\text{B.46})$$

² The transformation is unitary, the new operators still obey the fermionic commutator relations, thus are still describing fermions.

³ Some authors claim that one has to commute the operators to guarantee positive energies. For fermions the spectrum is restricted in either case, and the result is independent of this.

from which the grand canonical potential is calculated to be

$$\begin{aligned}\Omega &= -\beta^{-1} \ln Z \\ &= E^c + (-\beta)^{-1} \sum'_{k'\alpha} \ln(1 + \exp(-\beta E_{k'}^\alpha)).\end{aligned}\quad (\text{B.47})$$

The derivative of the grand canonical potential has to vanish, leading to

$$\begin{aligned}0 &= \frac{\partial E^c}{\partial \mathcal{F}_k} + \sum'_{k'} \sum_{\alpha} \frac{\partial E_{k'}^\alpha}{\partial \mathcal{F}_k} \frac{\exp(-\beta E_{k'}^\alpha)}{1 + \exp(-\beta E_{k'}^\alpha)} \\ &= \frac{\partial E^c}{\partial \mathcal{F}_k} + \sum'_{k'} \sum_{\alpha} \frac{\partial E_{k'}^\alpha}{\partial \mathcal{F}_k} f(E_{k'}^\alpha).\end{aligned}\quad (\text{B.48})$$

The derivative of the energy eigenvalues can be expressed by utilising the characteristic polynomial

$$0 = \frac{\partial}{\partial \mathcal{F}_k} |\mathcal{M}_{k'} - \mathbf{1}E_{k'}^\alpha| \equiv \frac{\partial}{\partial \mathcal{F}_k} |\mathbf{M}_{k'}^\alpha|, \quad (\text{B.49})$$

since, with (D.3), the derivative of any determinant can be expressed as

$$\frac{\partial}{\partial f} |A| = \sum_{i,j} \frac{\partial a_{ij}}{\partial f} \frac{\partial}{\partial a_{ij}} |A| \quad (\text{B.50})$$

$$= \sum_{i,j} (-1)^{i+j} \frac{\partial a_{ij}}{\partial f} |A_{ij}|, \quad (\text{B.51})$$

where a_{ij} is the element of the matrix in the i^{th} row and j^{th} column, and A_{ij} is the corresponding minor.

Due to this the derivative of the characteristic polynomial is

$$-\frac{\partial E_{k'}^\alpha}{\partial \mathcal{F}_k} \sum_l |\mathbf{M}_{ll}^\alpha| + \sum_{i,j} \frac{\partial m_{ij}}{\partial \mathcal{F}_k} (-1)^{i+j} |\mathbf{M}_{ij}^\alpha| = 0 \quad (\text{B.52})$$

where m_{ij} are the elements of \mathcal{M} , and the derivatives of the energies can be expressed as

$$\frac{\partial E_{k'}^\alpha}{\partial \mathcal{F}_k} = \left(\sum_l |\mathbf{M}_{ll}^\alpha|(k') \right)^{-1} \sum_{i,j}^{i \neq j} \frac{\partial m_{ij}(k')}{\partial \mathcal{F}_k} (-1)^{i+j} |\mathbf{M}_{ij}^\alpha|(k'). \quad (\text{B.53})$$

In the explicit form of the gap equation this expression is much more compact, as only few elements of the matrix depend on a certain mean-field.

To further simplify the gap equations the structure of the \mathcal{M} matrix will be used, being

$$\mathbf{M}_k^\alpha = \begin{pmatrix} D_k - \mathbf{1}E_k^\alpha & N_k \\ N_{k+Q} & D_{k+Q} - \mathbf{1}E_k^\alpha \end{pmatrix} \quad (\text{B.54})$$

from which it is apparent that $E_{k+Q}^\alpha = E_k^\alpha$ and

$$|\mathbf{M}_{ij}^\alpha|(k+Q) = |\mathbf{M}_{i+2,j+2}^\alpha|(k). \quad (\text{B.55})$$

Here $i + 2$ and $j + 2$ is to be understood modulo 4. After these remarks the gap equation are easily obtained in the following.

Superconducting Gap

First the SC gap equation is derived. It will be made use of the relation

$$\frac{\partial \Delta_{k'}}{\partial \mathcal{F}_k^o} = V_{kk'}^\Lambda. \quad (\text{B.56})$$

The derivative of the eigenvalues is, following (B.53)

$$\begin{aligned} \frac{\partial E_{k'}^\alpha}{\partial \mathcal{F}_k^o} &= \left(\sum_l |\mathbf{M}_{ll}^\alpha| \right)^{-1} \sum_{i,j} \frac{\partial m_{ij}}{\partial \mathcal{F}_k^o} (-1)^{i+j} |\mathbf{M}_{ij}^\alpha| \\ &= \left(\sum_l |\mathbf{M}_{ll}^\alpha| \right)^{-1} \left(-\frac{\partial \Delta_{k'}}{\partial \mathcal{F}_k^o} |\mathbf{M}_{12}^\alpha| - \frac{\partial \Delta_{k'+Q}}{\partial \mathcal{F}_k^o} |\mathbf{M}_{34}^\alpha| \right) \end{aligned} \quad (\text{B.57})$$

Combined with (B.48) and with (B.56), this leads to

$$\begin{aligned} -\frac{\partial E^c}{\partial \mathcal{F}_k^o} &= \Delta_k^* \\ &= -\sum_{k'} \sum_{\alpha} \frac{\frac{\partial \Delta_{k'}}{\partial \mathcal{F}_k^o} |\mathbf{M}_{12}^\alpha|(k') + \frac{\partial \Delta_{k'+Q}}{\partial \mathcal{F}_k^o} |\mathbf{M}_{34}^\alpha|(k')}{\sum_l |\mathbf{M}_{ll}^\alpha|(k')} f(E_{k'}^\alpha) \\ &= -\sum_{k'} \sum_{\alpha} \frac{4V_{kk'}^\Lambda |\mathbf{M}_{12}^\alpha|}{\sum_l |\mathbf{M}_{ll}^\alpha|(k')} f(E_{k'}^\alpha). \end{aligned} \quad (\text{B.58})$$

In the second line $E_{k'} = E_{k'+Q}$ and $|\mathbf{M}_{34}^\alpha|(k') = |\mathbf{M}_{12}^\alpha|(k' + Q)$ was used (B.55), from which directly $\sum_l |\mathbf{M}_{ll}^\alpha|(k') = \sum_l |\mathbf{M}_{ll}^\alpha|(k' + Q)$ follows, so that with (B.13) the sum can be rewritten to cover the whole BZ.

π -Pairing

The derivation of the gap equation for the π -pair proceeds analogously, using

$$\frac{\partial \pi_{k'}}{\partial \mathcal{F}_k^\pi} = W_{k,k'}^\Lambda \quad (\text{B.59})$$

and $|\mathbf{M}_{14}^\alpha|(k + Q) = |\mathbf{M}_{32}^\alpha|(k)$ (B.55), leading to

$$\pi_k^* = -\sum_{k'} \sum_{\alpha} \frac{W_{kk'}^\Lambda |\mathbf{M}_{14}^\alpha|(k')}{\sum_l |\mathbf{M}_{ll}^\alpha|(k')} f(E_{k'}^\alpha). \quad (\text{B.60})$$

Spin/Charge-Wave

The gap equation for the AF-gap requires a little more work, as none of the derivatives $\frac{\partial \mathcal{A}_{k\sigma}^{(*)}}{\partial \mathcal{F}_{k'\sigma'}}$ vanishes⁴, but is in principle absolutely parallel. First we

⁴ While in the SC and π case it is a matter of taste, whether one varies the gap or the expectation value, here the expectation value has to be used. Otherwise the variation of the c-number term is not so easy to evaluate.

note

$$\frac{\partial \mathcal{A}_{k'\sigma'}}{\partial \mathcal{F}_{k\sigma}} = \frac{1}{2} U^\Lambda \begin{pmatrix} \sigma & \sigma' \\ k & k' \end{pmatrix}. \quad (\text{B.61})$$

The derivative of the energy (B.53) can, with

$$\begin{aligned} & \sum_{i,j}^{i \neq j} \frac{\partial m_{ij}}{\partial \mathcal{F}_{k\sigma}} (-1)^{i+j} |\mathbf{M}_{ij}| \\ &= \left(\frac{\partial \mathcal{A}_{k'\uparrow}}{\partial \mathcal{F}_{k\sigma}} |\mathbf{M}_{13}^\alpha| - \frac{\partial \mathcal{A}_{-k'\downarrow}^*}{\partial \mathcal{F}_{k\sigma}} |\mathbf{M}_{24}^\alpha| + \frac{\partial \mathcal{A}_{k'\uparrow}^*}{\partial \mathcal{F}_{k\sigma}} |\mathbf{M}_{31}^\alpha| - \frac{\partial \mathcal{A}_{-k'\downarrow}}{\partial \mathcal{F}_{k\sigma}} |\mathbf{M}_{42}^\alpha| \right), \end{aligned}$$

be written as

$$\frac{\partial E_{k'}^\alpha}{\partial \mathcal{F}_{k\sigma}} = \frac{\frac{\partial \mathcal{A}_{k'\uparrow}}{\partial \mathcal{F}_{k\sigma}} |\mathbf{M}_{13}^\alpha| - \frac{\partial \mathcal{A}_{-k'\downarrow}^*}{\partial \mathcal{F}_{k\sigma}} |\mathbf{M}_{24}^\alpha| + \frac{\partial \mathcal{A}_{k'\uparrow}^*}{\partial \mathcal{F}_{k\sigma}} |\mathbf{M}_{31}^\alpha| - \frac{\partial \mathcal{A}_{-k'\downarrow}}{\partial \mathcal{F}_{k\sigma}} |\mathbf{M}_{42}^\alpha|}{\sum_l |\mathbf{M}_{ll}^\alpha|}. \quad (\text{B.62})$$

With $\mathcal{A}_{k'}^* = \mathcal{A}_{k'+Q}$ and $|\mathbf{M}_{24}^\alpha|(k'+Q) = |\mathbf{M}_{42}^\alpha|(k')$, $|\mathbf{M}_{13}^\alpha|(k'+Q) = |\mathbf{M}_{31}^\alpha|(k')$ the gap equation is found to be

$$\mathcal{A}_{k\sigma} = \sum_{k'} \sum_{\alpha} \frac{1}{2} \frac{U^\Lambda \begin{pmatrix} \sigma & \uparrow \\ k & k' \end{pmatrix} |\mathbf{M}_{13}^\alpha| - U^\Lambda \begin{pmatrix} \sigma & \downarrow \\ k & -k' \end{pmatrix} |\mathbf{M}_{42}^\alpha|}{\sum_l |\mathbf{M}_{ll}^\alpha|} f(E_{k'}^\alpha). \quad (\text{B.63})$$

Pomeranchuk Gap

To derive the gap equation for the Pomeranchuk gap $\delta\mu$ (B.28), note first that its derivative by the expectation value is given by

$$\frac{\partial \delta\mu_{k\sigma}}{\partial \langle n_{k'}^{\sigma'} \rangle} = \frac{1}{2} f_{k'k}^{\sigma'\sigma}. \quad (\text{B.64})$$

The derivation of the eigenvalues is calculated as before from the characteristic polynomial:

$$\begin{aligned} 0 &= \frac{\partial}{\partial \langle n_k^\sigma \rangle} |\mathcal{M}_{k'} - \mathbf{1} E_{k'}^\alpha| \\ &= \sum_i \frac{\partial m_{ii}^\alpha}{\partial \langle n_k^\sigma \rangle} |M_{ii}^\alpha| \end{aligned} \quad (\text{B.65})$$

$$\begin{aligned} &= \sum_i \frac{\partial E_{k'}^\alpha}{\partial \langle n_k^\sigma \rangle} |M_{ii}^\alpha| + \frac{1}{2} f_{k'k}^{\uparrow,\sigma} |M_{11}^\alpha| + \frac{1}{2} f_{k'+Q,k}^{\uparrow,\sigma} |M_{33}^\alpha| \\ &\quad - \frac{1}{2} f_{k'k}^{\downarrow,\sigma} |M_{22}^\alpha| - \frac{1}{2} f_{k'+Q,k}^{\downarrow,\sigma} |M_{44}^\alpha|, \end{aligned} \quad (\text{B.66})$$

where in the third line (B.64) was used. Thus the derivative of the energies is given by

$$\frac{\partial E_{k'}^\alpha}{\partial \langle n_k^\sigma \rangle} = \frac{1}{2} \frac{f_{k'k}^{\uparrow,\sigma} |M_{11}^\alpha| - f_{k'k}^{\downarrow,\sigma} |M_{22}^\alpha|}{\sum_i |M_{ii}^\alpha|} + R_{k+Q}, \quad (\text{B.67})$$

where R_{k+Q} represents a term identical with first term with the replacement $k' \rightarrow k' + Q$. From the variation of the grand canonical potential

$$\frac{\partial \Omega}{\partial \langle n_k^\sigma \rangle} = \frac{\partial E^c}{\partial \langle n_k^\sigma \rangle} + \sum_{k'}' \sum_{\alpha} \frac{\partial E_{k'}^\alpha}{\partial \langle n_k^\sigma \rangle} f(E_{k'}^\alpha) \quad (\text{B.68})$$

we get

$$\delta \mu_{k\sigma} = \sum_{k'} \sum_{\alpha} \frac{1}{2} \frac{f_{k',k}^{\uparrow,\sigma} |M_{11}^\alpha| - f_{-k',k}^{\downarrow,\sigma} |M_{22}^\alpha|}{\prod_{l \neq \alpha} (E_{k'}^l - E_{k'}^\alpha)} f(E_{k'}^\alpha) + \sum_{k'} 2f_{-k',k}^{\downarrow,\sigma} \quad (\text{B.69})$$

where the last term stems from the c-number term, going back to the commutation of the creator and annihilator in the 2nd and 4th diagonal element of the matrix part.

The Filling

The filling is given by

$$-n = \left(\frac{\partial \Omega}{\partial \mu} \right)_{\Delta(\mu)} = \frac{\partial \Omega}{\partial \mu} + \underbrace{\frac{\partial \Omega}{\partial \Delta}}_{=0} \frac{\partial \Delta}{\partial \mu} = \frac{\partial \Omega}{\partial \mu} \quad (\text{B.70})$$

where Δ here represents all different gaps. Thus only the direct dependence on μ has to be evaluated:

$$\frac{\partial \Omega}{\partial \mu} = \sum_{k'} \frac{\partial \xi_k}{\partial \mu} + \sum_{k' \alpha} f(E_{k'}^\alpha) \frac{\partial E_{k'}^\alpha}{\partial \mu}. \quad (\text{B.71})$$

The first term is due to $\sum_k \xi_k$ contribution of the c-number term, which stems from operator permutations.

Only the diagonal elements of the characteristic determinant depend on μ , so that the calculation for the derivation of the eigenvalues is parallel to the one of Pomeranchuk gap (B.65), leading to

$$\begin{aligned} 0 &= \frac{\partial}{\partial \mu} |\mathcal{M}_{k'} - \mathbf{1} E_{k'}^\alpha| \\ &= \sum_i |M_{ii}^\alpha| \frac{\partial}{\partial \mu} (\xi_k (-1)^{i+1} - E_{k'}^\alpha) \end{aligned} \quad (\text{B.72})$$

so that the derivative of the energies is

$$\frac{\partial E_{k'}^\alpha}{\partial \mu} = \frac{\sum_i (-1)^i |M_{ii}^\alpha|}{\sum_i |M_{ii}^\alpha|}. \quad (\text{B.73})$$

The expression for the filling therefore becomes

$$n = \sum_{k'} 1 - \sum_{k' \alpha} f(E_{k'}^\alpha) \frac{\sum_i (-1)^i |M_{ii}^\alpha|}{\sum_i |M_{ii}^\alpha|} \quad (\text{B.74})$$

The denominator can be rewritten, leading to

$$n = \sum_{k'} 1 - \sum_{k'\alpha} f(E_{k'}^\alpha) \frac{\sum_i (-1)^i |\mathbf{M}_{ii}^\alpha|}{\prod_{l \neq \alpha} (E_{k'}^l - E_{k'}^\alpha)} \quad (\text{B.75})$$

the first term can be absorbed into the second by (C.107) leading to the final result

$$n = - \sum_{k'\alpha} \sum_m f((-1)^{m+1} E_{k'}^\alpha) \frac{|\mathbf{M}_{mm}^\alpha|}{\prod_{l \neq \alpha} (E_{k'}^l - E_{k'}^\alpha)}. \quad (\text{B.76})$$

The expressions (B.75) and (B.76) have similar numerical costs, so it is a matter of taste which of both one prefers.

B.6 Grand Canonical Potential for $T = 0$

The grand canonical potential Ω is given by (B.47). In the limit $T \rightarrow 0$ the second part becomes

$$\sum_{k, \alpha; E_k^\alpha < 0} E_k^\alpha, \quad (\text{B.77})$$

which is just the sum over the negative eigenvalues.

To rewrite the c-number term in terms of the gaps, one has to invert the gap definitions (B.35), (B.36), (B.37) and (B.28) to eliminate the expectation values, which requires some care, if the interactions do not have full rank⁵. For example in the SC case, the potential can be written as

$$V_{k,k'} = \sum_i v_i e_k^i e_{k'}^i, \quad (\text{B.78})$$

where v_i are the eigenvalues and e_k^i are the elements of the eigenvectors. If the interaction is separable, only one eigenvalues is non-zero.

If one assumes that the gap is composed only of the eigenvectors of the potential with non-zero eigenvalues, which is the case for all self-consistent solutions, the gap can be re-expressed in amplitudes Δ^i in these eigenvectors:

$$\Delta_p = \sum_i e_p^i \Delta_i. \quad (\text{B.79})$$

Since the expectation values \mathcal{F} are multiplied with the gaps in the c-number term, other parts of the expectation values, not composed of these eigenvectors, are projected out, so that one can assume that also \mathcal{F} is composed of the eigenvectors:

$$\mathcal{F}_p = \sum_i e_p^i \mathcal{F}_i \quad (\text{B.80})$$

⁵ The calculation is done with regard to the numerics, where the interactions are discretised; nevertheless it should be valid for continuous interactions also.

Using the self-consistency equation we find

$$\Delta = \sum_i e^i \Delta^i = \sum_{i,j} e^i (e^j)^T v_j e^i \mathcal{F}_i = \sum_j e^j v_j F_j, \quad (\text{B.81})$$

so that $\Delta_i = v_i \mathcal{F}_i$ and the c-number term is given by⁶

$$-E^c = \sum_i \frac{\Delta_i^2}{v_i} + \sum_i \frac{\pi_i^2}{w_i} + \sum_i \frac{\mathcal{C}_i^2}{2u_i^C} + \sum_i \frac{\mathcal{S}_i^2}{2u_i^S} + \sum_i \frac{(\delta\mu_i^P)^2}{2f_i^C} + \sum_i \frac{(\delta\mu_i^m)^2}{2f_i^S}. \quad (\text{B.82})$$

Combining this rewritten c-number term with (B.77) leads to the desired zero-temperature grand canonical potential.

⁶ Where the various factors in front of the potential in the relation between the gaps and the expectation values have been absorbed into the eigenvalues of the potential.

Appendix C

Gap Equations in Path Integral Formalism

In this section the gap equations will in detail be derived within the functional integral formalism.

C.1 Effective Action

One would like to calculate the partition function

$$Z = \int \prod_K d\bar{\psi} d\psi \exp(S[\psi, \bar{\psi}]) \quad (\text{C.1})$$

with $S[\psi, \bar{\psi}] = S_0[\psi, \bar{\psi}] + S_I[\psi, \bar{\psi}]$, where the free part is given by

$$S_0[\psi, \bar{\psi}] = \sum_K \bar{\psi}_K C_K^{-1} \chi_k^{-1} \psi_K, \quad (\text{C.2})$$

with the sharp momentum-cut-off function

$$\chi_k^{-1} = \Theta(\Lambda - |\xi_k|), \quad (\text{C.3})$$

always used in this work. The interaction part is given by

$$S_I = - \sum_{K_1, K_2, K'_2, K'_1} \frac{1}{4} \Gamma^\Lambda(K_1, K_2, K'_2, K'_1) \bar{\psi}_{K_1} \bar{\psi}_{K_2} \psi_{K'_2} \psi_{K'_1}. \quad (\text{C.4})$$

$K = (\omega_n, k, \sigma)$ is the usual multi-index. Momentum, energy and total spin is assumed to be conserved.

To introduce symmetry-breaking, it is helpful to rewrite (C.1) in terms of a collective field. This is done by means of a Hubbard-Stratonovich transformation, which means completing the square in the exponent. The calculations are long but straightforward.

Introducing the Cooper Field (SC)

First the SC channel; the dependence of the Grassmann fields on the multi-index is rewritten, to avoid redefinition further down. The arguments of the potential are suppressed. Consider first only the terms with fixed (but arbitrary) momentum- (q) and energy-transfer ($\tilde{\omega}$) and fixed spins:

$$\begin{aligned} & \exp \left[-\frac{1}{4} \sum_{k,k'} \sum_{\omega_n \omega'_n} \Gamma \bar{\Psi} \begin{pmatrix} \omega'_n \\ k' \\ \sigma'_1 \end{pmatrix} \bar{\Psi} \begin{pmatrix} -\omega'_n + \tilde{\omega}_n \\ -k' + q \\ \sigma'_2 \end{pmatrix} \Psi \begin{pmatrix} -\omega_n + \tilde{\omega}_n \\ -k + q \\ \sigma_2 \end{pmatrix} \Psi \begin{pmatrix} \omega_n \\ k \\ \sigma_1 \end{pmatrix} \right] \\ &= \exp \left[\frac{1}{4} \sum_{k,k'} \sum_{\omega_n \omega'_n} \Gamma \bar{X}_{k',q,\sigma'_1\sigma'_2}^{\omega'_n \tilde{\omega}_n} X_{k,q,\sigma_1\sigma_2}^{\omega_n \tilde{\omega}_n} \right], \end{aligned} \quad (\text{C.5})$$

where the abbreviation $\bar{X} = \bar{\Psi}\bar{\Psi}$, $X = \Psi\Psi$ was introduced, indices like before. This can be rewritten by completing the square¹

$$\begin{aligned} C(q, \tilde{\omega}, \sigma) &= \int \mathcal{D}\varphi \mathcal{D}\varphi^* \exp \left[\frac{1}{4} \sum (\bar{X} - \varphi^*) \Gamma (X - \varphi) \right] \\ &= \exp \left[\frac{1}{4} \sum \bar{X} \Gamma X \right] \int \mathcal{D}\varphi \mathcal{D}\varphi^* \exp \left[\frac{1}{4} \sum \varphi^* \Gamma \varphi - \bar{X} \Gamma \varphi - \varphi^* \Gamma X \right] \end{aligned}$$

as

$$\int \mathcal{D}\varphi \mathcal{D}\varphi^* \exp \left[-\frac{1}{4} \sum_{k,k'} \sum_{\omega_n \omega'_n} -\varphi^* \Gamma \varphi + \varphi^* \Gamma X + X \Gamma \varphi \right] \quad (\text{C.6})$$

where bosonic fields have been introduced. The first term in (C.6) can be viewed as the free dispersion of the bosons, the second and third term as a coupling to the fermions (Yukawa coupling). The bosonic fields

$$\varphi^* = \varphi^*(k', \omega'_n; q, \tilde{\omega}_n, \sigma'_1 \sigma'_2) \quad (\text{C.7})$$

$$\varphi = \varphi(k, \omega_n; q, \tilde{\omega}_n, \sigma_2 \sigma_1) \quad (\text{C.8})$$

$$(\text{C.9})$$

are c-number fields. If more than one bosonic field is discussed the SC field is called φ^s .

To rewrite the complete interaction consider

$$\begin{aligned} & \exp \left[-\frac{1}{4} \sum_{\sigma'_1 \sigma'_2 \sigma_2 \sigma_1} \sum_{q \tilde{\omega}_n} \sum_{k \omega_n k' \omega'_n} \Gamma \bar{\psi} \bar{\psi} \psi \psi \right] \\ &= \prod_{\sigma'_1 \sigma'_2 \sigma_2 \sigma_1} \prod_{q \tilde{\omega}_n} \exp \left[-\frac{1}{4} \sum_{k \omega_n k' \omega'_n} \Gamma \bar{\psi} \bar{\psi} \psi \psi \right] \\ &= \prod_{\sigma'_1 \sigma'_2 \sigma_2 \sigma_1} \prod_{q \tilde{\omega}_n} \int \mathcal{D}\varphi^* \mathcal{D}\varphi \exp \left[-\frac{1}{4} \sum_{k \omega_n k' \omega'_n} (-\varphi^* \Gamma \varphi + \varphi^* \Gamma X + X \Gamma \varphi) \right] \\ &= \int \mathcal{D}\varphi^* \mathcal{D}\varphi \exp \left[-\frac{1}{4} \sum_{\sigma'_1 \sigma'_2 \sigma_2 \sigma_1} \sum_{q \tilde{\omega}_n} \sum_{k \omega_n k' \omega'_n} (-\varphi^* \Gamma \varphi + \varphi^* \Gamma X + X \Gamma \varphi) \right], \end{aligned} \quad (\text{C.10})$$

¹ Up to the constant from performing the Gaussian integral, which is unimportant here, as the focus in this work is only on the saddle point.

i.e., all the interactions are still fully taken into account, so that this step is still exact.

Since not all channels are expected to be of the same importance restrictions are employed to reduce the complexity. First set $q = 0$, i.e., pairs have not net momentum, and $\tilde{\omega} = 0$, i.e., pairs are static. Further $\sigma_2 = -\sigma_1 = -\sigma$, i.e., only singlet pairs ($\rightarrow \sigma'_2 = -\sigma'_1 \equiv -\sigma'$ from the spin-rotation symmetry) are considered. The interaction for the superconductor is, therefore, defined as

$$\begin{aligned} V \begin{pmatrix} \omega' & \omega & \sigma' \\ k' & k & \sigma' \end{pmatrix} &= \Gamma(K', -K'; -K, K) = \Gamma(-K', K'; K, -K) \\ &= V \begin{pmatrix} -\omega' & -\omega & -\sigma' \\ -k' & -k & -\sigma' \end{pmatrix}. \end{aligned} \quad (\text{C.11})$$

Like in the operator mean-field calculation the spin sum can be performed, but the symmetries of the bosonic fields are not as obvious as for the expectation values. To deduce them, consider first only one of the terms of the exponent of (C.10), say

$$\sum \varphi^*(k', \omega'_n; q, \tilde{\omega}_n, \sigma'_1 \sigma'_2) \Gamma \begin{pmatrix} \omega' & \omega & \tilde{\omega} \\ k' & k & q \end{pmatrix} \Psi \begin{pmatrix} -\omega_n + \tilde{\omega}_n \\ -k + q/2 \\ \sigma_2 \end{pmatrix} \Psi \begin{pmatrix} \omega_n + \tilde{\omega}_n \\ k + q/2 \\ \sigma_1 \end{pmatrix}. \quad (\text{C.12})$$

With the restrictions given above and the interaction V (C.11) we find

$$\begin{aligned} & T \sum \varphi^*(k', \omega', \sigma') V \begin{pmatrix} \omega' & \omega & \sigma' \\ k' & k & \sigma' \end{pmatrix} \Psi \begin{pmatrix} -\omega_n \\ -k \\ -\sigma \end{pmatrix} \Psi \begin{pmatrix} \omega_n \\ k \\ \sigma \end{pmatrix} \\ &= T \sum \varphi^*(k', \omega', \sigma') \times \\ & \quad \left[V \begin{pmatrix} \omega' & \omega & \uparrow \\ k' & k & \sigma' \end{pmatrix} \Psi \begin{pmatrix} -\omega_n \\ -k \\ \downarrow \end{pmatrix} \Psi \begin{pmatrix} \omega_n \\ k \\ \uparrow \end{pmatrix} - V \begin{pmatrix} \omega' & \omega & \downarrow \\ k' & k & \sigma' \end{pmatrix} \Psi \begin{pmatrix} \omega_n \\ k \\ \downarrow \end{pmatrix} \Psi \begin{pmatrix} -\omega_n \\ -k \\ \uparrow \end{pmatrix} \right] \\ &= T \sum \varphi^*(k', \omega', \sigma') \left[V \begin{pmatrix} \omega' & \omega & \uparrow \\ k' & k & \sigma' \end{pmatrix} - V \begin{pmatrix} \omega' & -\omega & \downarrow \\ k' & -k & \sigma' \end{pmatrix} \right] \Psi \begin{pmatrix} -\omega_n \\ -k \\ \downarrow \end{pmatrix} \Psi \begin{pmatrix} \omega_n \\ k \\ \uparrow \end{pmatrix} \\ &= T \sum [\varphi^*(k', \omega', \sigma') - \varphi^*(-k', -\omega', -\sigma')] V \begin{pmatrix} \omega' & \omega & \uparrow \\ k' & k & \sigma' \end{pmatrix} \Psi \begin{pmatrix} -\omega_n \\ -k \\ \downarrow \end{pmatrix} \Psi \begin{pmatrix} \omega_n \\ k \\ \uparrow \end{pmatrix}. \end{aligned} \quad (\text{C.13})$$

The expression in the last line

$$\varphi^*(k', \omega', \sigma') - \varphi^*(-k', -\omega', -\sigma') \quad (\text{C.14})$$

projects the antisymmetric part out. Thus, φ^* can be assumed to be antisymmetric, so that (C.14) becomes

$$\varphi^*(k', \omega', \sigma') + \varphi^*(k', \omega', \sigma') = 2\varphi^*(k', \omega', \sigma'). \quad (\text{C.15})$$

From

$$V \begin{pmatrix} \omega' & \omega & \uparrow \\ k' & k & \sigma' \end{pmatrix} = -V \begin{pmatrix} -\omega' & \omega & \uparrow \\ -k' & k & -\sigma' \end{pmatrix} \quad (\text{C.16})$$

we obtain in the same manner

$$\begin{aligned} & \sum_{\omega' k' \sigma'} \varphi^*(k', \omega', \sigma') V \begin{pmatrix} \omega' & \omega & \uparrow \\ k' & k & \sigma' \end{pmatrix} \\ &= \sum_{\omega' k'} (\varphi^*(k', \omega', \uparrow) - \varphi^*(-k', -\omega', \downarrow)) V \begin{pmatrix} \omega' & \omega & \uparrow \\ k' & k & \uparrow \end{pmatrix}. \end{aligned} \quad (\text{C.17})$$

Thus, we finally find (suppressing the spin indices in the interaction)

$$T \sum \varphi_{k',\omega'}^* V \begin{pmatrix} \omega' & \omega \\ k' & k \end{pmatrix} \Psi \begin{pmatrix} -\omega_n \\ -k \\ \downarrow \end{pmatrix} \Psi \begin{pmatrix} \omega_n \\ k \\ \uparrow \end{pmatrix}. \quad (\text{C.18})$$

The other terms in (C.10) are in a treated similar manner. The interaction in the SC-channel therefore becomes

$$S_I^{\text{SC}}[\psi, \bar{\psi}, \varphi] = S_I^{\text{SC},c}[\varphi] + S_I^{\text{SC},q}[\psi, \bar{\psi}, \varphi], \quad (\text{C.19})$$

with the condensation energy

$$S_I^{\text{SC},c}[\varphi] = \sum_{\omega,k} \Delta_{\omega,k}^* \varphi_{\omega,k} \quad (\text{C.20})$$

and the part quadratic in ψ

$$S_I^{\text{SC},q}[\psi, \bar{\psi}, \varphi] = - \sum_{\omega,k} \underline{\Psi}_2 \begin{pmatrix} & \Delta_{\omega,k} \\ \Delta_{\omega,k}^* & \end{pmatrix} \bar{\underline{\Psi}}_2 \quad (\text{C.21})$$

or, summing only over the magnetic BZ (indicated by the prime) to prepare the combination with the AF gap,

$$\begin{aligned} & S_I^{\text{SC},q}[\psi, \bar{\psi}, \varphi] \\ &= - \sum'_{\omega,k} \underline{\Psi}_4 \begin{pmatrix} & \Delta_{\omega,k} & & \\ \Delta_{\omega,k}^* & & & \\ & & \Delta_{\omega,k+Q} & \\ & \Delta_{\omega,k+Q}^* & & \end{pmatrix} \bar{\underline{\Psi}}_4, \end{aligned} \quad (\text{C.22})$$

where the gap was defined as

$$\Delta_{k\omega} = T \sum_{k'\omega'} V \begin{pmatrix} \omega' & \omega \\ k' & k \end{pmatrix} \varphi_{k'\omega'} \quad (\text{C.23})$$

and where the Nambu operators are

$$\underline{\Psi}_2 = \left(\bar{\Psi} \begin{pmatrix} \omega \\ k \\ \uparrow \end{pmatrix}, \Psi \begin{pmatrix} -\omega \\ -k \\ \downarrow \end{pmatrix} \right), \quad (\text{C.24})$$

for the 2×2 case and

$$\underline{\Psi}_4 = \left(\bar{\Psi} \begin{pmatrix} \omega \\ k \\ \uparrow \end{pmatrix}, \Psi \begin{pmatrix} -\omega \\ -k \\ \downarrow \end{pmatrix}, \bar{\Psi} \begin{pmatrix} \omega \\ k+Q \\ \uparrow \end{pmatrix}, \Psi \begin{pmatrix} -\omega \\ -k+Q \\ \downarrow \end{pmatrix} \right). \quad (\text{C.25})$$

for the 4×4 case, respectively.

Introducing the Pi-Pair

Parallel to the SC-pair the π -pair case is introduced. Instead of the restriction to zero-momentum pairs ($q = 0$), pairs with $q = (\pi, \pi) \equiv Q$ are considered. No double counting of degrees of freedom appears with respect to the superconducting channel. The potential is defined by

$$W \begin{pmatrix} \omega' & \omega & \sigma \\ k' & k & \sigma' \end{pmatrix} = \Gamma \begin{pmatrix} \omega' & -\omega' & -\omega & \omega \\ k'+Q/2 & -k'+Q/2 & -k+Q/2 & k+Q/2 \\ \sigma' & -\sigma' & -\sigma & \sigma \end{pmatrix}. \quad (\text{C.26})$$

From this again certain symmetries follow:

$$W \begin{pmatrix} \omega' & \omega \\ k' & k \\ \sigma' & \sigma \end{pmatrix} = W \begin{pmatrix} -\omega' & -\omega \\ -k' & -k \\ -\sigma' & -\sigma \end{pmatrix} = -W \begin{pmatrix} -\omega' & \omega \\ -k' & k \\ -\sigma' & \sigma \end{pmatrix}. \quad (\text{C.27})$$

A strictly parallel calculation to the SC case leads to the π -gap²

$$\pi_{\omega k} = T \sum_{\omega' k'} W \begin{pmatrix} \omega' & \omega \\ k' & k \end{pmatrix} \varphi_{\omega' k'}^{\pi} \quad (\text{C.28})$$

a contribution to the condensation energy

$$S_I^{\pi, c}[\varphi] = \sum_{\omega, k} \pi^*(\omega, k) \varphi^{\pi}(\omega, k), \quad (\text{C.29})$$

and a contribution to the quadratic part

$$\begin{aligned} & S_I^{\pi, q}[\psi, \bar{\psi}, \varphi] \\ &= \sum'_{\omega, k} \bar{\Psi}_4 \begin{pmatrix} & & \pi_{\omega, k} \\ & \pi_{\omega, k+Q} & \pi_{\omega, k+Q}^* \\ \pi_{\omega, k}^* & & \end{pmatrix} \bar{\Psi}_4, \end{aligned} \quad (\text{C.30})$$

with the same Nambu operators (C.25) as before.

Introducing the Spin/Charge-Wave (AF)

To prepare the HS-transformation in the AF channel the energy ω and momentum k dependence in the interaction is written as

$$\begin{aligned} S_I &= \sum_{K_1, K_2, K'_2, K'_1} \frac{1}{4} \Gamma(K_1, K_2, K'_2, K'_1) \bar{\Psi}_{K_1} \bar{\Psi}_{K_2} \Psi_{K'_2} \Psi_{K'_1} \\ &= \frac{1}{4} \sum \bar{\Psi} \begin{pmatrix} \omega' \\ k' \\ \sigma'_1 \end{pmatrix} \Psi \begin{pmatrix} \omega'+\tilde{\omega} \\ k'+q \\ \sigma'_1 \end{pmatrix} \bar{\Psi} \begin{pmatrix} \omega+\tilde{\omega} \\ k+q \\ \sigma'_2 \end{pmatrix} \Psi \begin{pmatrix} \omega \\ k \\ \sigma_2 \end{pmatrix} \Gamma(kk'\omega\omega', \tilde{\omega}q, \sigma) \\ &= \frac{1}{4} \sum \bar{X}(k'\omega'\sigma'_1, q, \tilde{\omega}\sigma_1) X(k\omega\sigma_2, q, \tilde{\omega}\sigma_2) \Gamma(kk'\omega\omega', \tilde{\omega}q, \sigma) \end{aligned} \quad (\text{C.31})$$

² With a different field than in the SC case φ^{π} .

Performing the Hubbard-Stratonovich transformation parallel as in (C.10), with a different field $\varphi^A \equiv \varphi$ in this section, one obtains

$$\begin{aligned} & \exp(S_I) \\ &= \int \mathcal{D}\varphi \mathcal{D}\varphi^* \left(-\frac{1}{4} \sum (-\varphi^* \Gamma \varphi + \varphi^* \Gamma X + \bar{X} \Gamma \varphi) \right), \end{aligned} \quad (\text{C.32})$$

where $\sum = \sum_{\sigma_i} \sum_{q\tilde{\omega}} \sum_{kk'\omega\omega'}$, X, \bar{X} like before, arguments of φ, φ^* like X, \bar{X} , and

$$\Gamma(K'_1, K'_2; K_2, K_1) = \Gamma \left(\begin{matrix} \omega' & \omega + \tilde{\omega} \\ k' & k+q \\ \sigma'_1 & \sigma'_2 \end{matrix}; \begin{matrix} \omega & \omega' + \tilde{\omega} \\ k & k'+q \\ \sigma_2 & \sigma_1 \end{matrix} \right). \quad (\text{C.33})$$

The channel considered to be relevant is given by the restriction to $\tilde{\omega} = 0$, i.e., static pairs, $q = (\pi, \pi) \equiv Q$, i.e., commensurate charge/spin-order, $\sigma_1 = \sigma'_1 \rightarrow \sigma_2 = \sigma'_2$, i.e., spin-projection axis in z -direction. The interaction in this channel is hence given by

$$\Gamma \left(\begin{matrix} \omega' & \omega \\ k' & k+Q \\ \sigma' & \sigma \end{matrix}; \begin{matrix} \omega' & \omega' \\ k' & k'+Q \\ \sigma' & \sigma' \end{matrix} \right) = U \left(\begin{matrix} \omega' & \omega \\ k' & k \\ \sigma' & \sigma \end{matrix} \right) = U \left(\begin{matrix} \omega & \omega' \\ k & k' \\ \sigma & \sigma' \end{matrix} \right) = U \left(\begin{matrix} \omega' & \omega \\ k'+Q & k+Q \\ \sigma' & \sigma \end{matrix} \right). \quad (\text{C.34})$$

While in the SC- and π -case the spin sum can be performed by using the symmetry of the potential, in the AF case the summation can be reduced in k -space to the magnetic BZ. This is seen by considering first the last two terms in the exponent of (C.32)

$$\begin{aligned} & \frac{1}{\beta} \sum_{\sigma\sigma'} \sum_{k\omega k'\omega'} \bar{\Psi} \left(\begin{matrix} \omega' \\ k' \\ \sigma' \end{matrix} \right) \Psi \left(\begin{matrix} \omega' \\ k'+Q \\ \sigma' \end{matrix} \right) \varphi \left(\begin{matrix} \omega \\ k \\ \sigma \end{matrix} \right) U \left(\begin{matrix} \omega' & \omega \\ k' & k \\ \sigma' & \sigma \end{matrix} \right) \\ &+ \frac{1}{\beta} \sum_{\sigma\sigma'} \sum_{k\omega k'\omega'} \varphi^* \left(\begin{matrix} k' \\ \omega' \\ \sigma' \end{matrix} \right) \bar{\Psi} \left(\begin{matrix} \omega \\ k+Q \\ \sigma \end{matrix} \right) \Psi \left(\begin{matrix} \omega \\ k \\ \sigma \end{matrix} \right) U \left(\begin{matrix} \omega' & \omega \\ k' & k \\ \sigma' & \sigma \end{matrix} \right) \\ &= \frac{1}{\beta} \sum_{\sigma\sigma'} \sum_{k\omega k'\omega'} \left(\varphi^* \left(\begin{matrix} k+Q \\ \omega \\ \sigma \end{matrix} \right) + \varphi \left(\begin{matrix} k \\ \omega \\ \sigma \end{matrix} \right) \right) \bar{\Psi} \left(\begin{matrix} \omega' \\ k' \\ \sigma' \end{matrix} \right) \Psi \left(\begin{matrix} \omega' \\ k'+Q \\ \sigma' \end{matrix} \right) U \left(\begin{matrix} \omega' & \omega \\ k' & k \\ \sigma' & \sigma \end{matrix} \right) \end{aligned} \quad (\text{C.35})$$

where (C.34) was used. Due to this the part anti-symmetric under translation and complex conjugation is projected out so that

$$\varphi^* \left(\begin{matrix} k+Q \\ \omega \\ \sigma \end{matrix} \right) = \varphi \left(\begin{matrix} k \\ \omega \\ \sigma \end{matrix} \right) \quad (\text{C.36})$$

can be assumed. With the definition of the gap as

$$\mathcal{A}^* \left(\begin{matrix} \omega \\ k \\ \sigma \end{matrix} \right) = \frac{1}{2} T \sum U \left(\begin{matrix} \omega' & \omega \\ k' & k \\ \sigma' & \sigma \end{matrix} \right) \varphi^* \left(\begin{matrix} \omega' \\ k' \\ \sigma' \end{matrix} \right) = \mathcal{A} \left(\begin{matrix} \omega \\ k+Q \\ \sigma \end{matrix} \right) \quad (\text{C.37})$$

both Yukawa terms in (C.32) are given by

$$\sum_{k\omega\sigma} \bar{\Psi} \left(\begin{matrix} \omega \\ k+Q \\ \sigma \end{matrix} \right) \Psi \left(\begin{matrix} \omega \\ k \\ \sigma \end{matrix} \right) \frac{1}{2} \mathcal{A}^* \left(\begin{matrix} \omega \\ k \\ \sigma \end{matrix} \right) + \sum_{k'\omega'\sigma'} \bar{\Psi} \left(\begin{matrix} \omega' \\ k' \\ \sigma' \end{matrix} \right) \Psi \left(\begin{matrix} \omega' \\ k'+Q \\ \sigma' \end{matrix} \right) \frac{1}{2} \mathcal{A} \left(\begin{matrix} \omega' \\ k' \\ \sigma' \end{matrix} \right). \quad (\text{C.38})$$

With the help of

$$\sum f(k) = \sum' (f(k) + f(k+Q)), \quad (\text{C.39})$$

the sum can be restricted to the magnetic BZ, indicated by the prime ', so that the factors 1/2 in (C.38) vanish

$$\sum'_{k\omega\sigma} \left[\bar{\Psi} \left(\begin{smallmatrix} \omega \\ k+Q \\ \sigma \end{smallmatrix} \right) \Psi \left(\begin{smallmatrix} \omega \\ k \\ \sigma \end{smallmatrix} \right) \mathcal{A}^* \left(\begin{smallmatrix} \omega \\ k \\ \sigma \end{smallmatrix} \right) + \bar{\Psi} \left(\begin{smallmatrix} \omega \\ k \\ \sigma \end{smallmatrix} \right) \Psi \left(\begin{smallmatrix} \omega \\ k+Q \\ \sigma \end{smallmatrix} \right) \mathcal{A} \left(\begin{smallmatrix} \omega \\ k \\ \sigma \end{smallmatrix} \right) \right] \quad (\text{C.40})$$

where (C.37) was used.

The contribution to the condensation term is

$$S_I^{\text{AF,c}} = \sum \varphi^* U \varphi = \sum \varphi^* \left(\begin{smallmatrix} \omega \\ k \\ \sigma \end{smallmatrix} \right) \frac{1}{2} \mathcal{A} \left(\begin{smallmatrix} \omega \\ k \\ \sigma \end{smallmatrix} \right) \quad (\text{C.41})$$

So that altogether the AF contribution is

$$S_I^{\text{AF}} = S_I^{\text{AF,c}} + S_I^{\text{AF,q}} \quad (\text{C.42})$$

where the quadratic part can be written in matrix form,

$$S_I^{\text{AF,q}} = - \sum'_{k\omega\sigma} \underline{\Psi}_2 \begin{pmatrix} & \mathcal{A}_{\omega,k,\sigma} \\ \mathcal{A}_{\omega,k,\sigma}^* & \end{pmatrix} \underline{\Psi}_2 \quad (\text{C.43})$$

$$= - \sum'_{k\omega} \underline{\Psi}_4 \begin{pmatrix} & & \mathcal{A}_{\omega,k,\uparrow} & \\ & & & -\mathcal{A}_{-\omega,-k,\downarrow}^* \\ \mathcal{A}_{\omega,k,\uparrow}^* & & & \\ -\mathcal{A}_{-\omega,-k,\downarrow} & & & \end{pmatrix} \underline{\Psi}_4 \quad (\text{C.44})$$

where the Nambu spinor is here

$$\underline{\Psi}_2 = \left(\bar{\Psi} \left(\begin{smallmatrix} \omega \\ k \\ \sigma \end{smallmatrix} \right), \bar{\Psi} \left(\begin{smallmatrix} \omega \\ k+Q \\ \sigma \end{smallmatrix} \right) \right) \quad (\text{C.45})$$

in the 2×2 case and

$$\underline{\Psi}_4 = \left(\bar{\Psi} \left(\begin{smallmatrix} \omega \\ k \\ \uparrow \end{smallmatrix} \right), \Psi \left(\begin{smallmatrix} -\omega \\ -k \\ \downarrow \end{smallmatrix} \right), \bar{\Psi} \left(\begin{smallmatrix} \omega \\ k+Q \\ \uparrow \end{smallmatrix} \right), \Psi \left(\begin{smallmatrix} -\omega \\ -k+Q \\ \downarrow \end{smallmatrix} \right) \right). \quad (\text{C.46})$$

in the 4×4 case as before (C.25), respectively.

The Pomeranchuk distortion (and magnetic gap) $\delta\mu_k$

The $q = 0$ terms of (C.32) can be interpreted as a distortion of the Fermi surface, which is the Pomeranchuk distortion if it is spin-independent and the ferromagnetic gap if it is spin-dependent. Therefore, define the interaction for $q = 0$ (with spins like in the AF case)

$$\Gamma \left(\begin{smallmatrix} \omega' & \omega \\ k' & k \\ \sigma' & \sigma \end{smallmatrix}; \begin{smallmatrix} \omega & \omega' \\ k & k' \\ \sigma & \sigma' \end{smallmatrix} \right) = f \left(\begin{smallmatrix} \omega' & \omega \\ k' & k \\ \sigma' & \sigma \end{smallmatrix} \right) = f \left(\begin{smallmatrix} \omega & \omega' \\ k & k' \\ \sigma & \sigma' \end{smallmatrix} \right). \quad (\text{C.47})$$

Due to this symmetry, $\varphi(\omega, k, \sigma) = \varphi^*(\omega, k, \sigma)|^3$ can be assumed so that the Ψ -dependent part reads

$$\frac{1}{2}T \sum_{\sigma\sigma'} \sum_{k\omega k'\omega'} \bar{\Psi} \begin{pmatrix} \omega \\ k \\ \sigma \end{pmatrix} \Psi \begin{pmatrix} \omega \\ k \\ \sigma \end{pmatrix} \varphi \begin{pmatrix} k' \\ \omega' \\ \sigma' \end{pmatrix} f \begin{pmatrix} \omega & \omega' \\ k & k' \\ \sigma & \sigma' \end{pmatrix}. \quad (\text{C.48})$$

Defining the gap as

$$\delta\mu_{\omega,k,\sigma} = \frac{1}{2}T \sum_{\omega'k'\sigma'} f \begin{pmatrix} \omega' & \omega \\ k' & k \\ \sigma' & \sigma \end{pmatrix} \varphi_{\omega',k',\sigma'}, \quad (\text{C.49})$$

this contribution has the form of a dispersion:

$$-\sum_{\omega k\sigma} \bar{\Psi} \begin{pmatrix} \omega \\ k \\ \sigma \end{pmatrix} \Psi \begin{pmatrix} \omega \\ k \\ \sigma \end{pmatrix} \delta\mu_{\omega,k,\sigma}. \quad (\text{C.50})$$

The contribution to the condensation energy is

$$\sum_{\omega,k,\sigma} \varphi_{\omega,k,\sigma} \frac{1}{2} \delta\mu_{\omega,k,\sigma}. \quad (\text{C.51})$$

C.2 Bosonic Action

Altogether, the sum of the different contributions for the SC-, π -, AF- and Pomeranchuk pair

$$S_I[\psi, \bar{\psi}, \phi] = S_I^{\text{SC}} + S_I^\pi + S_I^{\text{AF}} + S_I^{\text{f}} \quad (\text{C.52})$$

gives

$$\begin{aligned} S[\psi, \bar{\psi}, \varphi] &= S_0[\psi, \bar{\psi}] + S_I[\psi, \bar{\psi}, \varphi] \\ &= S^{\text{c}}[\varphi] - \sum'_{k\omega} \psi \mathcal{M} \bar{\psi} \end{aligned} \quad (\text{C.53})$$

with $\mathcal{M}(k, \omega) =$

$$\begin{pmatrix} \bar{\xi}_k - i\omega\chi_k^{-1} & \Delta_{\omega,k} & \mathcal{A}_{\omega,k,\uparrow} & \pi_{\omega,k} \\ \Delta_{\omega,k}^* & -\bar{\xi}_k - i\omega\chi_k^{-1} & \pi_{\omega,k+Q}^* & -\mathcal{A}_{-\omega,-k,\downarrow}^* \\ \mathcal{A}_{\omega,k,\uparrow}^* & \pi_{\omega,k+Q}^* & \bar{\xi}_{k+Q} - i\omega\chi_{k+Q}^{-1} & \Delta_{\omega,k+Q} \\ \pi_{\omega,k}^* & -\mathcal{A}_{-\omega,-k,\downarrow} & \Delta_{\omega,k+Q}^* & -\bar{\xi}_{k+Q} - i\omega\chi_{k+Q}^{-1} \end{pmatrix} \quad (\text{C.54})$$

denoting

$$\bar{\xi}_k = (\varepsilon_k - \mu)\chi_k^{-1} + \delta\mu_{\omega,k,\sigma} \quad (\text{C.55})$$

and the Nambu spinor

$$\underline{\Psi}_4 = \left(\bar{\Psi} \begin{pmatrix} \omega \\ k \\ \uparrow \end{pmatrix}, \Psi \begin{pmatrix} -\omega \\ -k \\ \downarrow \end{pmatrix}, \bar{\Psi} \begin{pmatrix} \omega \\ k+Q \\ \uparrow \end{pmatrix}, \Psi \begin{pmatrix} -\omega \\ -k+Q \\ \downarrow \end{pmatrix} \right). \quad (\text{C.56})$$

³ Meaning that the field is real, like one expects, as this field can be interpreted as a momentum- and spin-dependent density.

The condensation term is

$$\begin{aligned}
S^c[\varphi] &= \sum_{\omega,k} \varphi_{\omega,k}^s \Delta^*(\omega, k) + \sum_{\omega,k} \varphi_{\omega,k}^\pi \pi_{\omega,k}^* \\
&+ \sum_{\omega,k,\sigma} (\varphi_{\omega,k,\sigma}^A)^* \frac{1}{2} \mathcal{A}_{\omega,k,\sigma} + \sum_{\omega,k,\sigma} \varphi_{\omega,k,\sigma}^\delta \frac{1}{2} \delta \mu_{\omega,k,\sigma}. \quad (\text{C.57})
\end{aligned}$$

As the SC and Pi part on the one hand and the AF and Pomeranchuk part on the other hand are naïvely added, double counting appears, because the channels are not disjoint. For example the $\Gamma(k, -k, -k - Q, k + Q)$ is part of the SC and the AF potential, hence the relevant degrees of freedom are included twice. Since these elements form a space whose dimension is smaller the potential for the gap by one, it is of zero measure, so that this error is negligible⁴.

The action is quadratic in $\bar{\psi}$ and ψ , therefore the integral can be evaluated leading to

$$\begin{aligned}
Z &= \int \mathcal{D}\bar{\psi} \psi \mathcal{D}\varphi \exp(S[\psi, \bar{\psi}, \varphi]) \\
&= \int \mathcal{D}\varphi \mathcal{D}\bar{\psi} \psi \exp(S[\psi, \bar{\psi}, \varphi]) \\
&\equiv \int \mathcal{D}\varphi \exp(S^{\text{eff}}[\varphi]) \quad (\text{C.58})
\end{aligned}$$

with⁵

$$S^{\text{eff}}[\varphi] = S^c + \beta \sum' \ln \det \mathcal{M}. \quad (\text{C.59})$$

The obtained action is purely bosonic. It is no longer quadratic in φ , as expanding the logarithm leads to terms of all orders. Therefore, the integration cannot be performed exactly, and approximations have to be employed. If the employed approximations are valid, this model describes the same physics as the fermionic one. However, it paves the way into the symmetry-broken state.

C.3 Saddle-Point Approximation

The saddle-point approximation is equivalent to the mean-field approximation in the operator formalism. Thus we have to evaluate

$$\delta S^{\text{eff}}[\varphi] \equiv 0. \quad (\text{C.60})$$

The variation with respect to each field has to vanish, leading to (coupled) self-consistency equations, one for each pair-field – the gap equations.

⁴ In the numerics the BZ is discretised, so that one cannot speak of zero measure. But the error still should be small, as long as the interactions of the doubly counted elements do not become much larger compared with the others.

⁵ $\det \mathcal{M}$ is of dimension T^4 , so the log is not defined strictly. This could be corrected by an appropriate factor, which would drop out in the gap equations. The factor β in front of the sum, however, must not be omitted as this would alter the gap equations. It stems from the convention used here $\sum_{\omega_n} = T \sum_n$.

The gap equation for the SC gap

First the cooper-pair field, from

$$\frac{\delta}{\delta\varphi^s(\omega', k')} S^{\text{eff}}[\varphi] = \frac{\delta}{\delta\varphi^s(\omega', k')} \left[S^c - \beta \sum' \ln \det \mathcal{M} \right] = 0 \quad (\text{C.61})$$

with the help of ($\varphi \equiv \varphi^s$ in this section)

$$\frac{\delta}{\delta\varphi(\omega', k')} \Delta(\omega, k) = T^2 V \left(\begin{smallmatrix} \omega' & \omega \\ k' & k \end{smallmatrix} \right) \quad (\text{C.62})$$

the condensation term yields

$$\sum_{\omega, k} \Delta^*(\omega k) \delta_{\omega\omega'} = T \Delta^*(\omega', k'). \quad (\text{C.63})$$

The second term is

$$\beta \sum'_{\omega, k} \frac{1}{\det \mathcal{M}} \frac{\delta}{\delta\varphi(\omega', k')} \det \mathcal{M} \quad (\text{C.64})$$

with

$$\begin{aligned} & \frac{\delta}{\delta\varphi(\omega', k')} \det \mathcal{M} \\ &= -\det(\mathcal{M}_{12}) T^2 V \left(\begin{smallmatrix} \omega' & \omega \\ k' & k \end{smallmatrix} \right) - \det(\mathcal{M}_{34}) T^2 V \left(\begin{smallmatrix} \omega' & \omega \\ k' & k+Q \end{smallmatrix} \right). \end{aligned} \quad (\text{C.65})$$

Inserting (C.65) in (C.64) and summing with (C.39) over the whole BZ one obtains

$$T \sum_{k\omega} \frac{\det(\mathcal{M}_{12}) V \left(\begin{smallmatrix} \omega' & \omega \\ k' & k \end{smallmatrix} \right)}{\det \mathcal{M}}. \quad (\text{C.66})$$

The potential is assumed to be ω -independent, since the RG is done in the static approximation⁶. Thus it can be taken out of the Matsubara summation. The details can be found in appendix (D.4), formula (D.48). This leads to

$$T \sum_k \sum_\alpha \frac{\det(\mathbf{M}_{12}^\alpha) V_{k'k}}{\sum_l \det \mathbf{M}_{ll}^\alpha} \frac{-1}{1 + \exp(\beta E_k^\alpha)}, \quad (\text{C.67})$$

where $\mathbf{M} = \mathcal{M}(i\omega = E_k)$ has been introduced.

Combining (C.67) and (C.63) one gets the desired gap equation for the SC gap

$$\Delta_k^* = - \sum_{k'} \sum_\alpha \frac{\det(\mathbf{M}_{12}^\alpha(k')) V_{kk'}}{\sum_l \det \mathbf{M}_{ll}^\alpha(k')} f(E_{k'}^\alpha). \quad (\text{C.68})$$

⁶ From this follows also an ω_n -independent gap.

The denominator can be interpreted as the trace of the inverse matrix times the determinant, thus can be expressed in terms of the eigenvalues (D.27), giving

$$\Delta_k^* = - \sum_k \sum_\alpha \frac{\det(\mathbf{M}_{12}^\alpha(k')) V_{kk'}}{\prod_{i \neq \alpha} (E_{k'}^i - E_{k'}^\alpha)} f(E_{k'}^\alpha). \quad (\text{C.69})$$

With some further matrix algebra (D.31) this can be written as

$$\Delta_k^* = - \sum_k \sum_\alpha [V_{k'k} v_\alpha^2 (v_\alpha^1)^*] f(E_{k'}^\alpha) \quad (\text{C.70})$$

where v_α^i is the i^{th} component of the α^{th} normalised eigenvector of the matrix \mathcal{M} where the frequencies ω_n are set to zero. As in the four by four case the last two gap equations seem to have similar numerical requirements, so that any of them can be chosen in numerical calculations.

In case of a spin-rotational invariant interaction the potential can be decomposed in various ways. Here we employ the singlet–triplet decomposition is employed, which leads to

$$V_{kk'} = \frac{1}{2} (V_{kk'}^s + V_{kk'}^t) \quad (\text{C.71})$$

and to the gap

$$\Delta_k = T \sum_{k'} \frac{1}{2} (V_{kk'}^s + V_{kk'}^t) \varphi(k'). \quad (\text{C.72})$$

From the fact that $\Delta(k) = \Delta(-k)$ will be assumed, and from the symmetry of the potentials, namely $V_{kk'}^s = V_{-kk'}^s$ and $V_{kk'}^t = -V_{-kk'}^t$ it follows that the triplet potential will not contribute and thus can be ignored.

The gap equation for the Pi-pair

The calculation is parallel to the SC case. Evaluating

$$\frac{\delta}{\delta \varphi_{\omega', k'}^\pi} S^{\text{eff}}[\varphi] = \frac{\delta}{\delta \varphi_{\omega', k'}^\pi} \left[S^c + \beta \sum_{\omega, k} \ln \det \mathcal{M} \right] = 0 \quad (\text{C.73})$$

the condensation term gives

$$\sum_{k\omega} \pi_{k\omega}^* \delta_{\omega\omega'} = +T \pi_{k', \omega'}^* \quad (\text{C.74})$$

with the derivative of the gap

$$\frac{\delta}{\delta \varphi_{k', \omega'}^\pi} \pi_{k\omega} = T^2 W \begin{pmatrix} \omega' & \omega \\ k' & k \end{pmatrix}. \quad (\text{C.75})$$

The matrix term yields

$$T \sum_{k\omega} \frac{\det(\mathcal{M}_{14}) W \begin{pmatrix} \omega' & \omega \\ k' & k \end{pmatrix}}{\det \mathcal{M}}, \quad (\text{C.76})$$

leading, after performing the Matsubara summation, to the gap equation

$$\pi_k^* = - \sum_{k'} \sum_{\alpha} \frac{\det(\mathbf{M}_{14}^{\alpha}(k')) W_{kk'}}{\sum_l \det \mathbf{M}_{ll}^{\alpha}(k')} f(E_{k'}^{\alpha}), \quad (\text{C.77})$$

with $\mathbf{M} = \mathcal{M}(i\omega = E_k)$, which can be simplified to either

$$\pi_k^* = - \sum_{k'} \sum_{\alpha} \frac{\det(\mathbf{M}_{14}^{\alpha}(k')) W_{kk'}}{\prod_{i \neq \alpha} (E_{k'}^i - E_{k'}^{\alpha})} f(E_{k'}^{\alpha}) \quad (\text{C.78})$$

or

$$\pi_k^* = - \sum_{k'} \sum_{\alpha} [W_{kk'} v_{\alpha}^4 (v_{\alpha}^1)^*] f(E_{k'}^{\alpha}). \quad (\text{C.79})$$

The gap equation for the AF gap

The derivation of the gap equation for the AF order parameter is largely similar to the SC case. We have to evaluate

$$\frac{\delta}{\delta \varphi_{\omega, k, \sigma}^A} S^{\text{eff}}[\varphi] = \frac{\delta}{\delta \varphi_{\omega, k, \sigma}^A} \left[S^c + \beta \sum'_{\omega' k'} \ln \det \mathcal{M} \right] \quad (\text{C.80})$$

With ($\varphi \equiv \varphi^A$)

$$\frac{\delta}{\delta \varphi_{\omega, k, \sigma}} \mathcal{A}_{\omega', k', \sigma'} = T^2 \frac{1}{2} U \begin{pmatrix} k' & k \\ \omega' & \omega \\ \sigma' & \sigma \end{pmatrix} \quad (\text{C.81})$$

and, as $\delta \varphi^* / \delta \varphi \neq 0$ by (C.36)

$$\frac{\delta}{\delta \varphi_{\omega, k, \sigma}^A} \mathcal{A}_{\omega', k', \sigma'}^* = T^2 \frac{1}{2} U \begin{pmatrix} k'+Q & k \\ \omega' & \omega \\ \sigma' & \sigma \end{pmatrix} \quad (\text{C.82})$$

the condensation term leads to

$$\frac{\delta}{\delta \varphi_{\omega, k, \sigma}} \sum \varphi_{\omega', k', \sigma'}^* \frac{1}{2} \mathcal{A}_{\omega', k', \sigma'} = T \mathcal{A}_{\omega, k, \sigma}. \quad (\text{C.83})$$

The second term in (C.80) is

$$\frac{\delta}{\delta \varphi_{\omega, k, \sigma}^A} \left[\beta \sum' \ln \det \mathcal{M} \right] = \sum' \frac{1}{|\mathcal{M}|} \frac{\delta}{\delta \varphi} \det \mathcal{M}, \quad (\text{C.84})$$

the inner derivative yields

$$\begin{aligned} \frac{\delta}{\delta \varphi} \det \mathcal{M} = & + |\mathcal{M}_{13}| T^2 \frac{1}{2} U \begin{pmatrix} \omega & \omega' \\ k & k' \\ \sigma & \uparrow \end{pmatrix} + |\mathcal{M}_{31}| T^2 \frac{1}{2} U \begin{pmatrix} \omega & \omega' \\ k & k'+Q \\ \sigma & \uparrow \end{pmatrix} \\ & - |\mathcal{M}_{42}| T^2 \frac{1}{2} U \begin{pmatrix} \omega & -\omega' \\ k & -k' \\ \sigma & \downarrow \end{pmatrix} - |\mathcal{M}_{24}| T^2 \frac{1}{2} U \begin{pmatrix} \omega & -\omega' \\ k & -k'+Q \\ \sigma & \downarrow \end{pmatrix} \end{aligned} \quad (\text{C.85})$$

With this and (C.39) the second term (C.84) becomes

$$-\frac{1}{2}T \sum \frac{|\mathcal{M}_{13}|U \begin{pmatrix} \omega & \omega' \\ k & k' \\ \sigma & \uparrow \end{pmatrix} - |\mathcal{M}_{42}|U \begin{pmatrix} \omega & -\omega' \\ k & -k' \\ \sigma & \downarrow \end{pmatrix}}{|\mathcal{M}|} \quad (\text{C.86})$$

where the k' sum runs again over the whole BZ. Again the interaction is assumed to be ω and ω' -independent, so that with the help of (D.48) the Matsubara sum can be performed leading to

$$\frac{1}{2}T \sum_{k'} \sum_{\alpha} \frac{|\mathbf{M}_{13}^{\alpha}|U \begin{pmatrix} k & k' \\ \sigma & \uparrow \end{pmatrix} - |\mathbf{M}_{42}^{\alpha}|U \begin{pmatrix} k & -k' \\ \sigma & \downarrow \end{pmatrix}}{\sum_l |\mathbf{M}_{ll}|} f(E_{k'}^{\alpha}), \quad (\text{C.87})$$

where $i\omega_n$ is replaced by the different eigenvalues E_k^{α} , depicted by $\mathbf{M} = \mathcal{M}(\omega = E_k^{\alpha})$, over which is summed. This, combined with (C.83), leads to the gap-equation for the AF gap:

$$\mathcal{A}_{k,\sigma} = \frac{1}{2} \sum_{k'} \sum_{\alpha} \frac{|\mathbf{M}_{13}^{\alpha}|U \begin{pmatrix} k & k' \\ \sigma & \uparrow \end{pmatrix} - |\mathbf{M}_{42}^{\alpha}|U \begin{pmatrix} k & -k' \\ \sigma & \downarrow \end{pmatrix}}{\sum_l |\mathbf{M}_{ll}^{\alpha}|} f(E_{k'}^{\alpha}). \quad (\text{C.88})$$

Again, as in the SC case, the denominator can be rewritten with (D.27) as

$$\mathcal{A}_{k,\sigma} = \frac{1}{2} \sum_{k'} \sum_{\alpha} \frac{|\mathbf{M}_{13}^{\alpha}|U \begin{pmatrix} k & k' \\ \sigma & \uparrow \end{pmatrix} - |\mathbf{M}_{42}^{\alpha}|U \begin{pmatrix} k & -k' \\ \sigma & \downarrow \end{pmatrix}}{\prod_{i \neq \alpha} (E_{k'}^i - E_{k'}^{\alpha})} f(E_{k'}^{\alpha}) \quad (\text{C.89})$$

and further with (D.31) this can be rewritten as

$$\mathcal{A}_{k,\sigma} = \frac{1}{2} \sum_{k'} \sum_{\alpha} \left[v_{\alpha}^3 (v_{\alpha}^1)^* U \begin{pmatrix} k' & k \\ \uparrow & \sigma \end{pmatrix} - v_{\alpha}^2 (v_{\alpha}^4)^* U \begin{pmatrix} -k' & k \\ \downarrow & \sigma \end{pmatrix} \right] f(E_{k'}^{\alpha}). \quad (\text{C.90})$$

Again it is a matter of taste which of the last two one chooses.

If the original Hamiltonian is spin-rotation invariant, the spin dependence of U can be expressed in different ways, out of which only the singlet-triplet

$$U \begin{pmatrix} k & k' \\ \sigma & \sigma' \end{pmatrix} = U_{k,k'}^s \frac{1}{2} (1 - \delta_{\sigma,\sigma'}) + U_{k,k'}^t \frac{1}{2} (1 + \delta_{\sigma,\sigma'}) \quad (\text{C.91})$$

and the spin-charge decomposition, which seems more natural for the spin/charge-wave gap

$$U \begin{pmatrix} k & k' \\ \sigma & \sigma' \end{pmatrix} = U_{k,k'}^C + U_{k,k'}^S (2\delta_{\sigma,\sigma'} - 1) \quad (\text{C.92})$$

are used. The gap becomes

$$\begin{aligned} \mathcal{A}_{k\sigma} &= \frac{1}{2}T \sum_{k'} U_{k,k'}^s \varphi_{k'}^{-\sigma} + U_{k,k'}^t (2\varphi_{k'}^{\sigma} + \varphi_{k'}^{-\sigma}) \\ &= \frac{1}{2}T \sum_{k'} U_{k,k'}^C (\varphi_{k'}^{\sigma} + \varphi_{k'}^{-\sigma}) + U_{k,k'}^S (\varphi_{k'}^{\sigma} - \varphi_{k'}^{-\sigma}). \end{aligned} \quad (\text{C.93})$$

In the last line it becomes obvious that U^C couples to a charge-density wave, while U^S couples a spin-density wave, which can be exploited by decomposition of the gap into ($\sigma = 1$ for spin up, $\sigma = -1$ for spin down)

$$\mathcal{A}_{k,\sigma} = \mathcal{C}_k + \sigma \mathcal{S}_k, \quad (\text{C.94})$$

where \mathcal{C}_k represents the charge-density wave and \mathcal{S}_k the spin-density wave, i.e., the anti-ferromagnet.

The gap equation for $\delta\mu$

The gap equation for the Pomeranchuk gap is derived parallel to the anti-ferromagnetic gap.

With

$$\frac{\delta}{\varphi^\delta(\omega, k, \sigma)} \delta\mu(\omega', k', \sigma') = \frac{1}{2} T^2 f \left(\begin{array}{cc} \omega' & \omega \\ k' & k \\ \sigma' & \sigma \end{array} \right) \quad (\text{C.95})$$

we get from the condensation energy

$$\frac{\delta}{\delta\varphi} S^c = T \delta\mu(\omega, k, \sigma). \quad (\text{C.96})$$

With

$$\frac{\delta}{\varphi^\delta(\omega, k, \sigma)} |\mathcal{M}| = |\mathcal{M}_{11}| \frac{1}{2} T^2 f \left(\begin{array}{cc} \omega' & \omega \\ k' & k \\ \uparrow & \sigma \end{array} \right) - |\mathcal{M}_{22}| \frac{1}{2} T^2 f \left(\begin{array}{cc} -\omega' & \omega \\ -k' & k \\ \downarrow & \sigma \end{array} \right) + R_{k+Q}, \quad (\text{C.97})$$

where the reminder term equals the first two terms with k replaced by $k + Q$.

Assuming an ω -independent potential, we obtain from the second term in the usual way:

$$\frac{1}{2} T \sum_{k'\omega'} \frac{\exp(i\omega'\delta) |\mathcal{M}_{11}| f \left(\begin{array}{cc} k' & k \\ \uparrow & \sigma \end{array} \right) - \exp(-i\omega'\delta) |\mathcal{M}_{22}| f \left(\begin{array}{cc} -k' & k \\ \downarrow & \sigma \end{array} \right)}{|\mathcal{M}|}, \quad (\text{C.98})$$

where factors have to be introduced to guarantee convergence, as the determinants of the nominator is of order $(i\omega')^3$ and the denominator is of order $(i\omega')^4$. The signs are chosen to be the same as in the calculation of the filling further down. The result will prove to be consistent with a calculation in the operator formalism.

Thus the gap equation is

$$\begin{aligned} & \delta\mu_{k,\sigma} \\ &= \frac{1}{2} \sum_{k'\sigma'} \sum_{\alpha} \frac{|\mathbf{M}_{11}^{\alpha}| f \left(\begin{array}{cc} k' & k \\ \uparrow & \sigma \end{array} \right)}{\sum_l |M_{ll}^{\alpha}|} f(E_k^{\alpha}) + \frac{1}{2} \sum_{k'} \sum_{\alpha} \frac{|\mathbf{M}_{22}^{\alpha}| f \left(\begin{array}{cc} -k' & k \\ \downarrow & \sigma \end{array} \right)}{\sum_l |M_{ll}^{\alpha}|} f(-E_k^{\alpha}) \\ &= \frac{1}{2} \sum_{k'\alpha} \frac{|\mathbf{M}_{11}^{\alpha}| f \left(\begin{array}{cc} k' & k \\ \uparrow & \sigma \end{array} \right) - |\mathbf{M}_{22}^{\alpha}| f \left(\begin{array}{cc} -k' & k \\ \downarrow & \sigma \end{array} \right)}{\prod_{i \neq \alpha} (E_{k'}^i - E_{k'}^{\alpha})} f(E_k^{\alpha}) + \frac{1}{2} \sum_{k'} f \left(\begin{array}{cc} -k' & k \\ \downarrow & \sigma \end{array} \right) \end{aligned} \quad (\text{C.99})$$

where the last step was done to obtain the same form as the result of the operator calculation. It is parallel to the steps in the filling calculation.

Again using the spin-charge decomposition, we find

$$\delta\mu_{k,\sigma} = \frac{1}{2}T \sum_{k'\sigma'} f_{k'k}^C \left(\varphi_{k'\sigma}^\delta + \varphi_{k'-\sigma}^\delta \right) + f_{k'k}^S \left(\varphi_{k'\sigma}^\delta - \varphi_{k'-\sigma}^\delta \right) \quad (\text{C.100})$$

which implies

$$\delta\mu_{k,\sigma} = \delta\mu_k^P + \sigma\delta\mu_k^m, \quad (\text{C.101})$$

where $\delta\mu_k^P$ is the Pomeranchuk distortion of the Fermi surface with arbitrary form factor, and $\delta\mu_k^m$ is a ferromagnetic gap with arbitrary form factor.

Calculation of the Filling

The filling is given by

$$-n = \partial_\mu \Omega = -T \partial_\mu \ln Z. \quad (\text{C.102})$$

As the condensation term is independent of μ ⁷ we get

$$-n = -T \sum_{k,\omega_n}' \frac{\sum_m |M_{mm}| (-1)^m}{|M|}. \quad (\text{C.103})$$

As the integrand is of order $\sim (i\omega_n)^{-1}$ factors have to be introduced to get convergent expressions. A priori it is not clear whether $\exp(i\omega_n\delta)$ or $\exp(-i\omega_n\delta)$ has to be used. They are chosen in such a way that for vanishing gaps the density of the free electron gas is reproduced, which is

$$-n = -T \sum_{k,\omega_n}' \frac{\sum_m \exp((-1)^{m+1}i\omega_n\delta) |M_{mm}| (-1)^m}{|M|} \quad (\text{C.104})$$

Evaluating the Matsubara sum as before yields

$$= - \sum_{k,\alpha}' \sum_m \frac{|M_{mm}^\alpha|}{\sum_l |M_{ll}^\alpha|} f((-1)^{m+1} E_k^\alpha) \quad (\text{C.105})$$

$$= - \sum_{k,\alpha}' \sum_m \frac{(-1)^{m+1} |M_{mm}^\alpha|}{\sum_l |M_{ll}^\alpha|} f(E_k^\alpha) - \sum_{k,\alpha} \frac{|M_{22}^\alpha|}{\sum_l |M_{ll}^\alpha|} \quad (\text{C.106})$$

$$= - \sum_{k,\alpha}' \sum_m \frac{(-1)^{m+1} |M_{mm}^\alpha|}{\sum_l |M_{ll}^\alpha|} f(E_k^\alpha) - \sum_k (1) \quad (\text{C.107})$$

where the second steps follows from $M_{22}(k+Q) = M_{44}(k)$ and (C.39). The last step follows from $|M_{22}^\alpha|/\sum_l |M_{ll}^\alpha| = |v_\alpha^2|$ (D.31) and the fact that in a matrix formed of orthonormal column-vectors the row vectors are also orthonormal.

⁷ This is in contrast to the operator formalism.

The last step is done to give the equation the same form as in the operator formalism.

This can again be rewritten as

$$n = \sum_k 1 + \sum'_{k,\alpha} \sum_m \frac{(-1)^{m+1} |M_{mm}^\alpha|}{\sum_l |M_{ll}^\alpha|} f(E_k^\alpha) \quad (\text{C.108})$$

$$= \sum_k 1 + \sum'_{k,\alpha} \sum_m \frac{(-1)^{m+1} |M_{mm}^\alpha|}{\prod_{i \neq \alpha} (E_{k'}^i - E_{k'}^\alpha)} f(E_k^\alpha) \quad (\text{C.109})$$

$$= \sum_k 1 + \sum'_{k,\alpha} \sum_m (-1)^{m+1} |v_\alpha^m| f(E_k^\alpha). \quad (\text{C.110})$$

Appendix D

Mathematical Details

D.1 Determinants and Minors

In this section equations, necessary for deriving and simplifying the gap equations, will be derived.

Consider the Hermitian matrix \mathbf{M} with elements m_{ij} where i is the row and j the column index. The determinant is defined recursively by

$$|\mathbf{M}| = \det(\mathbf{M}) = \sum_i^N m_{ij} |\mathbf{M}_{ij}| (-1)^{i+j} \quad \forall j \quad (\text{D.1})$$

where $|\mathbf{M}_{ij}|$ is the Minor of the matrix \mathbf{M} , i.e., the determinant of the matrix which is obtained by removing the i^{th} row and j^{th} column.

It follows immediately that

$$\frac{\partial}{\partial m_{ij}} \det \mathbf{M} = (-1)^{i+j} \det \mathbf{M}_{ij}, \quad (\text{D.2})$$

and from this

$$\frac{\partial}{\partial x} \det \mathbf{M} = \sum_{i,j} (-1)^{i+j} \det(\mathbf{M}_{ij}) \frac{\partial}{\partial x} m_{ij}. \quad (\text{D.3})$$

To derive Cramer's rule, define the matrix

$$\mathbf{M}^0 = \{ |\mathbf{M}_{ij}| (-1)^{i+j} \}^{\text{tr}} = \begin{pmatrix} |\mathbf{M}_{11}| & -|\mathbf{M}_{21}| & \dots \\ -|\mathbf{M}_{12}| & |\mathbf{M}_{22}| & \dots \\ \vdots & \vdots & \ddots \end{pmatrix}. \quad (\text{D.4})$$

Multiplication with \mathbf{M} leads to

$$\mathbf{M}\mathbf{M}^0 = \mathbf{D} \quad (\text{D.5})$$

with the elements

$$d_{ij} = \sum_k^N m_{ik} |\mathbf{M}_{jk}| (-1)^{j+k}. \quad (\text{D.6})$$

For $i = j$ one finds, using (D.1):

$$d_{ii} = \sum_k^N m_{ik} |\mathbf{M}_{ik}| (-1)^{i+k} = \det(\mathbf{M}). \quad (\text{D.7})$$

For $i \neq j$ one obtains, again using (D.1):

$$d_{ij} = \sum_k^N m_{ik} |\mathbf{M}_{jk}| (-1)^{i+j} = \det(\mathbf{M}') \quad (\text{D.8})$$

where \mathbf{M}' is a matrix where the i^{th} and j^{th} row is identical, so that the determinant vanishes. Therefore \mathbf{D} is the identity times the determinant of \mathbf{M} so that Cramer's rule follows

$$\rightarrow \quad \mathbf{M}^0 = \{|\mathbf{M}_{ij}| (-1)^{i+j}\}^{\text{tr}} = \mathbf{M}^{-1} \cdot \det(\mathbf{M}) \quad (\text{D.9})$$

Note that \mathbf{M}^0 is still well-defined even if \mathbf{M} is singular.

In the following some properties of minors of matrices with at least one vanishing eigenvalue will be derived.

First consider

$$\sum_l |\mathbf{M}_{ll}| = \text{Tr}(\mathbf{M}^{-1}) \det \mathbf{M}, \quad (\text{D.10})$$

which is up to a factor the trace of the inverse matrix, see (D.9). As the trace is independent of the basis, the most convenient one will be chosen, which is the basis of eigenvectors, yielding

$$\begin{aligned} \mathbf{M} &= \text{diag}(\lambda_1, \dots, \lambda_N) \\ \mathbf{M}^{-1} &= \text{diag}(\lambda_1^{-1}, \dots, \lambda_N^{-1}) \end{aligned} \quad (\text{D.11})$$

and, of course, $\det(\mathbf{M}) = \prod_i \lambda_i$. It follows

$$\begin{aligned} \sum_l |\mathbf{M}_{ll}| &= \det(\mathbf{M}) \cdot \sum_m \frac{1}{\lambda_m} \\ &= \sum_m \prod_{i \neq m} \lambda_i. \end{aligned} \quad (\text{D.12})$$

if the eigenvalue α vanishes, all *terms* but the α^{th} one become zero in (D.12):

$$\sum_l |\mathbf{M}_{ll}| = \prod_{i \neq \alpha} \lambda_i \equiv \Lambda_\alpha, \quad \text{for } \lambda_\alpha = 0. \quad (\text{D.13})$$

Note that \mathbf{M} differs from the matrix in the gap equation, as here eigenvalues λ_i are assumed, while in the gap equation $E^\alpha - z$ is assumed.

The Hermitian matrix \mathbf{M} can in general be written in terms of the eigenvectors v_i and the associated eigenvalues λ_i as

$$\mathbf{M} = \sum_i v_i \lambda_i v_i^{ad}, \quad (\text{D.14})$$

as multiplication with the eigenvectors yields

$$\begin{aligned}\mathbf{M} &= \sum_i v_i \lambda_i v_i^{ad} v_j \\ &= \sum_i v_i \lambda_i \delta_{ij} \\ &= v_j \lambda_j,\end{aligned}\tag{D.15}$$

so that (D.14) has the same mapping as the matrix \mathbf{M} . Similarly the inverse matrix can be written as

$$\mathbf{M}^{-1} = \sum_i v_i (\lambda_i)^{-1} v_i^{ad},\tag{D.16}$$

since, assuming full rank,

$$\begin{aligned}\mathbf{M}\mathbf{M}^{-1} &= \sum_i v_i (\lambda_i)^{-1} v_i^{ad} \sum_i v_i \lambda_i v_i^{ad} \\ &= \sum_j v_j v_j^{ad} = \mathbf{1}.\end{aligned}\tag{D.17}$$

The last step follows from

$$\sum_i v_i v_i^{ad} v_j = v_j \quad \forall j.\tag{D.18}$$

D.2 Matrices with Big Values

In this section matrices with very large values, necessary to introduce the cut-off function in the Matsubara sum, are discussed.

Consider a matrix of the following

$$\mathbf{M} = \begin{pmatrix} a & \Delta & C \\ \Delta & a' & \\ \bar{C} & b & \Delta' \\ & \Delta' & b' \end{pmatrix}\tag{D.19}$$

where $a' = \mathcal{O}(a)$ and a is large. If we make the ansatz for the eigenvalue $E = \mathcal{O}(a)$ the eigenvalue equation reduces to

$$\begin{vmatrix} a - E & \Delta \\ \Delta & a' - E \end{vmatrix} E^2 + \mathcal{O}(a^2) = 0 \quad \Rightarrow \quad E = a \vee E = a',\tag{D.20}$$

i.e., the eigenvalue is the eigenvalue of the first diagonal block. The ansatz $E = \mathcal{O}(1)$ leads to

$$\begin{vmatrix} b - E & \Delta' \\ \Delta' & b' - E \end{vmatrix} \cdot a \cdot a' + \mathcal{O}(1) = 0,\tag{D.21}$$

i.e., the eigenvalue is determined by the second diagonal block.

Thus, the eigenvalues of a matrix with big values are given by the eigenvalues of the blocks with and without the big values.

The determinant is given by

$$\det \mathbf{M} = a \cdot a' \cdot \begin{vmatrix} b & \Delta' \\ \Delta' & b' \end{vmatrix}.\tag{D.22}$$

D.3 Simplification of the Gap Equations

The Matrix \mathbf{M} in the gap equations has the structure

$$\mathbf{M}(z) = \mathcal{M} - z\mathbf{1} \quad (\text{D.23})$$

where \mathcal{M} is a Hermitian matrix¹ and z a number. \mathcal{M} has eigenvalues and eigenvectors defined by

$$\mathcal{M}v_i = E^i v_i, \quad (\text{D.24})$$

so that \mathbf{M} has the same eigenvectors and different eigenvalues given by

$$\mathbf{M}v_i = (E^i - z)v_i. \quad (\text{D.25})$$

Thus, by (D.13) the denominator of the gap equations is given by:

$$\begin{aligned} \sum_l |\mathbf{M}_{ll}(z)| &= \sum_k \prod_{i \neq k} (E^i - z) \\ &\rightarrow \prod_{i \neq \alpha} (E^i - E^\alpha) \quad \text{for } z \rightarrow E^\alpha \end{aligned} \quad (\text{D.26})$$

$$\equiv \Lambda_\alpha \quad (\text{D.27})$$

where the product and the sum run over all eigenvalues.

Now the nominator can be expressed, due to (D.9), by elements of the inverse:

$$|\mathbf{M}_{ij}| = \frac{1}{\det(\mathbf{M})} \{\mathbf{M}^{-1}\}_{ji} (-1)^{i+j} \quad (\text{D.28})$$

while the inverse can be expressed by the eigenvalues and eigenvectors of the matrix due to (D.16)²

$$\{\mathbf{M}^{-1}\}_{ij} = \sum_l v_l^i (v_l^j)^* (E_l - z)^{-1} \quad (\text{D.29})$$

combining (D.28) and (D.29) and taking the limit $z \rightarrow \lambda_\alpha$ we obtain

$$|\mathbf{M}_{ij}^\alpha| = v_\alpha^j (v_\alpha^i)^* \Lambda_\alpha (-1)^{i+j} \quad (\text{D.30})$$

for the nominator, with Λ_α like (D.27). The fraction in the gap equation can thus be written as

$$\frac{|\mathbf{M}_{ij}^\alpha|}{\sum_l |\mathbf{M}_{ll}^\alpha|} = v_\alpha^j (v_\alpha^i)^* (-1)^{i+j}. \quad (\text{D.31})$$

¹ Here, the matrix \mathcal{M} of the operator formalism, or $\mathcal{M} \equiv \mathcal{M}(i\omega = 0)$ of the HS formalism is assumed.

² Observe that the definition of the matrix there differs slightly from this one.

D.4 Performing the Matsubara Sum

In this section the Matsubara sum, appearing in the MF equations with an ω -independent potential, is performed and the RG cut-off is introduced.

Terms like

$$\sum_{\omega_n} \frac{1}{\det \mathcal{M}(i\omega_n)} \det \mathcal{M}_{ij}(i\omega_n) = \frac{1}{\beta} \sum_n \frac{1}{\det \mathcal{M}(i\omega_n)} \det \mathcal{M}_{ij}(i\omega_n) \quad (\text{D.32})$$

have to be evaluated, with $\mathcal{M}(i\omega_n) = \mathcal{M}(0) - \mathbf{1}\omega_n$, where $\mathcal{M}(0)$ is a Hermitian matrix, independent of ω_n . Define

$$f(z) = \frac{1}{\det \mathcal{M}(z)} \det \mathcal{M}_{ij}(z) \quad (\text{D.33})$$

where $z = i\omega_n$. The auxiliary function

$$h(z) = (1 + \exp(\beta z))^{-1} \quad (\text{D.34})$$

has poles at $z_n = i\omega_n = i\frac{2n+1}{\beta}\pi$, with the residuum

$$\text{Res } h(z_n) = -\frac{1}{\beta} \quad \forall n. \quad (\text{D.35})$$

Define the complex function $g(z) = h(z)f(z)$. It is

$$\oint g(z) dz \rightarrow 0 \quad \text{for } r \rightarrow \infty, \quad (\text{D.36})$$

if $g(z)$ is of $\mathcal{O}(z^{-2})$ as $z \rightarrow \infty$.

Introducing the RG Cut-off

Here seems to be the best place to introduce the cut-off functions, but this is not essential for performing the Matsubara sum and can be skipped at first reading.

In the RG the cut-off is introduced by a cut-off function χ_k multiplied with the bare propagator. Assume k is such that $\chi_k = 1$, $1 \ll \chi_{k+Q}^{-1} \equiv \chi^{-1}$. Then, according to (D.2), the matrix can be represented as

$$\begin{aligned} |\mathcal{M}| &= \begin{vmatrix} C_{k,\omega}^{-1} & \Delta_k & \vdots & & 0 \\ \Delta_k^* & C_{k,\omega}^{-1} & \vdots & & \\ \dots & \dots & \dots & \dots & \dots \\ 0 & \vdots & \chi^{-1} C_{k+Q,\omega}^{-1} & & 0 \\ & \vdots & 0 & \chi^{-1} C_{-k+Q,-\omega}^{-1} & \end{vmatrix} \\ &= \chi^{-2} \begin{vmatrix} C_{k,\omega}^{-1} & \Delta_k \\ \Delta_k^* & C_{k,\omega}^{-1} \end{vmatrix} C_{k+Q,\omega}^{-1} C_{-k+Q,-\omega}^{-1} \end{aligned} \quad (\text{D.37})$$

The minor if of quadratic order in χ^{-1} in the SC case

$$\begin{aligned} |\mathcal{M}_{12}| &= \begin{vmatrix} \Delta_k^* & & \\ & \chi^{-1} C_{k+Q,\omega}^{-1} & \\ & & \chi^{-1} C_{-k+Q,-\omega}^{-1} \end{vmatrix} \\ &= \chi^{-2} \Delta_k^* C_{k+Q,\omega}^{-1} C_{-k+Q,-\omega}^{-1} \end{aligned} \quad (\text{D.38})$$

and of liner order in the AF case:

$$\begin{aligned} |\mathcal{M}_{13}| &= \begin{vmatrix} C_{k,\omega}^{-1} & \Delta_k & \\ \Delta_k^* & C_{k,\omega}^{-1} & \\ & & \chi^{-1} C_{-k+Q,-\omega}^{-1} \end{vmatrix} \\ &= \chi^{-1} \begin{vmatrix} C_{k,\omega}^{-1} & \Delta_k \\ \Delta_k^* & C_{k,\omega}^{-1} \end{vmatrix} C_{-k+Q,-\omega}^{-1}. \end{aligned} \quad (\text{D.39})$$

Thus

$$\frac{|\mathcal{M}_{ij}|}{|\mathcal{M}|} \quad (\text{D.40})$$

vanishes for the \mathcal{A} and π cases, and reduces in the SC case to the simple superconducting expression:

$$\frac{|\mathcal{M}_{ij}|}{|\mathcal{M}|} = \frac{\Delta_k^*}{\begin{vmatrix} C_{k,\omega}^{-1} & \Delta_k \\ \Delta_k^* & C_{k,\omega}^{-1} \end{vmatrix}} \quad (\text{D.41})$$

Back to the Matsubara sum:

The function $f(z)$ has the structure

$$f(z) = \frac{\det(\mathcal{M}_{ij}(z))}{\det \mathcal{M}(z)} \equiv \frac{f_1}{f_2} \quad (\text{D.42})$$

Poles can occur only if $f_2(z_\alpha) = 0$, implying

$$\det \mathbf{M}^\alpha = \det(\mathcal{M}(i\omega = z_\alpha)) = 0, \quad (\text{D.43})$$

i.e., if z_α is an eigenvalue of \mathcal{M} . Assuming that $\det(\mathbf{M}_{ij}) \neq 0$ and that the eigenvalues are not degenerate³

$$\text{Res } f(z_\alpha) = \frac{f_1(z_\alpha)}{f_2'(z_\alpha)}, \quad (\text{D.44})$$

³ The two assumptions do not always hold; in this case it is expected that the additionally zeros of numerator and denominator can be reduced.

holds, where, due to (D.3)

$$\begin{aligned}
f'(z) &= \frac{\partial}{\partial z} \det \mathcal{M}(z) \\
&= \sum_l (-1)^{l+l} \left(\frac{\partial}{\partial z} m_{ll} \right) \det (\mathcal{M}_{ll}) \\
&= - \sum_l \det (\mathcal{M}_{ll}), \tag{D.45}
\end{aligned}$$

so that

$$\text{Res } g(z_\alpha) = (1 + \exp(\beta z_\alpha))^{-1} (-1) \frac{\det \mathbf{M}_{ij}(z_\alpha)}{\sum_l \det \mathbf{M}_{ll}(z_\alpha)}. \tag{D.46}$$

All together

$$\begin{aligned}
0 &= \oint g(z) dz \\
&= \sum_n f(z_n) \text{Res } h(z_n) + \sum_\alpha h(z_\alpha) \text{Res } f(z_\alpha) \\
&= -\frac{1}{\beta} \sum_n \frac{1}{\det \mathcal{M}(z_n)} \det \mathcal{M}_{ij}(z_n) + \sum_\alpha \frac{-1}{1 + \exp(\beta z_\alpha)} \frac{\det \mathbf{M}_{ij}^\alpha}{\sum_l \det \mathbf{M}_{ll}^\alpha} \tag{D.47}
\end{aligned}$$

With our convention $\sum_{\omega_n} = T \sum_n$ for the ω_n sum we finally obtain

$$\sum_{\omega_n} \frac{1}{\det \mathcal{M}(\omega_n)} \det \mathcal{M}_{ij}(\omega_n) = \sum_\alpha \frac{-1}{1 + \exp(\beta z_\alpha)} \frac{\det \mathbf{M}_{ij}^\alpha}{\sum_l \det \mathbf{M}_{ll}^\alpha} \tag{D.48}$$

where $z_\alpha = E_k^\alpha$ is the eigenvalue of the matrix $\mathcal{M}(i\omega = 0)$.

Appendix E

Technical details

Here some technical details are discussed in brevity.

The numerics proved to be more costly than first expected. This is due to costly integrals and slow convergence of the iteration of the gap equations.

The costly integration is due to jumps in the integrand. Even if the jumps due to the patching are taken care of, the effective FSs of the AF yield further jumps, which are not easy to determine in the full scheme. The 2D integration was split into two 1D integrations by first integrating over energy shells (k_x as a variable or k_y) with respect to the free dispersion ε_k and second integrating over the energies. Since the energy shells of the effective dispersion E_k can cross the former ones this has no advantage and a simple k_x, k_y -integration might even be cheaper.

The convergence is poor due to limit cycles and due to RHSs which cross the bisector with a small angle. The first problem can be healed by a standard mixing factor, i.e., adding to the newly calculated gap-value a fraction of the old value, which is just Newton's method with a fixed value for the slope. The convergence can be drastically accelerated by a Shanks-transformation

$$S_n = \frac{A_{n+1}A_{n-1} - A_n^2}{A_{n+1} + A_{n-1} - 2A_n}$$

which maps a series $A_n = A + \alpha q^n \rightarrow A$. Such a behaviour is expected for self-consistency equations, as long as the relative angle of the two intersecting curves is finite. The transformation can be iterated, see [Bender and Orszag 1999]¹ for details.

Bisection does not always work for the AF gap due to metastable zero-gap solutions. Still something can be learned from chapter 4 (without proof): For $\mu_{vH} < \mu < 0$ the value of the RHS at the lower kink should be above the bisector to have a solution. Thus the position of the lower kink is a good lower point for a bisection. For $\mu < \mu_{vH}$, the solution has to be $|\mathcal{A}| > |\delta_{vH}|$, at least if no SC gap is present.

The potentials $V_{kk'}$, $W_{kk'}$ and $U_{kk'}$ are symmetric by construction. Due to the projection procedure in the RG, placing three of the momenta on the

¹Very much worth reading.

FS, the 4th momentum is by momentum conservation generally not on the FS. This unsymmetric treatment of the momenta leads to unsymmetric couplings for $W_{kk'}$ and $U_{kk'}$, which are symmetrised for the MF part. Also the $Q = (\pi, \pi)$ transfer is only an approximation, since the vector between the FSs is only in special cases exactly Q .

An eigenvalue decomposition of the interactions shows that they are usually dominated by one eigenvalue. The corresponding eigenvector determines the gap-structure to a large extent. Searching for solutions in this 1D subspace drastically reduces the computational effort and is suitable for getting a good overview. However, all data presented in this work were obtained with full momentum dependences.

The free energy is easy to program, computationally cheap for $T = 0$, and gives a first insight if combined with the eigenvalue decomposition mentioned above. It might therefore be a good starting point for similar numerics, even though determining the exact minima is again expected to be expensive.

Appendix F

Deutsche Zusammenfassung

Systeme mit verschiedenen konkurrierenden Instabilitäten stellen eine große Herausforderung der theoretischen Physik dar. Ein Paradebeispiel für solche Systeme ist die Stoffklasse der Kupferoxide, wie z.B. Ba-La-Cu-O. Während die Materialien im undotierten Zustand gewöhnlich Mott-Isolatoren sind, werden sie durch Dotierung zu Leitern bzw. unterhalb einer kritischen Temperatur zu Supraleitern. Diese supraleitenden Eigenschaften setzen bei für dieses Phänomen hohen Temperaturen ein, weshalb sie auch als Hoch- T_c -Materialien bezeichnet werden. Auch der normalleitende, unmagnetische Zustand weist ungewöhnliche und weitestgehend unverstandene Eigenschaften auf. So ist unterhalb einer gewissen Temperatur die Zustandsdichte in der Nähe der Fermifläche unterdrückt; weiterhin ist die Temperaturabhängigkeit des Widerstandes linear, im Gegensatz zu dem aus der Fermiflüssigkeits-Theorie erwarteten quadratischen Verhalten.

Es liegt die Vermutung nahe, dass diese Eigenschaften ihren Ursprung in dem Wechselspiel verschiedener Instabilitäten finden. Eine kontrollierte Rechnung, die verschiedene Instabilitäten gleichberechtigt zulässt, ist also wünschenswert. Leider ist bisher keine praktikable Methode bekannt, die für typische Parameter der Hoch- T_c -Materialien anwendbar wäre.

Die in dieser Arbeit vorgestellte Methode ist eine Kombination aus funktionaler Renormierungsgruppe (RG) und einer erweiterten Molekularfeld-Rechnung. Die RG ist kontrolliert für kleine Wechselwirkungen (WW), nicht jedoch für die relativ starken WW des oben beschriebenen Problems; jedoch kann man etwas über die Hoch- T_c -Systeme durch Untersuchung des Limes schwacher Kopplungen lernen, zumindest unter der Annahme, dass das Verhalten kontinuierlich von der Wechselwirkungsstärke abhängt.

Die störungstheoretische Berechnung verschiedener Größen führt zu Divergenzen verschiedener Klassen von Diagrammen. Für kontrollierte Rechnungen ist es daher unumgänglich, diese Beiträge gleichberechtigt zu erfassen, d.h. aufzusummieren. Nur in speziellen Fällen ist dieses analytisch möglich. Die Idee der Renormierung besteht darin, das ursprüngliche Problem in Moden hoher und Moden niedriger Energie zu zerlegen. Dazu wird eine Regularisierungsskala (Cut-Off) Λ eingeführt und entsprechende skalenabhängige n -Punkt-Funktionen, die nur Beiträge hoher Energie enthalten. Die Änderung

dieser Funktionen mit der Skala Λ wird durch die Renormierungsgruppengleichungen oder Flussgleichungen beschrieben. Das Lösen dieser Differentialgleichungen summiert im Limes $\Lambda \rightarrow 0$ systematisch die führenden Beiträge. Auch diese Integration kann zu Divergenzen führen; diese sind jedoch keine Artefakte der Störungstheorie, sondern Zeichen einer Instabilität zu einer symmetriebrochenen Phase. Diese Divergenzen verhindern die Ausintegration ($\Lambda \rightarrow 0$) der RG-Gleichungen. In der Herleitung gemachte Näherungen werden durch das Anwachsen verschiedener Kopplungen ungültig. Daher ist es naheliegend, die Integration nur bis zu einer Skala Λ_{MF} durchzuführen, und die weiteren Freiheitsgrade auf andere Weise zu behandeln. Tatsächlich lassen sich die n -Punkt-Funktionen zusammen mit dem Cut-Off im in dieser Arbeit verwendeten RG Schema als skalenabhängiges Niederenergie-Modell auffassen.

Dieses Niederenergie-Modell wird im Rahmen einer erweiterten Molekularfeldnäherung (MF) behandelt. Die Molekularfeld-Rechnung erlaubt die gleichzeitige Berücksichtigung verschiedener Ordnungsparameter. Dabei stehen d -Wellen-Supraleitung und Spin-Dichte-Wellen (Antiferromagnet) im Mittelpunkt. Diese kombinierte MF+RG Theorie erlaubt deren Wechselspiel und eine mögliche Koexistenz zu untersuchen. Die Energielücken-Struktur (Gap-Struktur) und die Gapamplituden können berechnet werden.

F.1 Übersicht der Arbeit

Im Kapitel 2 wird das in dieser Arbeit verwendete Renormierungsschema, das Wick-geordnete Schema, motiviert und hergeleitet. Um eine numerische Behandlung zu ermöglichen werden Näherungen gemacht; die erhaltene ein-Schleifen Gleichung berücksichtigt nur die zur Fermifläche tangentialen Impulsabhängigkeiten, vernachlässigt jedoch die radialen Impulsabhängigkeiten und die Energieabhängigkeit. Das Wick-geordnete Schema ist im Kontext dieser Arbeit besonders geeignet, da eine Interpretation als Niederenergie-Modell möglich ist.

Um zu klären, welche Beiträge in der verwendeten Näherung enthalten sind, wird die Lösung grafisch als die sogenannte Parquet-Approximation interpretiert. Das Niederenergie-Modell wird beschrieben und der Übergang zur Molekularfeld-Rechnung motiviert.

Symmetriebrechung und Molekularfeldtheorie werden in Kapitel 3 kurz allgemein eingeführt um dann das konkrete Problem zu behandeln: die gekoppelte MF-Theorie verschiedener Ordnungsparameter. Die gekoppelten MF-Gleichungen werden auf zwei Weisen hergeleitet. Zum einen mit Hilfe des Pfadintegralformalismus; das Einführen bosonischer Felder mittels einer Hubbard-Stratonovich-Transformation erlaubt den Übergang zu einer rein bosonischen Wirkung, die im Rahmen einer Sattelpunktsintegration behandelt wird, was zu den MF-Gleichungen führt. Zum anderen kann der Hamiltonoperator durch eine MF-Entkopplung auf quadratische Form gebracht werden, so dass die Zustandssumme unmittelbar angegeben werden kann. Die Variation des großkanonischen Potentials führt zu den MF-Gleichungen.

Während sich die erste Herleitung nahtlos an die Renormierungsgruppe anfügt, und sich daher auch leicht auf andere Cut-Off Schemata als dem hier

verwendeten erweitern läßt, hat die Molekularfeldentkopplung des Hamiltonoperators den Vorteil größerer Übersichtlichkeit.

Die hier berücksichtigten Ordnungsparameter (OP) sind die Supraleitung und eine Spin/Ladungs-Dichte-Welle mit Modulation $Q = (\pi, \pi)$; bei einer Anwesenheit dieser beiden OP ergibt sich bei endlicher Kopplung auch ein Gap durch Paare mit Gesamtimpuls Q , das π -Paar.

Beide Herleitungen machen wenig Gebrauch von der speziellen Gap-Struktur oder dem Modell und lassen sich daher leicht auf mehr oder andere Gaps oder andere Modelle verallgemeinern.

Die MF-Rechnung für den Antiferromagneten hat gegenüber der Rechnung für den Supraleiter einige Besonderheiten, die in Kapitel 4 diskutiert werden. Insbesondere kann es bei endlichem Ordnungsparameter effektive Fermiflächen geben, die sich von der nackten Fermifläche unterscheiden; für ein endliches übernächstes-Nachbar-Hüpfen t' kann solch ein OP sogar die einzig stabile Lösung sein. Das Verhalten der MF-Lösung wird zu einem großen Teil von diesen effektiven Fermiflächen bestimmt, die daher ausführlich diskutiert werden.

Im letzten Abschnitt des Kapitels 4 wird das Zusammenwirken der Renormierung und der Molekularfeldtheorie im Spezialfall rein antiferromagnetischer Wechselwirkung untersucht. Es stellt sich heraus, dass die RG unphysikalische Niederenergie-Modelle erzeugen kann. Dieses hängt eng zusammen mit der Möglichkeit von Phasenübergängen erster Ordnung; beides wird zurückgeführt auf die Existenz effektiver Fermiflächen in Gegenwart des AF Gaps, und deren Abhängigkeit von diesen.

Die Eigenschaften der Lösung der AF-Gapgleichung sind wichtig zum Verständnis des Wechselspiels mit der Supraleitung (SL) und zur Interpretation der numerischen Rechnungen.

In Kapitel 5 werden kurz die MF-Rechnung für die Supraleitung und das π -Paar diskutiert. Während die Rechnung für erstere als bekannt vorausgesetzt wird stellt sich heraus, dass das π -Paar von untergeordneter Bedeutung ist. Weiterhin wird das Wechselspiel zwischen Supraleitung, Antiferromagnetismus und π -Paarung diskutiert. Die Anwesenheit eines AF-OP kann die rechte Seite des SL-Gapgleichung verkleinern oder auch vergrößern. Letzteres steht im Gegensatz zur allgemeinen Erwartung. Entsprechendes gilt für die rechte Seite des AF-OP. Da beide Gapgleichungen Ableitungen des großkanonischen Potentials sind, sind die jeweiligen Abhängigkeiten verknüpft.

Numerische Ergebnisse der RG+MF Kombination werden in Kapitel 6 präsentiert. Die numerische Implementierung der RG stammt von [Rohe 2005].

Es wird kurz auf das attraktive Hubbard Modell ($U < 0$) eingegangen, was u.a. Aussagen über die Qualität der gemachten Näherungen erlaubt. Es findet sich die erwartete Reduktion des SL-Gaps durch Fluktuationen.

Der Hauptteil des Kapitels beschäftigt sich mit dem repulsiven Hubbard-Modell ($U > 0$). Ohne übernächstes-Nachbar-Hüpfen ($t' = 0$) sind die gefundenen Lösungen entweder antiferromagnetisch, isolierend und halb gefüllt oder rein supraleitend. Für endliches t' kann es trotz eines endlichen AF Fermiflächen geben. Dies erlaubt Dotierung und Koexistenz mit Supraleitung.

Für Parameter, die Dotierung und Koexistenz erlauben, wird die t' - und U -Abhängigkeit der Gapamplituden untersucht. Für einen Parametersatz werden die effektiven Fermiflächen und Gapstrukturen in Abhängigkeit vom chemischen Potential μ angegeben. Schließlich wird beispielhaft gezeigt, dass das bis dahin vernachlässigte π -Paar-Gap klein gegenüber den anderen Gaps ist.

Anhang A enthält ein pädagogisches Beispiel der Renormierung. Störungsrechnung in gewöhnlichen, nichtlinearen Differentialgleichungen kann zu strukturell falschen Ergebnissen führen. Die Flussbedingung der Differentialgleichung hat die selbe Gruppenstruktur wie die funktionale Renormierungsgruppe. Unter Ausnutzung dieser Gruppeneigenschaft ergeben sich Flussgleichungen, deren Integration zu einer strukturell sinnvollen Näherung des ursprünglichen Problems führt.

Bibliography

- D. J. Amit, *Field theory, the renormalization group, and critical phenomena*, McGraw-Hill, New York, 1978.
- P. W. Anderson, *The resonating valence bond state in La_2CuO_4 and superconductivity*, *Science* **235**, 1196 (1987).
- P. W. Anderson, G. Baskaran, Z. Zou, and T. Hsu, *Resonating-valence-bond theory of phase transitions and superconductivity in La_2CuO_4 -based compounds*, *Physical Review Letters* **58**, 2790 (1987).
- J. F. Annett, *Superconductivity, superfluids, and condensates*, Oxford Univ. Press, Oxford, 2004.
- J. Bardeen, L. N. Cooper, and J. R. Schrieffer, *Theory of Superconductivity*, *Physical Review* **108**, 1175 (1957).
- S. E. Barrett, D. J. Durand, C. H. Pennington, C. P. Slichter, T. A. Friedmann, J. P. Rice, and D. M. Ginsberg, *^{63}Cu Knight shifts in the superconducting state of $\text{YBa}_2\text{Cu}_3\text{O}_{7-\delta}$ ($T_c = 90\text{K}$)*, *Phys. Rev. B* **41**, 6283 (1990).
- J. Bednorz and K. Müller, *Possible high T_c superconductivity in the Ba-La-Cu-O system*, *Zeitschrift für Physik B* **64**, 189 (1986).
- C. Bender and S. Orszag, *Advanced Mathematical Methods for Scientists and Engineers*, Springer, New York, 1. edition, 1999.
- J. Berges, N. Tetradis, and C. Wetterich, *Non-perturbative renormalization flow in quantum field theory and statistical physics*, *Phys. Rep.* **363**, 223 (2002), hep-ph/0005122.
- B. Binz, D. Baeriswyl, and B. Douçot, *Weakly interacting electrons and the renormalization group*, *Annalen der Physik* **12**, 704 (2003), cond-mat/0309645.
- L.-Y. Chen, N. Goldenfeld, and Y. Oono, *Renormalization group and singular perturbations: Multiple scales, boundary layers, and reductive perturbation theory*, *Phys. Rev. B* **54**, 376 (1996).
- A. V. Chubukov and D. M. Frenkel, *Renormalized perturbation theory of magnetic instabilities in the two-dimensional Hubbard model at small doping*, *Phys. Rev. B* **46**, 11884 (1992).

- I. T. Diatlov, V. V. Sudakov, and K. A. Ter-Martirosian, *Asymptotic Meson-Meson Scattering Theory*, Zh. Eksp. Teor. Fiz. **5**, 631 (1957).
- A. C. Durst and P. A. Lee, *Impurity-induced quasiparticle transport and universal-limit Wiedemann-Franz violation in d-wave superconductors*, Phys. Rev. B **62**, 1270 (2000).
- I. Dzyaloshinskii, , Zh. Eksp. Teor. Fiz. **93**, 1487 (1987).
- T. Enss, *Renormalization, Conservation Laws and Transport in Correlated Electron Systems*, PhD thesis, University of Stuttgart, Germany, 2005, cond-mat/0504703.
- D. Esteve, J. Martinis, C. Urbina, M. Devoret, G. Collin, P. Mondo, M. Ribault, and A. Revcolevschi, *Observation of the a.c. Josephson Effect Inside Copper-Oxide-Based Superconductors*, Europhys. Lett. **3**, 1237 (1987).
- P. Fazekas, *Lecture notes on electron correlation and magnetism*, World Scientific, Singapore, 2003.
- J. Feldman, J. Magnen, V. Rivasseau, and E. Trubowitz, *An intrinsic $1/N$ expansion for many-fermion systems*, Europhysics Letters **24**, 437 (1993).
- A. L. Fetter and J. D. Walecka, *Quantum theory of many-particle systems*, MacGraw-Hill, New York, 1971.
- P. L. Gammel, D. J. Bishop, G. J. Dolan, J. R. Kwo, C. A. Murray, L. F. Schneemeyer, and J. V. Waszczak, *Observation of hexagonally correlated flux quanta in $YBa_2Cu_3O_7$* , Physical Review Letters **59**, 2592 (1987).
- M. Gaudin, *Sur le développement de la grande fonction de partition por des systèmes de particules identiques*, Nuclear Physics **20**, 513 (1960).
- R. Gersch, C. Honerkamp, D. Rohe, and W. Metzner, *Fermionic renormalization group flow into phases with broken discrete symmetry: charge-density wave mean-field model*, European Physical Journal B **48**, 349 (2005).
- R. Gersch, J. Reiss, and Honerkamp, *In preparation*, (2006).
- C. J. Halboth, *Niederenergie-Eigenschaften zweidimensionaler Fermi Systeme*, PhD thesis, RWTH Aachen, Germany, 1999.
- C. J. Halboth and W. Metzner, *d-Wave Superconductivity and Pomeranchuk Instability in the Two-Dimensional Hubbard Model*, Phys. Rev. Lett. **85**, 5162 (2000).
- C. J. Halboth and W. Metzner, *Renormalization-group analysis of the two-dimensional Hubbard model*, Phys. Rev. B **61**, 7364 (2000), cond-mat/9908471.
- J. E. Hirsch, *Two-dimensional Hubbard model: Numerical simulation study*, Phys. Rev. B **31**, 4403 (1985).

- W. Hofstetter and D. Vollhardt, *Frustration of antiferromagnetism in the t - t' -Hubbard model at weak coupling*, Annalen der Physik **7**, 48 (1998), cond-mat/0309645.
- C. Honerkamp, D. Rohe, S. Andergassen, and T. Enss, *Interaction flow method for many-fermion systems*, Phys. Rev. B **70**, 235115 (2004), cond-mat/0403633.
- C. Honerkamp and M. Salmhofer, *The temperature-flow renormalization group and the competition between superconductivity and ferromagnetism*, Phys. Rev. B **64**, 184516 (2001), cond-mat/0105218.
- C. Honerkamp and M. Salmhofer, *Eliashberg Equations Derived from the Functional Renormalization Group*, Progress of Theoretical Physics **113**, 1145 (2005), cond-mat/0501674.
- C. Honerkamp, M. Salmhofer, N. Furukawa, and T. M. Rice, *Breakdown of the Landau-Fermi liquid in Two Dimensions due to Umklapp Scattering*, Phys. Rev. B **63**, 035109 (2001), cond-mat/9912358.
- J. Hubbard, *Calculation of Partition Functions*, Physical Review Letters **3**, 77 (1959).
- M. S. Hybertsen, E. B. Stechel, W. M. C. Foulkes, and M. Schlüter, *Model for low-energy electronic states probed by x-ray absorption in high- T_c cuprates*, Phys. Rev. B **45**, 10032 (1992).
- M. Inui, S. Doniach, P. J. Hirschfeld, and A. E. Ruckenstein, *Coexistence of antiferromagnetism and superconductivity in a mean-field theory of high- T_c superconductors*, Phys. Rev. B **37**, 2320 (1988).
- A. P. Kampf and A. A. Katanin, *Competing phases in the extended U - V - J Hubbard model near the Van Hove fillings*, Phys. Rev. B **67**, 125104 (2003), cond-mat/0212190.
- A. A. Katanin, *Fulfillment of Ward identities in the functional renormalization group approach*, Phys. Rev. B **70**, 115109 (2004).
- A. A. Katanin and A. P. Kampf, *Renormalization group analysis of magnetic and superconducting instabilities near van Hove band fillings*, Phys. Rev. B **68**, 195101 (2003), cond-mat/0304189.
- A. A. Katanin and A. P. Kampf, *Order-parameter symmetries for magnetic and superconducting instabilities: Bethe-Salpeter analysis of functional renormalization-group solutions*, Phys. Rev. B **72**, 205128 (2005), cond-mat/0408246.
- W. Kohn and J. M. Luttinger, *New Mechanism for Superconductivity*, Physical Review Letters **15**, 524 (1965).

- Š. Kos, A. J. Millis, and A. I. Larkin, *Gaussian fluctuation corrections to the BCS mean-field gap amplitude at zero temperature*, Phys. Rev. B **70**, 214531 (2004).
- M. Y. Kuchiev and O. P. Sushkov, *Many-body correlation corrections to superconducting pairing in two dimensions*, Phys. Rev. B **53**, 443 (1996).
- T. Kunihiro and K. Tsumura, *Application of the Renormalization-group Method to the Reduction of Transport Equations*, ArXiv High Energy Physics - Theory e-prints (2005), [arXiv:hep-th/0512108](https://arxiv.org/abs/hep-th/0512108).
- B. Kyung, *Mean-field study of the interplay between antiferromagnetism and d-wave superconductivity*, Phys. Rev. B **62**, 9083 (2000).
- J. S. Langer, *Perturbation Expansions and Functional Integrals in the Theory of Superconductivity*, Physical Review **134**, 553 (1964).
- E. Langmann and M. Wallin, *Mean-field approach to antiferromagnetic domains in the doped Hubbard model*, Phys. Rev. B **55**, 9439 (1997).
- E. Langmann and M. Wallin, *Phase diagrams of the 2D t-t'-U Hubbard model from an extended mean field method*, 2004, URL <http://www.citebase.org/abstract?id=oai:arXiv.org:cond-mat/0406608>.
- F. Lederer, G. Montambaux, and D. Poilblanc, , J. Phys. (Paris) **48**, 1613 (1987).
- H. Q. Lin and J. E. Hirsch, *Two-dimensional Hubbard model with nearest- and next-nearest-neighbor hopping*, Phys. Rev. B **35**, 3359 (1987).
- A. Martín-Rodero and F. Flores, *Solution for the U-negative Hubbard superconductor including second-order correlation effects*, Phys. Rev. B **45**, 13008 (1992).
- R. D. Mattuck and B. Johansson, *Quantum field theory of phase transitions in Fermi systems*, Advances in Physics **17**, 509 (1968).
- N. D. Mermin and H. Wagner, *Absence of Ferromagnetism or Antiferromagnetism in One- or Two-Dimensional Isotropic Heisenberg Models*, Physical Review Letters **17**, 1133 (1966).
- T. R. Morris, *The Exact Renormalisation Group and Approximate Solutions*, Int. J. Mod. Phys. A **9**, 2411 (1994), [hep-ph/9308265](https://arxiv.org/abs/hep-ph/9308265).
- B. Mühlischlegel, *Asymptotic Expansion of the Bardeen-Cooper-Schrieffer Partition Function by Means of the Functional Method*, J. Math. Phys. **3**, 522 (1962).
- M. Murakami, *Possible Ordered States in the 2D Extended Hubbard Model*, J. Phys. Soc. Jpn. **69**, 1113 (2000).
- M. Murakami and H. Fukuyama, *Backward Scattering and Coexistent State in Two-Dimensional Electron Systems*, JPSJ **67**, 2784 (1998).

- A. Neumayr and W. Metzner, *Renormalized perturbation theory for Fermi systems: Fermi surface deformation and superconductivity in the two-dimensional Hubbard model*, Phys. Rev. B **67**, 035112 (2003), cond-mat/0208431.
- J. Polchinski, *Renormalization and effective lagrangians*, Nucl. Phys. B **231**, 269 (1984).
- G. C. Psaltakis and E. W. Fenton, *Superconductivity and spin-density waves: organic superconductors*, Journal of Physics C Solid State Physics **16**, 3913 (1983).
- D. Rohe, *Renormierungsgruppenanalyse des Hubbard-Modells in zwei Dimensionen*, PhD thesis, University of Stuttgart, Germany, 2005.
- D. Rohe and W. Metzner, *Pseudogap at hot spots in the two-dimensional Hubbard model at weak coupling*, Phys. Rev. B **71**, 115116 (2005), cond-mat/0406164.
- S. Sachdev, A. V. Chubukov, and A. Sokol, *Crossover and scaling in a nearly antiferromagnetic Fermi liquid in two dimensions*, Phys. Rev. B **51**, 14874 (1995).
- M. Salmhofer, *Continuous Renormalization for Fermions and Fermi Liquid Theory*, Commun. Math. Phys. **194**, 249 (1998), cond-mat/9706188.
- M. Salmhofer and C. Honerkamp, *Fermionic renormalization group flows: Technique and theory*, Prog. Theor. Phys. **105**, 1 (2001).
- M. Salmhofer, C. Honerkamp, W. Metzner, and O. Lauscher, *Renormalization group flows into phases with broken symmetry*, Prog. Theor. Phys. **112**, 943 (2004), cond-mat/0409725.
- D. J. Scalapino, *The case for $d_{x^2-y^2}$ pairing in the cuprate superconductors*, Phys. Rep. **250**, 329 (1995).
- J. R. Schrieffer, X.-G. Wen, and S.-C. Zhang, *Spin-bag mechanism of high-temperature superconductivity*, Physical Review Letters **60**, 944 (1988).
- H. J. Schulz, Europhys. Lett. **4**, 609 (1987).
- R. Shankar, *Renormalization-group approach to interacting fermions*, Reviews of Modern Physics **66**, 129 (1994), cond-mat/9307009.
- Z.-X. Shen, D. S. Dessau, B. O. Wells, D. M. King, W. E. Spicer, A. J. Arko, D. Marshall, L. W. Lombardo, A. Kapitulnik, and P. Dickinson, *Anomalously large gap anisotropy in the a-b plane of $\text{Bi}_2\text{Sr}_2\text{CaCu}_2\text{O}_{8+\delta}$* , Physical Review Letters **70**, 1553 (1993).
- A. Singh and Z. Tešanović, *Collective excitations in a doped antiferromagnet*, Phys. Rev. B **41**, 614 (1990).

- R. L. Stratonovich, , Soviet Phys.–Doklady **2**, 416 (1958).
- X. F. Sun, S. Ono, Y. Abe, S. Komiya, K. Segawa, and Y. Ando, *Electronic Inhomogeneity and Breakdown of the Universal Thermal Conductivity of Cuprate Superconductors*, Physical Review Letters **96**, 017008 (2006).
- M. Sutherland, D. G. Hawthorn, R. W. Hill, F. Ronning, S. Wakimoto, H. Zhang, C. Proust, E. Boaknin, C. Lupien, L. Taillefer, R. Liang, D. A. Bonn, W. N. Hardy, R. Gagnon, N. E. Hussey, T. Kimura, M. Nohara, and H. Takagi, *Thermal conductivity across the phase diagram of cuprates: Low-energy quasiparticles and doping dependence of the superconducting gap*, Phys. Rev. B **67**, 174520 (2003), cond-mat/0301105.
- M. Takigawa, P. C. Hammel, R. H. Heffner, Z. Fisk, K. C. Ott, and J. D. Thompson, *^{17}O NMR study of $\text{YBa}_2\text{Cu}_3\text{O}_{7-\delta}$* , Physica C Superconductivity **162**, 853 (1989).
- C. C. Tsuei, J. R. Kirtley, C. C. Chi, L. S. Yu-Jahnes, A. Gupta, T. Shaw, J. Z. Sun, and M. B. Ketchen, *Pairing symmetry and flux quantization in a tricrystal superconducting ring of $\text{YBa}_2\text{Cu}_3\text{O}_{7-\delta}$* , Physical Review Letters **73**, 593 (1994).
- P. G. J. van Dongen, *Thermodynamics of the extended Hubbard model in high dimensions*, Phys. Rev. Lett. **67**, 757 (1991).
- C. Wetterich, *Exact evolution equation for the effective potential*, Phys. Lett. B **301**, 90 (1993).
- C. Wetterich, *Bosonic effective action for interacting fermions*, ArXiv Condensed Matter e-prints (2002), cond-mat/0208361.
- K. G. Wilson, *The renormalization group: Critical phenomena and the Kondo problem*, Reviews of Modern Physics **47**, 773 (1975).
- K. G. Wilson and J. Kogut, *The renormalization group and the ϵ expansion*, Phys. Rep. **12**, 75 (1974).
- H. Yamase and H. Kohno, *Coexistence of antiferromagnetism and d -wave singlet state controlled by long-range hopping integral*, Phys. Rev. B **69**, 104526 (2004).
- H. Yamase, V. Oganessian, and W. Metzner, *Mean-field theory for symmetry-breaking Fermi surface deformations on a square lattice*, Phys. Rev. B **72**, 035114 (2005), cond-mat/0502238.
- D. Zanchi and H. J. Schulz, *Weakly correlated electrons on a square lattice: A renormalization group theory*, Europhys. Lett. **44**, 235 (1998), cond-mat/9703189.
- D. Zanchi and H. J. Schulz, *Weakly correlated electrons on a square lattice: Renormalization-group theory*, Phys. Rev. B **61**, 13609 (2000), cond-mat/9812303.

- F. C. Zhang and T. M. Rice, *Effective Hamiltonian for the superconducting Cu oxides*, Phys. Rev. B **37**, 3759 (1988).
- S. C. Zhang, *A Unified Theory Based on $SO(5)$ Symmetry of Superconductivity and Antiferromagnetism*, Science **275**, 1089 (1997).

Danksagungen

Zuerst danke ich meinem Doktorvater Prof. Dr. Metzner für das interessante Thema und die freundliche und gute Betreuung, die auch Zeit ließ, eigene Ideen zu verfolgen.

Weiterhin danke ich Daniel Rohe, dass er mir sein RG-Programm zur Verfügung gestellt und folgenreiche Sonderwünsche erfüllt hat. Hochachtung verdient, dass er meine westfälische Gemütsruhe, die für rheinländische Verhältnisse wohl manchmal an Lethargie grenzt, erduldet hat.

Danken möchte ich der EDV-Abteilung für die stets wieselflinke und äußerst hilfreiche Arbeit.

Roland Gersch danke ich für die engelsgleiche Geduld beim Korrekturlesen.

Tilman Enss danke ich, dass er geduldig mit mir diskutierte, auch in dem Jahr als ich beim Verständnis des anharmonischen Oszillators keine Fortschritte machte. Danke auch, dass ich einige seiner Feynman-Diagramme verwenden durfte.

Mein weiterer Dank gilt Sabine Andergassen, Dmitry Aristov, Heinz Barentzen, Maria Daghofer, Karsten Held, Carsten Honerkamp, Peter Horsch, Andrey Katanin, Ingrid Knapp, Dirk Manske, Andrzej Oleś, Ulrich Schollwöck, Philipp Strack, Oleg Sushkov, Hiroyuki Yamase und Roland Zeyher für die vielen, angeregten und nützlichen Diskussionen über Physik und Nichtphysik und die schöne Zeit.